POLITECNICO DI MILANO

Facoltà di Ingegneria dei Processi Industriali
Dipartimento di Energia
Dipartimento di Chimica, Materiali e Ingegneria Chimica "Giulio Natta"

A COMPUTATIONAL FRAMEWORK FOR THE SIMULATION OF GAS-SOLID CATALYTIC REACTORS BASED ON A MULTIREGION APPROACH

Relatori: **Prof. Alberto CUOCI**
Prof. Matteo MAESTRI

Tesi di Laurea in Ingegneria Chimica di:
Matteo CALONACI **Matr. 760875**
Federica FURNARI **Matr. 764864**

Anno Accademico 2011-2012

Abstract

A fundamental understanding of a catalytic chemical reactor is a prerequisite for the development and optimization of industrial catalytic technologies. In particular, this requires the interplay of phenomena occurring at different time and length scales.

In a previous work (Goisis and Osio 2011) a dedicated numerical tool has been developed (called catalyticFOAM), to allow for the CFD of heterogeneous catalytic reactor based on a detailed microkinetic description of the surface reactivity. In that tool the transport phenomena within the porous medium were neglected in first place. Aim of this work is the development of a numerical framework which allows the description of the actual physics of the system in both fluid and solid phase, handling in detail the coupling at the interface. This leads to a full comprehension of the catalytic process, being an accurate description of both phases, essential when considering systems in which heat and mass transfer limitations inside the catalyst play a major role and the catalyst morphology can thus not be neglected.

In order to achieve this objective, a multi-region structure has been developed, which allows the solver to investigate systems with an arbitrary number of different domains with their own properties, whose geometry can be of arbitrary complexity. A segregated approach for physical coupling of neighboring regions at the interface has been implemented, involving the solution on each domain and the achievement of convergence on the boundary conditions through an iterative loop. Furthermore, an operator splitting technique has been adopted to overcome the complexity of the numerical problem.

The solver developed (catalyticFOAM-multiRegion) thus allows for the dynamic solution of reacting flows over solid catalysts, through a mathematical model detailing both intra-phase phenomena

occurring inside the fluid and solid phase and inter-phase phenomena occurring between them. The surface reactivity is described with detailed kinetic mechanisms with no theoretical limits to the number of species or reactions involved, and the possibility to investigate systems with geometries of arbitrary complexity confers generality and flexibility to the solver.

The resulting numerical framework has been tested by simulating cases of increasing complexity. Moreover, a validation has been performed in order to investigate the reliability of the solver. In particular, the fuel-rich H_2 combustion over Rh catalyst has been analyzed and the simulation results have been compared with experimental data. The capability to detail intra-phase phenomena inside the catalytic volume is proven to be critical to describe the real physics of the system, providing a better fit with experimental data with respect to the models in the literature.

Sommario

La conoscenza approfondita di un reattore catalitico è un prerequisito fondamentale per lo sviluppo e l'ottimizzazione delle tecnologie catalitiche industriali. In particolare, ciò richiede la descrizione di fenomeni che avvengono a diverse scale spaziali e temporali.

In un lavoro di Tesi precedente (Goisis e Osio 2011) è stato sviluppato uno strumento destinato alla simulazione CFD di reattori catalitici eterogenei basata su una descrizione microcinetica dettagliata della reattività di superficie. Tuttavia, in questo modello, i fenomeni di trasporto all'interno del mezzo poroso erano stati trascurati in prima approssimazione.

Scopo di questo lavoro è lo sviluppo di un framework numerico che permetta di descrivere la reale fisica del problema sia all'interno della fase fluida che all'interno della fase solida, gestendo inoltre in dettaglio l'accoppiamento in corrispondenza dell'interfaccia. Solo in questo modo è possibile arrivare a una piena comprensione del processo catalitico, soprattutto quando si considerano sistemi in cui limitazioni al trasporto di materia ed energia all'interno del catalizzatore giocano un ruolo importante (e la morfologia del catalizzatore non può quindi essere trascurata).

Per raggiungere questo obiettivo è stato sviluppato un codice di calcolo fluidodinamico multi-regione, che permette di studiare sistemi costituiti da un numero arbitrario di domini differenti con proprietà distinte, la cui geometria può essere di arbitraria complessità. L'accoppiamento sull'interfaccia delle diverse regioni è stato gestito attraverso una tecnica segregata, che prevede l'ottenimento delle soluzioni su ogni dominio e il raggiungimento della convergenza sulle condizioni al contorno attraverso una procedura iterativa. Inoltre, per superare le difficoltà numeriche caratteristiche del problema, è stata adottata la tecnica dell'operator-splitting.

Il codice di calcolo sviluppato (catalyticFOAM-multiRegion) permette quindi di descrivere la dinamica dei flussi reattivi su catalizzatori solidi, attraverso un modello matematico che descrive in modo dettagliato sia i fenomeni intra-fase che avvengono nelle fasi fluida e solida, sia i fenomeni inter-fase che avvengono fra di loro. La reattività della superficie catalitica è descritta con schemi cinetici dettagliati, in modo che non vi sia un limite teorico al numero di specie o di reazioni coinvolte. Inoltre la possibilità di studiare sistemi aventi geometrie di arbitraria complessità, considerando un numero arbitrario di regioni diverse caratterizzate da diverse proprietà, conferisce

generalità e flessibilità al solutore.

Il framework risultante è stato testato attraverso simulazioni di casi di complessità crescente. Inoltre è stata condotta una convalida del solutore al fine di studiarne l'affidabilità. In particolare, è stata analizzata la combustione su Rh di una corrente ricca in H2 ed i risultati sono stati confrontati con i dati sperimentali. La descrizione dettagliata dei fenomeni intra-fase all'interno del volume catalitico si è rivelata in questo caso essere di fondamentale importanza per descrivere la reale fisica del problema, permettendo di ottenere un migliore accordo con i dati sperimentali rispetto ai modelli proposti nella letteratura.

Table of contents

Figures index

Tables Index

Chapter 1

Introduction

1.1 Motivation

The reactor is the heart of the chemical process, and a thorough understanding of the phenomena occurring during the transformation of reactants into the desired products is of vital importance for the development and optimization of the entire process. It is thus essential to have a deep knowledge of the fundamental parameters critical to chemical reactor design, such as reactor sizing and optimal operating conditions.

Catalytic reactions and reactors have widespread applications in the production of chemicals in bulk, petroleum and petrochemicals, pharmaceuticals, specialty chemicals, etc. The simultaneous developments in catalysis and reaction engineering in 1930s and 1940s acted as a driving force for the onset of rational design of catalytic reactors. These detailed design efforts, firmly based on sound mathematical principles, in turn triggered the development of several profitable catalytic processes. Various authors studied the engineering aspects of diffusion mass transport and reaction rate interaction. In particular, Thiele explained the fractional reduction in catalyst particle

activity due to intra-particle mass transfer limitations and proposed the concept of effectiveness factor reflecting the extent of utilization of the catalyst pellet (Thiele, E.W. 1939).

On the other hand, another simplification usually considered in catalytic reactors models is the uniform temperature inside the solid particle, which means a complete neglect of heat transfer limitations.

The main aim of this work is to get a more accurate description of the physical domain through a detailed description of heat and mass transfer inside the solid domain, which can be crucial in some systems, as well as of inter-phase transport phenomena between the solid and fluid phase. In this way, thanks to the simulation of the actual physics of the system, it is possible to get rid of most of the restrictive approximations often introduced, related to simplified forms of governing equations or specific geometries.

1.2 General overview

Without any doubts, one of the main difficulties encountered in the numerical modeling of the catalytic reactors is the great gap of different time and length scales involved, since the dominant reaction pathway is the result of the interplay between micro-, meso- and macro-scale phenomena (Figure 1.1).

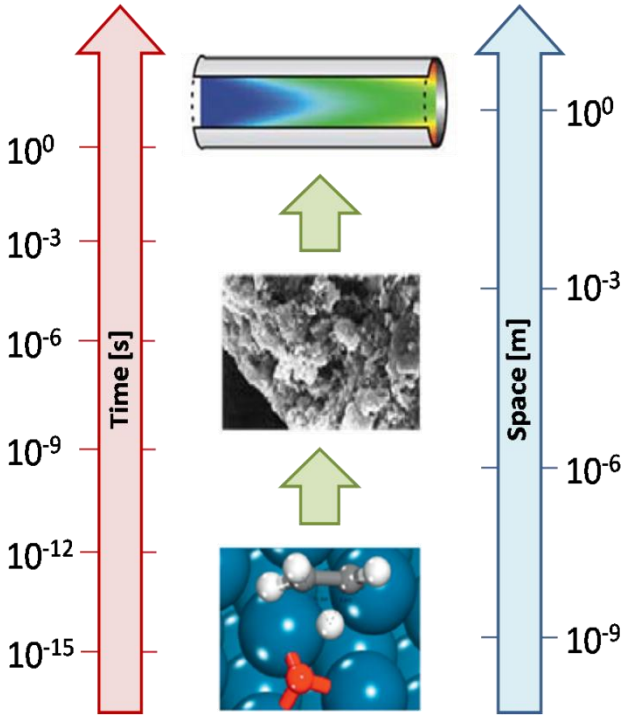

Fig. 1.1 - Time and length scales involved in heterogeneous catalytic processes.

The microscopic scale is associated with making and breaking of chemical bonds between atoms and molecules. At the mesoscale the interplay between all the elementary steps involved in the catalytic process determines the main reaction pathway. At the macroscopic scale the transport of mass, energy and momentum determines local composition, temperature and pressure.

This means that the dominant reaction mechanism is a multi-scale property of the system (Maestri 2011). The description of different phenomena is achieved by employing a "first principles approach", i.e. at each scale the fundamental governing equations are used. In particular:

- ✓ at the molecular scale the behavior of the system is described through detailed kinetic models, whose parameters are computed via first-principles electronic-structure calculations;

- ✓ at the meso-scale statistical methods give a rigorous representation of mechanisms taking place at the catalytic surface. Anyway the most common approach used in literature is the mean field approximation (Vlachos, Stamatakis et al. 2011). This approach assumes a perfect and rapid mixing of reactants, products, and intermediates on the surface;
- ✓ at the macro-scale methods based on continuum approximation are employed, e.g. resolution of Navier-Stokes equations with Computational Fluid Dynamics (CFD) (Reuter 2009).

Such a fundamental approach implies the development of efficient methodologies to connect the fundamental aspects across all the scales involved and link them in one multi-scale simulation.

Unluckily, the resulting numerical problem places highly computational demands mainly related to:

- ✓ the dimensions of the system are proportional to the number of species involved in the reacting process. Therefore, the more detailed the kinetic scheme is, the higher the required time is;
- ✓ ta proper discretization of the geometric domain is required to solve the problem. The number of cells in which the volume is divided is proportional to the accuracy and to the dimensions of the problem;
- ✓ the problem is very stiff because of the difference among the characteristic times and the characteristic lenghts;
- ✓ the presence of a reacting term implies a strong non-linearity of the governing equations.

Furthermore, an accurate description of the problem should include a characterization of the catalytic phase and model intra-solid phenomena constituting the true nature of the diffusion-reaction mechanism. This acquires particular importance, especially when dealing with systems where heat and mass transfer limitations play a major role in determining the conditions holding on the catalytic surface. In these cases, neglecting the catalyst morphology can have a critical impact on the description of the system.

In the following, a summary on the most interesting approaches to these problems available in literature is provided.

1.3 State of the Art

The development of tools capable to describe the actual behavior of catalytic systems via first principles and multi-scale approaches is still in the initial phase. This is due to the complexity of the numerical problem that one has to handle. Recent advances in this field are owed to the vast diffusion of CFD applications.

Nowadays CFD is able to predict very complex flow fields due to the recent development of numerical algorithms and the availability of more performing computer hardware. However, CFD still lacks in the efficient handling of detailed kinetic schemes, mainly due to the difficult management of the huge number of reactions and species involved and to the stiffness of the resulting equations.

Recently the attention has been focused on the development of tools that implement heterogeneous kinetic models. In this section the most recent and challenging studies on coupling of microkinetic modeling and CFD are provided.

The most noticeable advances in this framework have been provided by (Deutschmann, Tischer et al. 2008) with the development of the DETCHEM^{TM} software. This is a FORTRAN based collection of softwares designed to couple detailed chemistry models and CFD. The software package contains tools able to simulate time dependent gas-phase systems, with homogeneous gas-phase and/or heterogeneous surface chemical reactions. The list of tools contained in the DETCHEM library is presented below, together with mathematical aspects and range of applicability (Deutschmann, Tischer et al. 2011):

- ✓ DETCHEMBATCH and DETCHEMCSTR are computational tools that simulate homogeneous and heterogeneous reactions taking place respectively in a batch and CSTR reactor;
- ✓ DETCHEMPLUG is an application able to simulate the behavior of plug flow chemical reactors for gas mixtures. The model is mono-dimensional and it has been developed in the assumption of negligible axial diffusion and absence of variations in transverse direction;
- ✓ DETCHEMPACKEDBED is a tool for the simulations of packed bed reactors. The model is one-dimensional heterogeneous and assumes that there is no axial diffusion and no radial variations in the flow properties;
- ✓ DETCHEMCHANNEL is a computational tool that simulates the steady state chemically reacting gas flow through cylindrical channels using the boundary-layer approximation;

- ✓ DETCHEMMONOLITH is a simulation code that is designed to simulate transient problems of monolithic reactors, used whenever the interactions of chemistry, transport and reactor properties shall be investigated in monolithic structures of straight channels. It is assumed that there is no gas exchange between the channels and that the residence time of the gas inside the channels is small compared with the response time scale of the monolith. Furthermore, it is assumed that the cross-section of the monolith does not change along the channel axis;
- ✓ DETCHEMRESERVOIR is an application that allows to simulate isothermal transient behavior of monolith reactors. Only selected surface concentrations are assumed to vary over time (storage concentrations). The used approach consists in iterating steady-state and transient calculations. For each time step the DETCHEMCHANNEL or DETCHEMPLUG routines are called. The obtained steady-state values are then used by DETCHEMRESERVOIR as initial values in the integrations of site conservation balances of storage species;
- ✓ DC4FLUENT is a collection of user defined functions and works by coupling the DETCHEM routine with the commercial CFD code FLUENT. Furthermore the routines of the DETCHEM library are used to calculate source terms for the governing equations of mass, species and energy by the DC4FLUENT plugin.

As regards solid volume description, DETCHEM^{TM} provides two different models: (i) a simple model, which is based on the concept of effectiveness factors, and (ii) a detailed approach, which is based on solving reaction-diffusion equations within the solid volume. The former is a very fast model, but it introduces a strong simplification; the latter is a time consuming model because it solves the reaction-diffusion equations for every species within the solid volume.

The studies that have been developed by using this software package are presented in the following.

In (Deutschmann, Correa et al. 2003) the start-up of the catalytic partial oxidation (CPO) of methane over rhodium/alumina in a short contact times reactor was investigated. The study was conducted by employing the DETCHEM^{MONOLITH} code. The triangular shape of the single channel of the monolith was approximated with a cylindrical structure. Five representative channels were simulated in order to describe the behavior of the monolith. The kinetic scheme adopted comprehends both gas-phase and surface reaction mechanism.

A study on the abatement of automotive exhaust gases on platinum catalysts was performed by (Koop and Deutschmann 2009), by using the DETCHEM^{CHANNEL} application. The two-dimensional flow-field has been described and a detailed reaction mechanism for the conversion of CO, CH_4, C_3H_6, H_2, O_2 and NO_x has been included. Based upon experiments with a platinum catalyst in an isothermal flat bed reactor, a detailed surface reaction mechanism has been developed. Numerical simulations of the thermodynamic equilibrium of nitrogen oxides and calculations of surface coverage on platinum have been performed.

Mladenov and co-workers (Mladenov 2010) performed a CFD study in order to understand the impact of the real wash-coat shape on the overall reaction rate. The computational tools used from the DETCHEM package are DETCHEM^{CHANNEL} and DC4FLUENT plugin. The aim of the work was to study mass transfer in single channels of a honeycomb-type automotive catalytic converter operated under direct oxidation conditions. Specifically, 1D, 2D and 3D simulations were performed on channels of different shapes, respectively circular cross section, square cross section and square cross section with rounded corners. Furthermore, the effect of diffusion in a porous wash-coat was investigated. The reaction mechanism comprehends 74 reactions among 11 gas-phase and 22 adsorbed surface species.

An example of multiphase CFD with reactionis performed in a study by Tischer et al. (Tischer et al., 2007), where a PDEX (Nowak et al. 1996) 1D transient Model of Gas Flow and Temperature Profile is compared with a Detchem^{TM} solver for the simulation of a three-way catalyst. Although DETCHEM is also capable of surface reaction mechanisms simulation, the same global-step reaction mechanism was used in order to make kinetics consistent. As regards the solid phase description, instead of including the diffusion limitations of the wash-coat through an efficiency factor for the reaction, DETCHEM^{TM} makes use of a wash-coat diffusion sub-model in order to describe the influence of the wash-coat thickness. Finally the DETCHEM^{TM} results were compared with experimental data.

Beside these works developed with the DETCHEM library, another interesting study has been realized by Vlachos and co-workers (Vlachos, Kaisare et al. 2008). They performed a study on catalytic combustion of propane on platinum in micro-reactors under laminar conditions. A comprehensive parametric analysis was made investigating the role of inlet velocity, equivalence ratio and reactor size. A two-dimensional model was used. The kinetic model adopted consisted of

a one-step reaction mechanism, obtained via a-posteriori model reduction of detailed microkinetic mechanism.

An interesting work, aiming at considering all the scales involved in catalytic reactors, has been made by (Goisis and Osio 2011) where a CFD solver has been built up in the OpenFOAM® (OpenFOAM® 2011) framework, an open source CFD code. Its characteristics are summarized below:

- it can handle detailed kinetic mechanisms without any constraint on the number of species and reactions involved. The microkinetic description is provided by the CatalyticSMOKE libraries (Goisis and Osio 2011). These adopt standard CHEMKIN (ReactionsDesign 2008) correlations and can handle both classical and UBI kinetic schemes (Maestri and Reuter 2011, Goisis and Osio 2011);

- good efficiency in handling multi-scale coupling thanks to the splitting operator method, which solves the main problem (PDEs system, stiff, non-linear and fully coupled) through the solution of two sub-problems: the chemical reaction (a coupled, non-linear and stiff system of ODEs) and the transport (a decoupled, quasi linear, non-stiff system of PDEs). In this way the problem can be efficiently solved (Strang 1968; Pope and Zhuyin 2008);

- solution of the Navier-Stokes equations with the Pressure Implicit Splitting Operator (PISO) (Issa 1986) method;

- no limitations in the shape of the geometric domain: any three-dimensional domain can be investigated. If the system has specific symmetry properties, it can be studied with a 2D simulation, saving a considerable amount of time (Goisis and Osio, 2011).

A missing feature in the mentioned work is the detailed description of the phenomena occurring inside the catalytic phase, leading to a multi-region approach to the problem. This is one of the main breakthroughs developed in this thesis. The implementation of this feature inside the OpenFOAM® framework is still debated within the Open Source community, where two different approaches have been proposed:

✓ **monolithic:** this approach involves a single coupled system of equations on a single matrix taking into account both the phases involved. When dealing with multiple regions with different properties, this approach can work just for loose inter-equation coupling (Clifford 2011). Furthermore, the management of the constitutive equations, the storage of field

variables and all post-processing operations would become harder with a single matrix approach;

- ✓ **partitioned:** this approach involves governing equations solved separately on each of the coupled regions, imposing appropriate boundary conditions on both ends. To make the coupling effective, the procedure must be iterated until convergence is reached (Craven and Campbell 2011). If this can be seen as a negative aspect in terms of computational time, the advantage of this approach is that it works on multiple meshes even for stiff inter-equation coupling.

The latter approach has been adopted in this work in order to avoid all the approximations usually introduced when modeling the catalytic pellets and, instead, to simulate the reaction environment (both solid and fluid) with equations describing the actual physics of the system.

Furthermore, it is important to consider that in general real systems present different diffusivities for different materials, and it is important to take into account for effective properties in the different solid phase domains considered accordingly.

Another phenomenon which can be crucial for a correct model of a real system is the heat conduction and heat transfer limitations in the solid phase. The correct modeling of heat exchange phenomena makes it possible to predict the temperature in any point of the solid domain and, as a consequence, to get a numerical estimation of the catalyst activity and to identify hotspots in the reactor design.

Of course, besides working in a reacting environment, the tool proposed can also be used to simulate simpler non-reacting multi-region systems, such as heat exchangers, or complex systems composed of reacting regions and non-reacting ones.

The methodologies followed in this work to accomplish these objectives are explained in the next paragraph.

1.4 Methodologies and main results

The tool developed in this work, named `catalyticFOAM-multiRegion`, was built up in the OpenFOAM® framework (OpenFOAM® 2011), an open source CFD code.

As extensively stated in the previous sections, the main aim of this solver is to model in detail both the solid and the fluid phases of catalytic reactors, through the resolution of the fundamentals equations describing the physics of the system in each phase. The tools available for the implementation are the OpenFOAM® libraries, able to handle variable fields in order to dynamically describe the system, and kinetic libraries, giving the solver the possibility to simulate complex kinetic schemes. An accurate description of the physical problem and the mathematical model developed to describe the system, together with an insight on the tools used for the development, are provided in ***Chapter 2***.

The available CFD tools that solve this class of heterogeneous reacting problems have large difficulties in handling multi-scale coupling efficiently. On one side, fully coupled methods are suitable only for problems of small dimensions. On the other side, segregated methods are inappropriate for the solution of stiff and non-linear problems. To overcome these difficulties a new approach based on the splitting operator method has been proposed (Goisis and Osio, 2011). This allows to split the problem in two sub-problems and to solve them decoupled. In Figure 1.2 a schematization of the splitting operator method is presented.

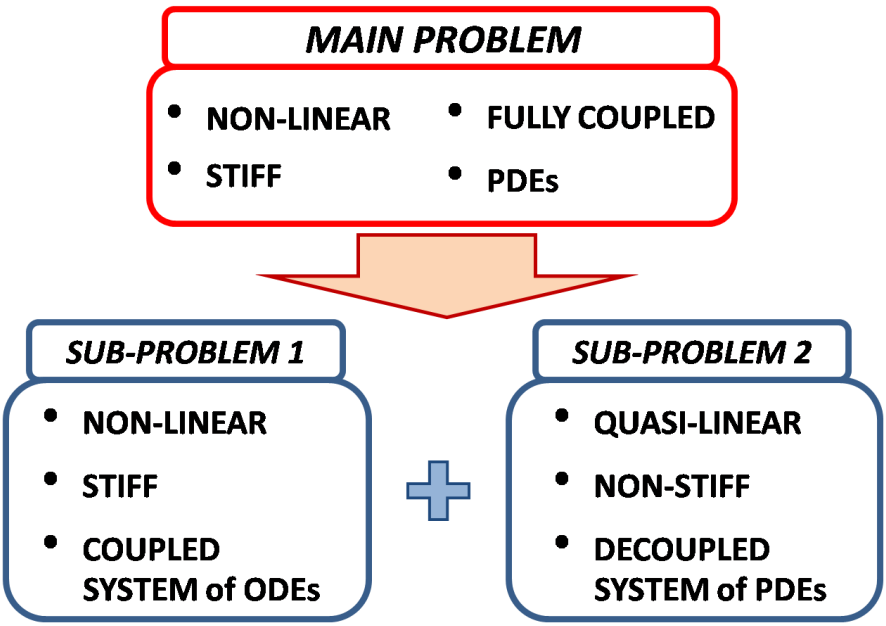

Fig. 1.2 - Schematization of the splitting operator method.

This implies the following advantages:

- ✓ possibility to select the best numerical algorithm for each sub-problem;
- ✓ stiffness and non-linearity are enclosed only in one sub-problem;
- ✓ low stiffness and quasi-linearity permit to adopt a fully segregated approach in the transport step.

Consequently the problem can be efficiently solved (Strang 1968; Pope and Zhuyin 2008).

The application of a splitting operator scheme to our problem has been achieved by separating the portions of the governing equations containing chemical reaction terms from those containing the transport terms. The latter are solved in sequence, each one decoupled from the others, as prescribed by the segregated approach. Instead of having a huge system of PDEs, one has to solve each equation of the system decoupled. A special attention has to be paid to the Navier-Stokes equations. Indeed, the strong coupling with the continuity equation makes it necessary to treat the inter-equation coupling in an explicit manner. The procedure followed is the Pressure Implicit Splitting Operator (PISO) method (Issa 1986). PISO and their derivatives are the most popular methods for dealing with inter-equation coupling in the pressure-velocity system for transient solutions (Jasak 1996). In addition to that, to handle multiple regions and their interaction, a partitioned approach is adopted: governing equations are solved separately on each of the coupled regions, imposing appropriate boundary conditions (mixed boundary conditions) at the interface between two different phases. To make the coupling effective, the procedure must be iterated until convergence is reached (PIMPLE Loop). Further information about the numerical strategies adopted throughout the solver, as well as the final architecture of the solver for both the description of intra-phase phenomena and inter-phase phenomena occurring at coupled interfaces, can be found in ***Chapter 3***.

The application of these methodologies led to the development of the catalyticFOAM-multiRegion solver. The work was mainly focused on the implementation of the code. This was made by adding one feature at a time and validating it before proceeding. The main features of this tool are:

- ✓ the possibility to solve homogeneous reacting flows in the fluid zones and both homogeneous and heterogeneous reacting flows in the solid zones;

- ✓ the ability to perform simulations with an accurate description of the velocity field by the resolution of the Navier-Stokes equations in both laminar and turbulent conditions, with any arbitrary geometric domain;
- ✓ the possibility to solve heat conduction problems and to model adiabatic or isothermal systems;
- ✓ the possibility to describe the reaction mechanisms with detailed kinetic models;
- ✓ the capability to handle an arbitrary number of different regions and phases, each with its own properties and meshed separately;
- ✓ the attribution of distinct governing equations and properties on each region;
- ✓ the physical sound description of intra-solid heat and mass transfer phenomena, making possible to account for diffusive limitations inside the catalytic phase;
- ✓ the effective description of conjugate heat-mass transfer inter-phase phenomena through the implementation of new libraries managing coupling boundary conditions at the interface

All the features described above are tested in ***Chapter 4***, performing numerical tests on different parts of the solver architecture by approaching test cases of increasing complexity, in order to prove the validity and effectiveness of the segregated numerical approach proposed for both inter-phase coupling and intra-phase phenomena description in both the fluid and the solid phase. The solver solution has been compared to analytical or numerical, fully-coupled solutions when possible.

Finally, in order to investigate the reliability of the solver, a validation has been performed in ***Chapter 5***. The fuel-rich H_2 combustion over Rh catalyst in an annular reactor has been analyzed and the simulation results have been compared with experimental data. Specifically, data on oxygen conversion achieved in the reactor at different temperatures have been compared with isothermal simulations performed with the solver developed in this work. In particular, the attention has been focused on the temperature range where previous works (Maestri et al. 2008, Goisis and Osio 2011) over-estimated oxygen conversion and were not able to reproduce the experimental data properly, due to the lack of description of intra-phase phenomena inside the solid phase. Thanks to its capability to reproduce the physics of both inter-phase interaction and intra-phase phenomena inside the solid catalyst, the developed tool provides a satisfactory fit with

experimental data in these temperature ranges, describing accurately concentration profiles inside the solid phase and being thus able to represent both chemical controlled regime and mass-transfer controlled regime.

Chapter 2

Physical Problem and Computational Tools Available

In this chapter, we first describe the physical problem we aim to solve, which is the generic catalytic reacting system, and the mathematical model used to describe this system, after introducing the solid phase and its characterization. Secondly, we briefly describe the main tools that will be used in order to develop and build the solver: the OpenFOAM® framework, and the OpenSMOKE and catalyticSMOKE kinetic libraries.

2.1 Physical problem and mathematical model

The aim of the work herein presented is the detailed description of gas-solid catalytic reactors. In order to properly model this system, it is necessary to address different phenomena, such as heat and mass transfer occurring both in the gas and solid phase (intra-phase phenomena) and between them (inter-phase phenomena), the velocity and pressure fields due to the fluid flow in the reactor, and the gas-phase and surface reactivity.

The most important phenomena taking place in a catalytic reaction can be summarized as shown in Fig. 2.1:

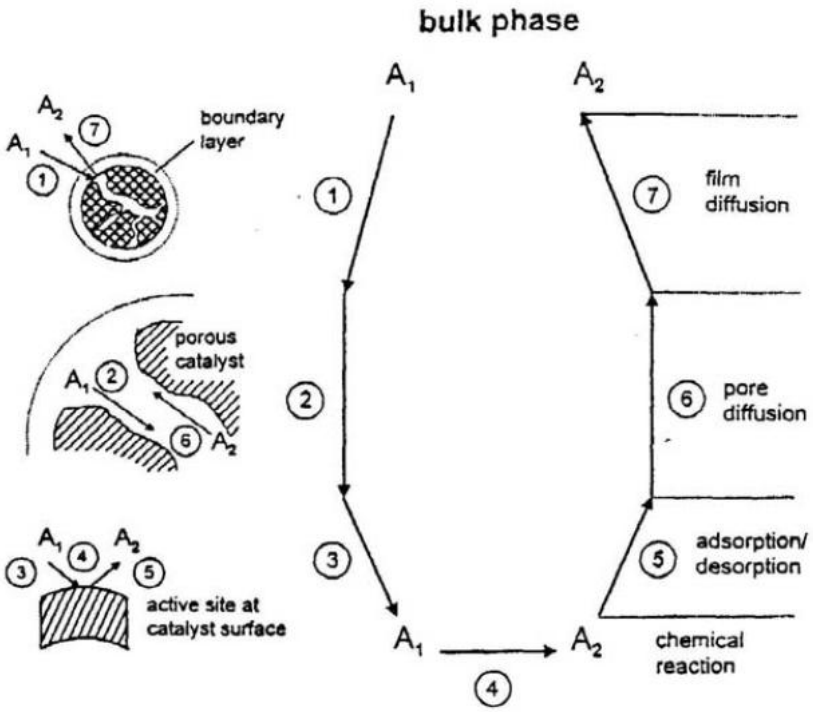

Fig. 2.1 – Individual steps of a simple, heterogeneous catalytic fluid-solid reaction A_1->A_2 carried out on a porous catalyst (Bird,Stewart, Lightfoot 2002)

1) film diffusion: the reactants diffuse from the bulk phase to the boundary layer surrounding the solid phase;
2) pore diffusion: the reactants diffuse from the boundary layer to the solid phase through the catalyst pores;
3) adsorption: the reactants physically or chemically adsorb on the solid surface. If the adsorption is chemical, a free active site is necessary for the adsorption to take place;
4) surface reaction: the adsorbed species react between each other or with gas-phase species;
5) desorption: the reaction products desorb from the catalytic surface;
6) pores back-diffusion: the reaction products diffuse from inside the catalyst to the boundary layer surrounding the solid;
7) film back-diffusion: the reaction products diffuse from the boundary layer to the bulk.

Moreover heat transfer phenomena are associated with this steps and need to be considered.

In a previous work (Goisis and Osio 2011) the attention was focused on the interplay between the Navier-Stokes equation and the surface reactivity based on a micro-kinetic description of the

surface reactivity. Nevertheless, intra-phase mass and energy phenomena inside the catalyst were neglected. The aim of this work is to describe in detail every single phase mentioned above, in order to fully account for diffusive limitations and phenomena occurring inside the catalytic solid itself.

Beside the wide variety of different reactors which can be found in reality, their description is not based on the external form of the apparatus nor on the reaction taking place in it, nor even on the nature of the medium-homogeneous or not. The phenomena occurring in a reactor may be broken down to reaction, transfer of mass, heat, and momentum. The modeling and design of reactors is therefore based on the equations describing the previously listed phenomena:

- the continuity equation
- the momentum equation
- the energy equation
- the species transport equation

The solution of these equations will provide a full characterization of the system in terms of its main variables for each phase considered:

- Velocity
- Pressure
- Density
- Temperature
- Gas species concentrations
- Adsorbed species concentrations

The form and complexity of the mathematical model dealing with these equations will be discussed in 2.1.2, while in 2.1.1 a deeper description of the solid phase is given.

2.1.1 The introduction of the solid phase

2.1.1.1 The need for fluid and solid cells

In a previous work (Goisis and Osio 2011) the catalyst morphology was not detailed, and the presence of that phase was taken into account by endowing the cells close to the catalytic layer itself with an additional heterogeneous reactive term and a boundary condition imposing continuity between the reactive flux and the diffusive flux to and from the catalytic surface. As discussed previously, this approach was not capable of taking into account diffusive limitations in the solid phase or in general intra-solid transport phenomena occurring there. In this work, a new approach has been developed, capable of taking into account both the phenomena occurring in the fluid and in the catalytic solid phases.

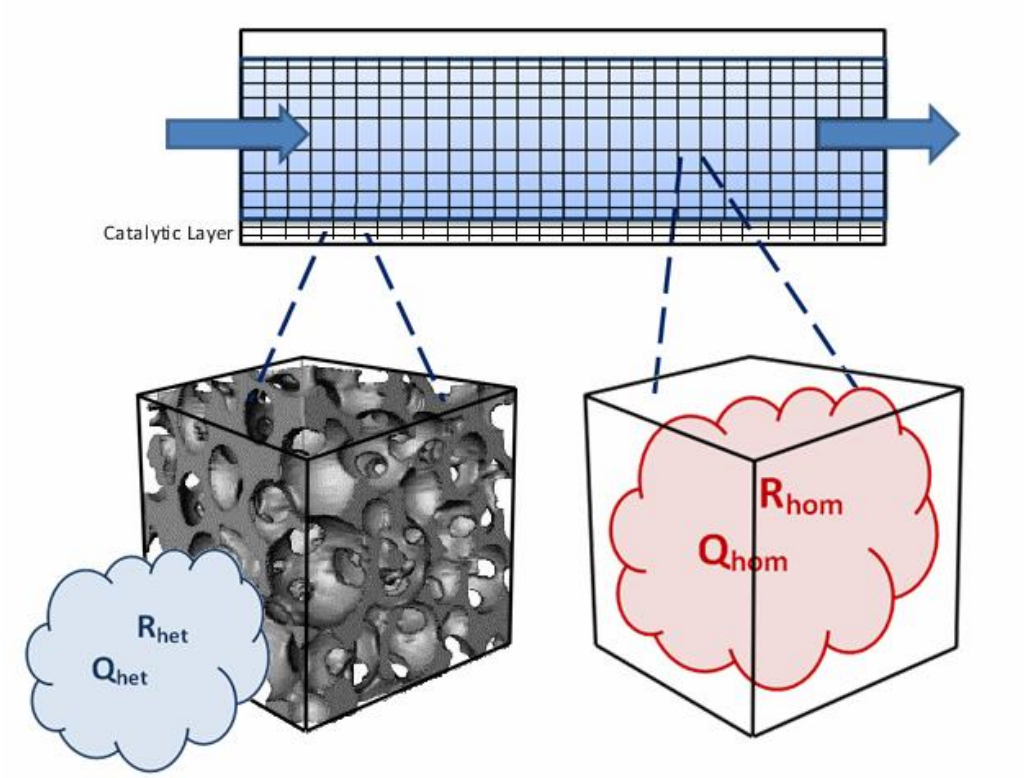

Fig. 2.2 - Fluid and solid cells schematization

Aim of this work is thus to provide a tool capable of describing both the inter-phase and the intra-phase phenomena occurring in both the fluid and solid phase of a catalytic reactor. In particular,

the latter has been considered as a porous pseudo-homogeneous phase, including both the solid catalytic surface and the fluid contained inside its pores, as shown in Figure 2.2.

Thus, two different types of cell zones have been accounted for in the solver: (i) the "homogeneous" cells, which contain only the gas phase reactions, and (ii) the "catalytic" cells, which involve the heterogeneous reactions. In the following only heterogeneous phenomena have been considered to take place in catalytic cells, as the low gaseous volumes present in the solid pores and the presence of the catalytic surface inhibit heavily homogeneous reactions occurring in the gas phase inside the catalyst pores.

2.1.1.2 Catalytic solid phase characterization

As regards the physical characterization of the catalytic cells, properties are considered to be uniform in every portion of the catalytic volume. The main parameters used to describe the catalyst morphology embedded into the model are:

- the void fraction ε, representing the volume of voids over the total volume of the cell, allowing the gaseous phase inside the pores to be taken into consideration;
- the effective catalytic surface per unit of volume a_{cat} , which can be often found in the literature as a characteristic parameter of a catalytic geometry.

When this parameter is not known, it is still possible to estimate it if other physical properties of the catalyst are available. For example, in the case of supported catalysts, it is possible to compute it as:

$$a_{cat} = \frac{W_{cat} \cdot \xi \cdot \delta}{\mathrm{MW_{Rh}} \cdot \Gamma_{\mathrm{sites}} \cdot \mathrm{V}} \tag{2.1}$$

where ξ is the fraction of the active phase over the total catalyst mass [kg_{Active}/kg_{Cat}], δ is the fraction of active sites available over the total active sites [$mol_{AvailableAct}/mol_{TotAct}$], Γ_{sites} is the density of sites per unit area [$mol_{AvailableSites}/m^2$].

2.1.2 Mathematical Model

As mentioned at the beginning of this chapter, the most general equations to represent the physics of the system to be modeled are the equations of continuity, momentum, energy, and species (gaseous and adsorbed). In this paragraph it will be shown how these conditions have been implemented into a mathematical model, with the aim of describing the whole range of phenomena occurring in both the fluid and the solid catalyst.

2.1.2.1 Navier-Stokes Equations

For a correct description of the flow field it is necessary to solve the Navier-Stokes equations for the momentum transport under the hypothesis of Newtonian fluids:

$$\frac{\partial(\rho \boldsymbol{U})}{\partial t} + \nabla(\rho \boldsymbol{U}\boldsymbol{U}) = -\nabla p + \nabla(\mu \nabla \boldsymbol{U}) + \rho \boldsymbol{g} \qquad (2.2)$$

where μ is the dynamic viscosity, $\mathbf{g}$ is the gravity acceleration, $\boldsymbol{U}$ is the velocity vector, ρ is fluid mixture density and p is the pressure.

Being the density field interconnected with the velocity and pressure fields, it is necessary to add the continuity equation:

$$\frac{\partial \rho}{\partial t} + \nabla(\rho \boldsymbol{U}) = 0 \qquad (2.3)$$

For compressible fluids it is requested the knowledge of the pressure field, described by the equation of state. Since the technological interest is focused on processes where the flowing phase is gaseous, the ideal gas approximation is adopted:

$$\rho = \frac{pMW}{R\,T}$$

where MW is the molecular weight and R is the universal gas constant.

2.1.2.2 Species transport equation

As we want to consider multicomponent mixtures, we solve the transport equation of species under the hypothesis of Fickian diffusion, as follows:

$$\frac{\partial(\rho\omega_i)}{\partial t} + \nabla(\rho \boldsymbol{U}\omega_i) = \nabla(\rho D_i \nabla\omega_i) + \sum_j R_j \nu_{ij} MW_i \qquad (2.4)$$

where ω_i is the mass fraction of the *i*th component, MW_i is the molecular weight of the ith species, D_i represents the mass diffusivity of the *i*th species in the reacting mixture and υ_{ij} is the stoichiometric coefficient of the *i*th species in the *j*th reaction. R_j is the rate of the *j*th reaction.

2.1.2.3 Energy trasport equation

In order to describe the temperature field, the solution of the energy balance is required.

$$c_p \frac{\partial(\rho T)}{\partial t} + c_p \nabla(\rho \boldsymbol{U} T) = \nabla(\mathrm{k}\nabla\mathrm{T}) + \sum_j R_j \Delta H_j \qquad (2.5)$$

where *T* is the temperature, C_p is the specific heat of the gas mixture and ΔH_j is the heat of reaction of the *j*th reaction. The energy dissipation due to the viscosity of the fluid is neglected. Furthermore, the pressure term can be ignored (Bird 2002).

2.1.2.4 Transport equations in the solid phase

When considering the solid phase, the equations previously shown will have slight differences related mainly to the absence of flow through the solid phase. In the latter, in fact, a diffusion and reaction model will be considered:

- ✓ there is no need to solve the Navier-Stokes equation in the solid phase, in the hypothesis of absence of flow through the catalytic solid pores;
- ✓ in the heat and mass transfer equations, for the same reason, no convective term has been considered (respectively $\nabla(\rho \boldsymbol{U}\omega_i)$ and $c_p\nabla(\rho \boldsymbol{U} T)$ shown in the equations above). The resulting equations for species and energy transport in the solid phase are then:

$$\frac{\partial(\rho_{mix}\omega_i)}{\partial t} = \nabla\left(\rho_{mix} D_{eff,i} \nabla\omega_i\right) + \sum_j R_j \nu_{ij} MW_i \qquad (2.6)$$

$$C_{p,sol} \frac{\partial(\rho_{sol} T)}{\partial t} = \nabla\left(\mathrm{k}_{eff}\nabla\mathrm{T}\right) + \sum_j R_j \Delta H_j \qquad (2.7)$$

where ω_i is the mass fraction of the *i*th component, $D_{eff,i}$ and λ_{eff} represents the effective diffusivity of the *i*th species and effective conductivity, ρ_{sol} and ρ_{mix} are respectively the apparent density of the solid phase and density of the gas phase inside the catalyst pores, v_{ij} is the stoichiometric coefficient of the *i*th species in the *j*th reaction. R_j is the rate of the *j*th reaction and includes both homogeneous and heterogeneous reactions.

2.1.2.5 Effective properties in the solid phase

The means to predict mass and heat transport of gases in porous solids in present days are inaccurate as a consequence of the inherent difficulties encountered in properly relating the local transport coefficients to the highly complex pore space. Due to the complexity of the catalysts morphology, the solid phase has been characterized with effective properties uniform in the whole catalytic volume, as already widely done in literature. The effective diffusivity inside the solid phase has been espressed as a function of the diffusivity computed in the gaseous bulk phase through a reduction factor, making it possible to take into account for transport limitations in the catalytic phase and incomplete use of the catalyst volume:

$$k_{diffusivity} = \frac{D_{solid}}{D_{bulk}} \tag{2.8}$$

When this parameter is not known from experimental measurements, such as mercury penetration methods (Kim,Ochoa et al. 1987), it is still possible to obtain it from catalyst porosity values with predictive models based on experimental measures (Mezedur, Kaviany et al. 2002) or on random porous solid 3-D models capable of taking into account micro-morphology features such as pore sizes, pore orientations, interconnections, dead ends, etc. (Mu,Liu et al. 2007).

Here below an example of the expressions which can be found in the literature is reported (Mu,Liu et al. 2007) :

$\frac{D_{eff}}{D_{bulk}} = \frac{2\varepsilon}{3-\varepsilon}$
$\frac{D_{eff}}{D_{bulk}} = \varepsilon^{1.5}$
$\frac{D_{eff}}{D_{bulk}} = \frac{2\varepsilon}{1-0.5ln\varepsilon}$
$\frac{D_{eff}}{D_{bulk}} = 1-(1-\varepsilon)^{0.46}$

Table 3.1 - Expressions for the effective diffusivity

Another effective property of the solid phase which has been considered in the mathematical model is the effective conductivityλ_{eff}, which needs to be evaluated through predictive models or experimental measurements.

2.1.2.6 Reactive term in different phases

In order to model properly the multiphase system, it is necessary to mathematically describe all the phenomena taking place both in the solid and in the fluid phase. All the species can:

- ✓ lead to homogeneous reactions in the fluid phase;
- ✓ diffuse from the fluid to the solid phase and vice-versa.

Once inside the solid phase, reactants can

- ✓ adsorb on the catalytic surface and lead to heterogeneous reactions;
- ✓ react in the fluid phase inside the solid pores.

As previously stated, homogeneous reactions taking place inside the catalyst pores will be reasonably neglected. Naturally, the reaction creates a concentration gradient which makes new reactants move from the fluid to the solid phase until a steady state is reached, and all the reactions will be accompanied by heat generation.

Now that the solid phase has been characterized, it is possible to write again the mathematical model described in the previous paragraph, detailing the reactive terms which have not been

detailed yet. These equations express species and heat transport and generation due to the reaction, and their derivations are provided in Appendix A.

- ✓ In the homogeneous phase:

$$\begin{cases} \dfrac{\partial(\rho\omega_i)}{\partial t} + \nabla(\rho \boldsymbol{U}\omega_i) = \nabla(\rho D_i \nabla\omega_i) + \sum_j R_{hom,j}\nu_{ij}MW_i \\ c_p \dfrac{\partial(\rho T)}{\partial t} + c_p\nabla(\rho \boldsymbol{U}T) = \nabla\big(\mathrm{k}\nabla(\mathrm{T})\big) + \sum_j R_j \Delta H_j \end{cases} \tag{2.9}$$

- ✓ In the heterogeneous phase cells, on the other hand:

$$\begin{cases} \dfrac{\partial(\rho^{mix}\omega_i)}{\partial t} = \nabla\big(\rho^{mix} D_{eff,i}\nabla\omega_i\big) + (\sum_j R_{het,j}\nu_{ij}MW_i)\cdot a_{cat} \\ c_{p,sol} \dfrac{\partial(\rho_{sol}T)}{\partial t} = \nabla\big(\mathrm{k}_{eff}\nabla\mathrm{T}\big) + \sum_j R_{het,j}\Delta H_j \cdot a_{cat} \end{cases} \tag{2.10}$$

where $R_{hom,i}$ is the homogeneous reaction rate for the i-th specie $in\ [\frac{kmol_i}{m^3_{reatt}s}]$ and $R_{het,i}$ is the heterogeneous surface reaction rate $\mathrm{in}\ [\frac{kmol_i}{m^2_{CAT}s}]$, which needs to be multiplied by the specific catalytic area $a_{cat}\ [\frac{m^2_{CAT}}{m^3_{REATT}}]$. As regards the properties of the solid, $D_{eff,i}$and λ_{eff} are the effective properties of the catalytic pseudo-phase, as described in the previous paragraph.

Furthermore, site conservation balances have to be written as follows:

$$\Gamma_{site}\frac{\partial\vartheta_i}{\partial t} = R_{i,surf} \tag{2.11}$$

where ϑ_i is the site fraction of the *i*th species and Γ_{site} is the sites density and $R_{i,sur}$ is the production rate of the ith surface species.

After presenting the mathematical model adopted, it is necessary to address the numerical issues related to its solution and to develop a solver which can handle the computational structure defined. This has been done in Chapter 3.

The model shown above results in a system of Partial Differential Equations (PDEs), which requires a computational tool in order to be solved. For its increasing popularity in the CFD community and its versatility, the OpenFOAM® framework has been chosen for this scope, and it will be briefly described in the next paragraph, together with the libraries adopted for the computation.

2.2 Tools available

2.2.1 OpenFOAM framework

2.2.1.1 General overview

The aim of this section is to introduce the main features of OpenFOAM® as support code for CFD simulations and its practical use.

OpenFOAM® is a C++ library created in 1993 and it is an object-oriented numerical simulation toolkit for continuum mechanics. Its popularity is increasing in the last years because OpenFOAM is released under General Public License (GPL), including the possibility to have at disposal the whole code and eventually modify it as needed. It is capable to support all the typical features of C++ programming, e.g. creation of new types of data specific for the problem to be solved, construction of data and operations into hierarchical classes, handling of a natural syntax for user defined classes (i.e. operator overloading) and it easily permits the code re-use for equivalent operations on different types (Mangani 2008).

OpenFOAM® is not meant to be a ready-to-use software, even if it can be used as a standard simulation package. Rather, it offers a support in building user specific codes.

Like the widest part of CFD software, OpenFOAM® provides tools not only for the finite volumes calculations, but also for pre and post processing. A schematic of the library structure is given in Figure 2.3.

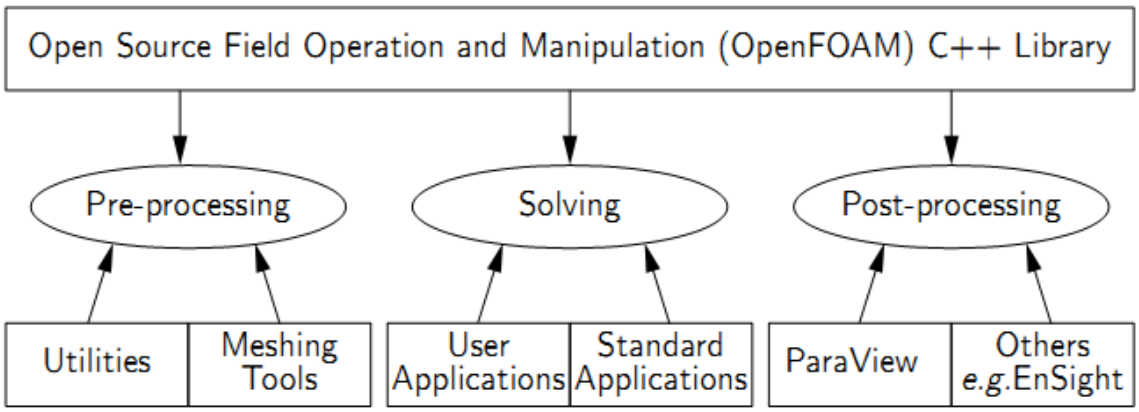

Fig. 2.3 - OpenFOAM® library structure (OpenFOAM user guide, 2011).

Pre-processing tools enable the set-up of the simulations by the generation of the computational

mesh, only with the corresponding initial and boundary conditions. Post-processing utilities allow one to view and analyze simulations results. The computational part is based on solvers, applications designed to solve specific classes of engineering problems, e.g. aerospace, mechanics, chemistry.

The latest OpenFOAM® version (2.1.1) includes over 80 solver applications and over 170 utility applications that perform pre- and post-processing tasks, e.g. meshing, data visualization, etc.
In the following we present the structure and organization of an OpenFOAM® case. In general the sequence of work in OpenFOAM® can be divided into three consecutive steps:

- *pre-processing*: firstly it is necessary to set-up the problem;
- *processing*: the simulation is performed by a solver;
- *post-processing*: results are displayed with specific application for data analysis and manipulation.

Pre-processing

The basic directory structure for the set-up of an OpenFOAM®case is represented in Figure2.4.

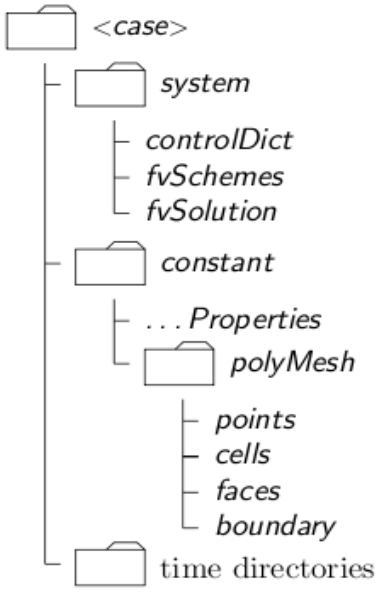

Fig. 2.4 - Directory structure for the set-up of an OpenFOAM® case.

The case folder includes:

- The `polyMesh` folder providing a full description of the case mesh.

- The `constant` directory containing information about physical properties.
- The `time` directories containing individual data files for each field (e.g. temperature, pressure, compositions) at different times of simulation.
- The `system` directory for setting numerical parameters associated with the solution procedure.

It is necessary to pay great attention to the creation of the computational mesh in order to ensure a valid and accurate solution.

OpenFOAM® provides a mesh generation utility called `blockMesh` that creates parametric meshes with specified grading and arbitrary curved edges. The mesh is generated from a dictionary file named `blockMeshDict` located in the `constant/polyMesh` directory. The utility reads this dictionary, generates the mesh and creates the mesh data.

In order to easily generate elaborate meshes it is possible to use a variety of software, such as *GAMBIT* (Fluent 2004), a mesh generation software owned by Ansys FLUENT®, which writes mesh data to a single file. OpenFOAM® provides a tool for the conversion of GAMBIT meshes to the OpenFOAM® format.

Initial and boundary conditions for a certain number of fields are required in order to start the simulation. These data are stored in the `0` folder: each file contains for every variable the initial conditions for the internal field and the declaration of each boundary condition. The latter has to be chosen from a list of pre-built standard conditions (OpenFOAM® 2012).

The `system` directory contains at least the following three files: `controlDict`, `fvSchemes` and `fvSolution`. In the first one run control parameters are set, including start/end time, time step and other specifications. The `fvSchemes` file contains the discretization schemes used in the solution. Typically one has to assign the discretization methods for gradient, divergence etc. In the `fvSolution` file algorithms for the solution of each equation are selected and tolerances for each variables are set.

Processing and post-processing

During the calculations the solver iterates the numerical procedure and periodically writes results at intermediate times. It is possible to choose how often taking note of the results (setting the `writeInterval = timeIntervalBetweenSuccessiveRecords` in the `controlDictionary` file) and/or how many time folders to write (setting the `purgeWrite`≠0

in the `controlDictionary` file). It is also possible to choose between two different format of writing files:

- `writeFormat` = BIN: faster writing operation, output files unreadable with text editor tool, but observable through sampling and plotting or classical post processing;

- `writeFormat` = ASCII: slower writing operation, output files readable with text editor tool as well as observable with more classical methods.

There are some tricks to make the simulations faster. For example it is possible to run a simplified and lightened form of the solver (`simpleFoam`) just to get the stationary field for velocities and take it as starting point: in this way the field variables involved in the Navier-Stokes equations are closer to their stationary value.

OpenFOAM® is supplied with the post-processing utility ParaView (Ahrens, Geveci et al. 2005), an open source multi-platform data analysis and visualization application which provides a lot of useful tools for these scopes.

2.2.1.2 The math behind OpenFOAM®

The widest part of complex engineering systems is described by one or more Partial Differential Equations (PDEs). Since the majority of these equations does not have an analytical solution, it is necessary to solve them with numerical methods (Quarteroni and Valli 1999).

In this paragraph the fundamentals of numerical procedures of discretization and solution are presented.

Discretization algorithm

The purpose of any discretization practice is to transform one or more PDEs into the resulting system of algebraic equations to allow the numerical solution. The discretization process consists of splitting of the computational domain into a finite number of discrete regions, called control volumes or cells. For transient simulations, it is also required to divide the time domain into a finite number of time-steps. Finally, it is necessary to re-write equations in a suitable discretized form.

The approach of discretization adopted by OpenFOAM® is the Finite Volume Method (FVM) (Versteeg and Malalalsekera 1995). The main features of this method are listed below:

- the governing equations are discretized in the integral form;
- equations are solved in a fixed Cartesian coordinate system on the computational mesh. Solution can be evaluated both for steady-state and transient behaviors;
- the control volumes can have a generic polyhedral shape: together they form an un-structured mesh (Patankar and Spalding 1972; Van Doormaal and Raithby 1985).

In the following we provide a short description of discretization of domain, time and equations.

Domain discretization

The discretization via FVM entails the subdivision of the domain in control volumes or cells. These have to completely fill the domain without overlapping. The point in which variables are calculated is located in the centroid of the control volume of each cell, defined as:

$$\int_{V_P} (\boldsymbol{x} - \boldsymbol{x_P}) dV = \mathbf{0} \qquad (2.12)$$

where $\boldsymbol{x_P}$ stands for the coordinate of the centroid, as shown in Figure 2.3.

The domain faces can thus be divided in two classes: internal faces, between two control volumes, and boundary faces, which coincide with the boundaries of the domain. A simple example of domain discretization is showed in Figure 2.5.

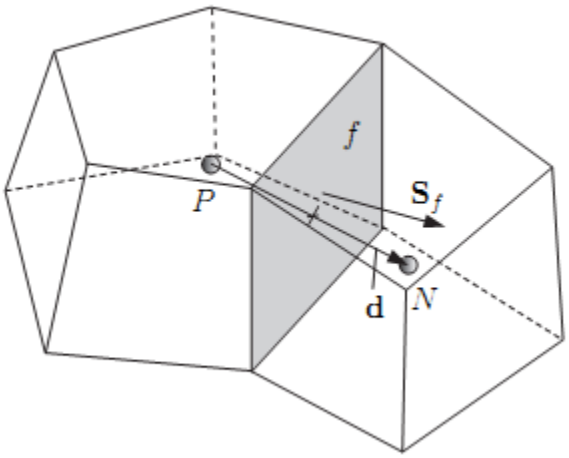

Fig. 2.5 - Example of finite volume discretization (OpenFOAM® User guide, 2011).

In Figure 2.3 the point *P* and *N* represents the centroid of the cells of the geometric domain. The vector **d** represents the distance between the two centroids. The vector $\mathbf{S_f}$ is the surface vector outgoing from the generic flat face *f*.

Equations discretization

Let us consider the standard form of the transport equation of a generic scalar field ϕ:

$$\frac{\partial(\rho\phi)}{\partial t} + \nabla(\rho \boldsymbol{U}\phi) - \nabla(\Gamma\nabla\phi) = 0 \tag{2.13}$$

where $\boldsymbol{U}$ is the velocity vector and Γ is the generic diffusion coefficient (e.g. thermal conductivity). For the sake of clarity the source term has been neglected. Further details on the discretization of the source term can be found in section 2.3.3.

The finite volume method requires that Eq. (2.14) is satisfied over the control volume V_P in the integral form:

$$\int_t^{t+\Delta t} \left[\frac{\partial}{\partial t}\int_{V_P} \rho\phi dV + \int_{V_P} \nabla\cdot(\rho\boldsymbol{U}\phi)dV - \int_{V_P} \nabla\cdot(\rho\Gamma\nabla\phi)dV\right] dt = 0 \tag{2.14}$$

The discretization of each term of Eq. (2.15) is achieved by applying the Gauss theorem in its general form:

$$\int_V \nabla\phi dV = \oint_{\partial V} \phi dS \tag{2.15}$$

Having in mind that each cell with volume V is bounded by a list of flat faces, it is possible to re-write the integral of Eq. (2.16) as a sum over all faces. The combination of Eq. (2.15) and (2.16) leads to:

$$(\nabla\phi)V_P = \sum_f S_f\phi_f \tag{2.16}$$

where V_P is the volume of the cell, S_f is the surface of the cell and ϕ_f is the flux of the generic scalar ϕ through the face *f*.

Time discretization

In transient problems it is fundamental to adopt numerical methods to handle temporal integration. Let us consider the first term of Eq. (2.15):

$$\int_t^{t+\Delta t} \left[\frac{\partial}{\partial t}\int_V \rho\phi dV + \int_V \Psi(\phi)dV\right] dt \tag{2.17}$$

where $\Psi(\phi)$ is a generic non-linear function.

The time integration can be evaluated in three different ways in OpenFOAM®:

- **Euler implicit:** the time term is discretized in an implicit way (Buzzi-Ferraris 1998), thereby taking current values ϕ^n:

$$\int_t^{t+\Delta t} \Psi(\phi) dt \cong \Psi_D(\phi^n)\Delta t \tag{2.18}$$

where $\Psi_D(\phi^n)$ is the discretized form of the spatial quantity $\Psi(\phi)$ and *n* indicates the new computed value. This method provides first order accuracy, guarantees boundedness and is always stable (Jasak 1996).

- **Explicit:** the spatial term is discretized in explicit way, which means that old values of ϕ are used:

$$\int_t^{t+\Delta t} \Psi_D(\phi^n)\, dt \cong \Psi_D(\phi^o)\Delta t \tag{2.19}$$

where ϕ^o are the old values of ϕ. This method is first order accurate and the solution depends only on previous times. The main disadvantage is that this method becomes unstable when too big time steps are adopted for the integration.

- **Crank-Nicholson:** a trapezoid rule is used to discretize the temporal integral:

$$\int_t^{t+\Delta t} \Psi_D(\phi)\, dt \cong \Psi_D\left(\frac{\phi^n + \phi^o}{2}\right)\Delta t \tag{2.20}$$

This method is second order accurate and stable, but does not guarantee boundedness of the solution (Ferziger and Peric 1999).

In this work the Euler implicit method has been always adopted.

Boundary conditions

In order to complete the formulation of the discretized problem one has to set boundary conditions. First of all, it is important to separate physical and numerical conditions:

- **Physical conditions:** these conditions are derived from engineering interpretation of the true system behavior. These conditions are set during the creation of a mesh. Each physical condition is the union of several numerical conditions. Here we provide some significant examples:

- ✓ Inlet: the velocity profile at inlet is assigned and, for consistency, pressure gradient is set to zero.
- ✓ Outlet: the pressure profile is assigned and velocity gradient is set to zero.
- ✓ Symmetry plane: in 2D cases it is necessary to specify the symmetry plane of the system. The related boundary condition implies that the components of the gradient normal to the surface are set to zero.

- **Numerical conditions:** these conditions provide a suitable expression for the value of variables at boundaries. Their values are specified with the initial conditions. Specifically, the most important conditions are Dirichlet (or fixed value) and Neumann (or fixed gradient).

Algebraic linear systems

OpenFOAM® implements different algorithms for the solution of linear algebraic systems of equations. Algorithms are selected by specifying the following features:

- *Preconditioner*: allow one to choose a method for the preconditioning of the system. More details on this methods are given in (OpenFOAM® 2012). This improves the conditioning of the problem and save computational time.

- *Linear solver*: specifies which solver has to be used. Here we cite Krylov subspace solvers and GAMG (OpenFOAM® 2012), which evaluate the solution on a coarse grid and then refine it on a finer mesh.

- *Smoothers*: improve computational speed reducing the number of iterations required to reach the convergence.

2.2.2 The kinetic library

In this section a detailed description of the kinetic library is provided. A general introduction is reported in 2.2.2.1. The gas-phase kinetic is handled by the `OpenSMOKE` library, described in 2.2.2.2, while the heterogeneous kinetic mechanism is implemented in the `CatalyticSMOKE` library, illustrated in 2.2.2.3.

2.2.2.1 General overview

In the chemical industry the need to control reactions at the molecular level quickly increased within the requirement of more energy efficient and selective processes. In order to achieve this goal during most of the 20th century the approach consisted in proposing a rate equation and fitting it with experimental data to obtain the most suitable rate constants. Even though this method leads to powerful results, these models give satisfying results only in a narrow range of operating conditions (Dumesic, Huber et al. 2008).

In recent years kinetic models have been reinterpreted thanks to the possibility of modeling in detail the surface chemistry. Indeed, the aim of kinetic modeling is to provide valuable tools for the design of chemical reactors under a wide range of conditions and for the analysis and optimization of catalytic processes (Gokhale, Kandoi et al. 2004).

During the last years the attention has been focused on kinetic models that try to incorporate the basic surface chemistry involved in the catalytic reaction (Schlögl 2001). This new perspective leads to the development of a new rational design of the catalyst based on predictive capability of first-principles models, without any experimental input. Anyway this approach still presents many challenges to overtake, in order to have a full description and control of all chemical transformations.

In order to provide a predictive ability to the heterogeneous kinetics model, it has been useful to employ some specific libraries. In particular, the kinetic scheme handling relies on two libraries, one for the homogeneous and the other for the heterogeneous phase. These are presented in the following section.

2.2.2.2 The OpenSMOKE library

The gas-phase is entirely managed by the `OpenSMOKE` library. This has been written in C++ by the CRECKmodeling group at Politecnico di Milano and provides an efficient handling of thermodynamic, transport, and kinetic data.

In order to use the `OpenSMOKE` library two steps are required:

- ✓ the first one is the interpretation of the input files: in this phase the interpreter program reads information from files, checks if these are correct and consistent, elaborates data and puts them in binary files. The input files contain respectively thermodynamic, transport and

kinetic information and are written in the standard CHEMKIN® format (ReactionsDesign 2008).

- ✓ the second one is the computation of desired properties: binary files are read, data are saved in the Random Access Memory (RAM) to improve the speed of access and the requested properties are calculated by calling the required functions.

The structure of the `OpenSMOKE` library is described in Figure 2.6.

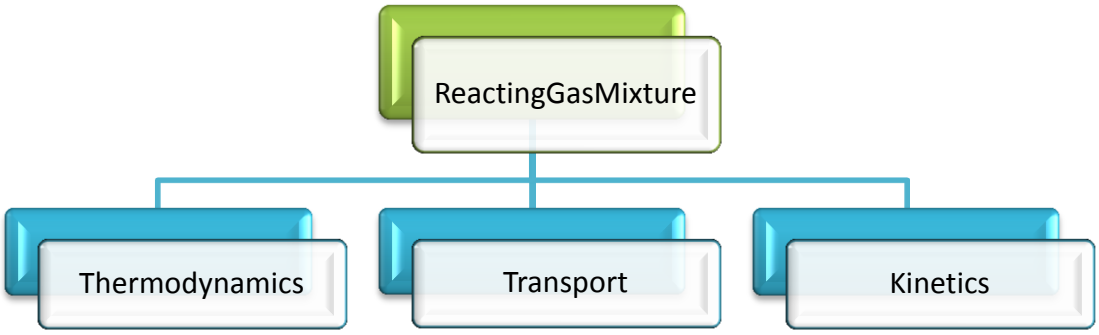

Fig. 2.6 - Schematization of the `OpenSMOKE` object-oriented library.

The main class is the `ReactingGasMixture` class, which contains species data, e.g. molecular weight and species names, and a number of useful functions, e.g. conversion from molar to massive fractions and computation of the mean molecular weight of the gas mixture. Furthermore, it includes references to:

- ✓ the `Thermodynamic` class, which contains functions for the computation of thermodynamic properties such as enthalpy, entropy and specific heats;
- ✓ the `Transport` class, which provides methods for the calculation of mass diffusivities, viscosity and thermal conductivities;
- ✓ the `Kinetics` class, which comprises all the necessary functions for the computation of reaction rates, formation rates and heats of reaction.

2.2.2.3 The CatalyticSMOKE library

For the handling of the heterogeneous kinetic scheme tool that has been chosen in this work is the CatalyticSMOKE library. The main purposes of this tool are:

- ✓ to provide an efficient handling of traditional kinetic schemes based on the SURFACE CHEMKIN® standard format;
- ✓ to give the possibility to implement non-standard kinetic schemes, such as mechanisms based on Unity Bond Index-Quadratic Exponential Potential (UBI-QEP) framework (Shustorovich and Sellers 1998).

The organization of this tool is based on the OpenSMOKE library structure. Thus, two applications are required: the first one to read and interpret input files, the second to compute the desired properties.

Input file

The input file has to be written in the SURFACE CHEMKIN® format (ReactionsDesign 2008). The main features of this format are:

- ✓ broad generality: the SURFACE CHEMKIN® standard is adopted by the widest part of the scientific community;
- ✓ flexibility: there is no limit to the number of materials, catalytic sites, adsorbed species and surface reactions in a single kinetic scheme;
- ✓ possibility to take into account standard, stick and coverage-dependent reactions;
- ✓ intuitive and easy-to-use interface.

One of the main tasks of this interpreter is that it is able to read and process data for UBI-QEP schemes. This feature has been coded as an extension of the standard CHEMKIN® format and it was one of the main purposes of a previous work (Goisis and Osio 2011).

It is thus possible to adopt both classic kinetic mechanisms and UBI ones, because semi-empirical methods provide an efficient approach for the detailed description of microkinetic behavior of reacting systems (Maestri, Vlachos et al. 2009; Maestri and Reuter 2011).

CatalyticSMOKE Library structure

The kinetic parameters stored in the binary file can be read by the `CatalyticSMOKE` library. The structure of this computational tool is described in Figure 2.7.

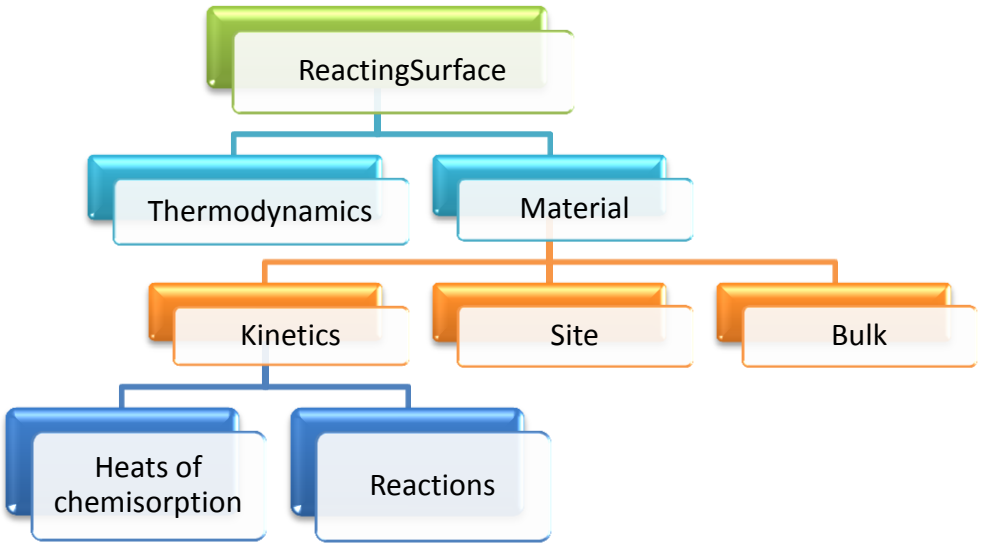

Fig. 2.7 - Schematization of the structure of the `CatalyticSMOKE` library.

The main class is `ReactingSurface` and contains references to `Thermodynamics` and `Material` classes. The former provides information on the thermodynamic properties, the latter contains the material properties and is linked to the classes `Site`, `Bulk` and `Kinetics`, which contains information about the kinetic scheme adopted and manages the calculations of heats of chemisorption. For this reason, it is linked to the `Reactions` class, which comprises all the reaction parameters and methods.

In order to exploit the potentiality of C++ language and in particular of object-oriented design, each component of the `CatalyticSMOKE` library is arranged as a class. Specifically, each class has its own methods and can be called by hierarchically superior classes. The function that computes the reaction rates is one of the most used of the `CatalyticSMOKE` library. It can be recalled from the main program by pointing to the main class. The function executes a loop over the materials considered in the kinetic scheme. Since the single material can be composed by one or more active elements, the computation of the reaction rates is accomplished for each kind of site. The information about the kinetic schemes is contained in the `Kinetic` class, while the properties of each site, e.g. site density, are grouped in the `Site` class. The reaction rate

evaluation in made by recalling each `Reaction` object, which contains all the necessary data, e.g. activation energy, pre-exponential factor, etc.

Chapter 3

From The Physical problem to the Development of a multi-region solver in the OpenFOAM® framework

In this chapter, we describe the development process of the solver, from the mathematical model to the coding of a computational and numerical structure for problem simulation. In the first part, the main numerical issues related to the solution of the previously described mathematical model in complex catalytic systems have been shown, leading to the choice for a segregated approach for the solving process. Secondly, the numerical structures adopted to overcome the intrinsic issues of a segregated approach have been presented, as well as the final architecture of the solver as regards the solution process in each phase. In a second part of the chapter, the attention has been focused on the implementation of the main features required to make the solver fully predictive of inter-phase phenomena as well, namely the capability to handle multiple meshes for multiple regions and the coupling procedure at the interface, both as a mathematical condition and from a numerical point of view. Several tests on the numerical architecture built has been then be performed in Chapter 4.

3.1 Numerical Challenges

The complexity of the system, physically and mathematically described in Chapter 2, leads to a series of numerical and computational challenges:

• Detailed kinetic schemes usually consist of hundreds of chemical species (molecular and radical species) and thousands of elementary direct and inverse reactions. Consequently, the direct coupling of a CFD code with detailed kinetic schemes is complex and disposes severe demands of computational resources.

For instance, it is quite simple to get an idea of the global dimensions of the numerical problem since they are proportional to the product between the number of computational cells (N_C), in which the system is discretized, and the number of chemical species (N_S), along with a few additional variables (e.g. temperature, pressure, and momentum). Consequently, it would be quite common to have some millions of variables describing the coupled CFD and kinetic problem (Manca, Buzzi-Ferraris et al. 2009).

• Additionally, in a catalytic process extremely different time and length scales are involved. Elementary steps of reaction concern atoms and molecules at a length scale of 0.1 nm. The characteristic time for a single chemical event varies in the order of femto-seconds for a single dissociation and picoseconds for diffusion over a distance of 10 nm. Chemical species continuously adsorb and desorb on the catalytic surface with a characteristic time of microseconds. Variables at the molecular scale are influenced by transport phenomena of mass, energy and momentum taking place at the reactor scale.

The coupling among these scales is crucial in determining the real behavior of the system (Maestri 2011). Consequently the resulting numerical problem can be very stiff. This means that, in order to solve the problem considering properly every phenomena at each scale, it would be necessary to adopt an integration step of magnitude smaller than the characteristic time of the fastest process.

• Moreover, in case of reacting systems, strong non-linearities are present in the equations. The diffusion and convection terms are slightly non-linear, and therefore they can be easily lagged or linearized without large losses of accuracy in the solution (Jasak 1996). Nevertheless the source term due to the reaction is highly non-linear: in fact the widest part of kinetic constants are expressed in the Arrhenius form and the reaction rate is proportional to concentrations at the

power of the respective reaction order. For this reason, in order to solve the problem it is necessary to adopt specific algorithms.

Nowadays, available CFD codes encounter a large amount of difficulties in the solution of these problems, especially in case of the use of detailed microkinetic description of the surface chemistry. For all the reasons presented above, it is compulsory to rely on numerical techniques that allow to overtake these difficulties and obtain a satisfying and accurate solution.

3.2 Need for a segregated approach and related issues

Since the fully coupled problem is too computationally demanding to be solved mainly due to the dimensions of complex chemical systems, it is necessary to adopt a segregated approach. This means that equations are solved once at a time with the inter-equation coupling eventually treated in the explicit manner. The application of this method to our problem is however affected by two main issues:

✓ The first problem is owed to the presence of the pressure explicit term in the Navier-Stokes equations. Indeed, in order to solve the momentum equations, it is necessary to know the pressure field. Since we solve them decoupled, an explicit inter-equation coupling is required. In section 3.3.1, the PISO procedure proposed by (Issa 1986) is described, which is consolidated and largely used in the CFD field. In transient calculations, all inter-equation couplings apart from the pressure-velocity system are lagged.

✓ The second problem is that the segregated approach can be adopted only in case of slightly non-linear and, most important, non stiff problems. On the other hand, chemical reactions and especially heterogeneous catalytic reactions lead to the introduction of a source term in the speciesand temperature equations, which is highly non-linear and makes the system of equations very stiff. In order to overtake these problems, a possible solution is to use a splitting method (Ren and Pope 2008). In section 3.3.2 an overview of the staggered time splitting scheme adopted is given by following the description reported in (Pope and Zhuyin 2008). In the next paragraphs, the chosen approach to overcome these numerical issues is shown.

3.2.1 Pressure-velocity Coupling

The pressure-velocity coupling is taken into account by the PISO loop, a transient splitting method for the solution of the Navier-Stokes equations. This algorithm is composed by three steps:

1. firstly, the Navier-Stokes equations are solved assuming a constant pressure field. Its value is assigned at the previous step. This stage is called momentum predictor and an approximated value of the velocity field is obtained;
2. using the predicted velocity value obtained it is possible to solve the continuity equation and consequently get the correct pressure field: this step is called pressure solution;
3. the velocity field is corrected in an explicit manner making it consistent with the new pressure field. This is the explicit correction stage.

The PISO loop is iterated until the tolerance for the pressure-velocity system is reached: at this point it is possible to obtain the pressure and velocity fields for the current time step.

The correction of velocity actually consists of two parts: an adjustment due to the change in the pressure gradient and another one due to the variation of the neighboring velocities. In the PISO algorithm, velocity is corrected explicitly: this means that the second correction is neglected and the whole error is assumed to be due to the error in the pressure term. This assumption is not true and makes it necessary to iterate the calculus procedure to achieve the correct solution. In other words, the PISO loop consists of an implicit momentum predictor followed by a series of pressure solutions and explicit velocity corrections (Jasak 1996).

The transient solution procedure we use for the solution of the entire problem can be summarized as follows:

1. Assembling and solving the momentum predictor equation.
2. Go through the PISO loop till the tolerance for pressure-velocity system is reached. At this stage, pressure and velocity fields for the current time-step are obtained.
3. Solve all the other equations in the system.

The procedure has to be iterated till the reaching of the final integration time.

3.2.2 The Operator-Splitting Technique

The numerical scheme consists of splitting the equations into sub-equations, and integrating each one separately and sequentially. Typically, each sub-equation describes only one part of the physics

of the problem. The results of the integration at each sub-step are combined to approximate the final solution with high accuracy (Strang 1968).

Let us consider the equations of transport:

$$\frac{\partial \boldsymbol{\varphi}}{\partial t} = \boldsymbol{M}(\boldsymbol{\varphi}, t) + \boldsymbol{S}(\boldsymbol{\varphi}) \tag{3.1}$$

where $\boldsymbol{\varphi}$ comprehend the entire set of species composition and the temperature. Therefore it is a vector of NS+1 variables written as $\boldsymbol{\varphi}$=[ω_1, ω_2,… ω_{NS}, T], where NS is the number of species. Furthermore $\boldsymbol{M}$ denotes the transport processes due to diffusion and convection, and $\boldsymbol{S}$ denotes the source term due to chemical reactions.

In our case the $\boldsymbol{S}$ term is stiff and highly non-linear in concentrations and temperature. The $\boldsymbol{M}$ term instead presents a low stiffness and a quasi-linear nature. In fact the non-linearity is dictated only by the presence of the secondary variables, e.g. density dependence on temperature.

Instead of solving the entire system, operator splitting methods provide the splitting of these equations in two systems of equations, the first taking into account only the reaction term and the second one considering only the transport term. The resulting system can be represented in this way:

$$\begin{cases} \dfrac{\partial \varphi_1}{\partial t} = S\big(\varphi_1, u(\varphi_1)\big) \\ \dfrac{\partial \varphi_2}{\partial t} = M(\varphi_2, u(\varphi_2), t) \end{cases} \qquad \frac{\partial \varphi}{\partial t} = M(\varphi, u(\varphi), t) + S(\varphi, u(\varphi)) \tag{3.2}$$

The Jacobian matrix of the whole system of PDEs that takes into account the reaction is block-unstructured and sparse (Figure 3.1). The Jacobian matrix has the dimension of $(N_C \times NU) \times (N_C \times NU)$, where N_C is the total number of computational cells and NU is the number of unknowns (NS+1, since we also have the T equation), given by the sum of species, three components of velocity, pressure and temperature. The Jacobian of each cell is dimensioned as $NU \times NU$.

By adopting the operator splitting scheme in the segregated approach the Jacobian matrix of convective and diffusive terms is transformed into a group of Jacobians with the same sparseness of the global matrix and dimensioned $N_C \times NU$.

The Jacobian matrix that describes the reactive step becomes a block diagonal matrix. Indeed the rate of production of each cell depends only on the conditions of the cell itself. This implies that the system of PDEs can be turned into a group of decoupled Ordinary Differential Equations (ODEs) system. The resulting numerical problem is constituted by a system of quasi-linear PDEs and a group of non-linear ODEs system.

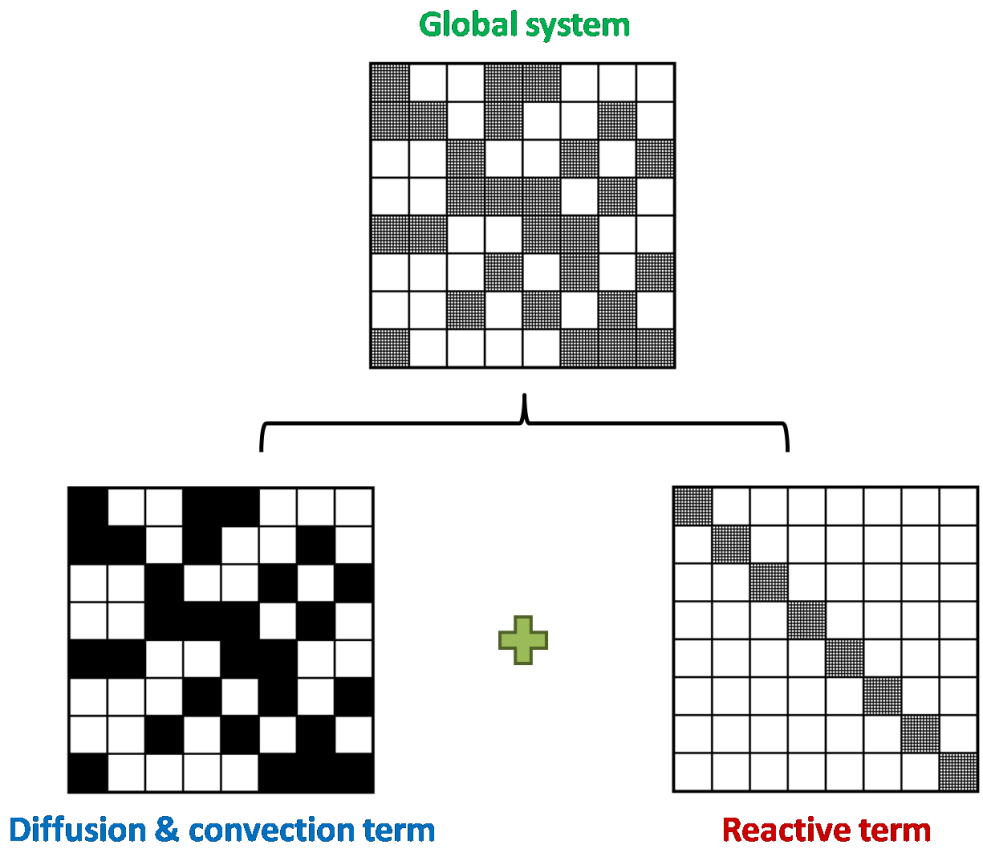

Fig. 3.1 - Jacobian matrix of the PDEs and ODEs systems.

Among this type of computational methods, two classes of splitting schemes can be distinguished: one is based on the Strang splitting scheme, and the other is based on staggered time steps.

- Strang Spliiting Scheme: For each time step dt, schemes based on Strang splitting require two reaction sub-steps of length $dt/2$ and one transport sub-step of length dt. The classical analysis (Sportisse 2000, Strang 1968) (which considers the limit $dt \rightarrow 0$) shows that the splitting error in the Strang splitting scheme is of order dt^2. If each of the three sub-steps in the above splitting

procedure is solved accurately (with at least second-order accuracy in time), the Strang splitting scheme is second-order accurate in time.

- Staggered Time Steps: Schemes based on staggered time steps require a single transport sub-step of length dt and a single reaction fractional step of length dt. As the computational cost scales with the number of reaction sub-steps that need to be performed, these methods result much more computationally feasible when dealing with complex chemical systems and will thus be chosen as the method of choice in this work.

This method computes the predictor value integrating the transport equations PDEs system on a time step Δt in order to obtain first-guess values of temperature and massive fractions.

Then the ODEs system is solved using the obtained values as initial conditions (corrector step): once again integration is performed over the same time step Δt. The systems solved are stiff, decoupled and dimensioned $NS + 1$.

When every sub-problem is solved using a second order accurate in time numerical method, the final solution is assured to be second order accurate in time as well as for the Strang Splitting scheme (Pope and Zhuyin 2008). In Figure 3.2 a schematization of the integration over time according to the staggered time splitting scheme is provided.

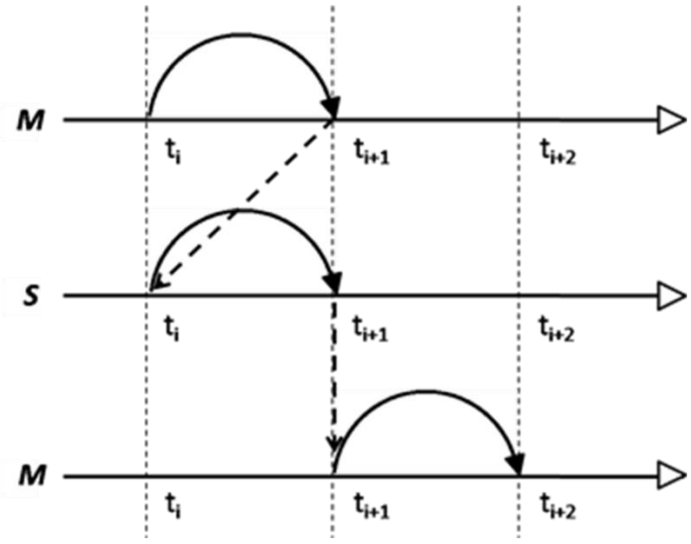

Fig. 3.2 - Schematization of staggered time splitting scheme.

The main advantage of using a splitting scheme is the possibility to adopt the best numerical algorithm for each sub-system. In Figure 3.3 a schematization of the described predictor-corrector method is given.

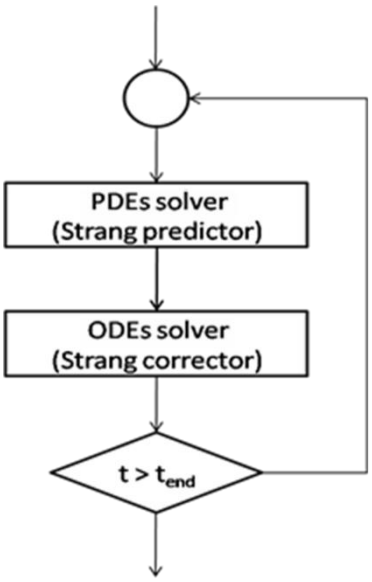

Fig. 3.3 - Diagram of the staggered time split predictor-corrector method.

The reacting sub-system requires a specific integrator for non-linear and stiff ODEs systems. In our case we use the `BzzOdeStiffObject` class (Buzzi-Ferraris 2011) based on the Gear's algorithms (Gear 1971). Nevertheless, in principle any available solver for stiff ODE systems can be adopted. The transport sub-system has a low stiffness and is quasi-linear: it is then possible to adopt a segregated approach.

3.3 Solver numerical structure

As extensively discussed in the previous chapter (2.1.1), we are going to consider two distinct types of cell, solid, and fluid, each of them characterized by a specific mathematical model. Moreover, the approaches adopted to overcome numerical issues have been discussed. In the following, it will be shown how the operator-splitting approach can be applied to the equations discussed in chapter 2 and in 3.1.3, as well as the resulting numerical structure for the solver developed.

3.3.1 Implementing the splitting operator technique

The predictor step consists of the solution of a PDEs system describing the heat and mass transport between the solid and fluid cells. The numerical problem associated is quasi-linear and has a low stiffness degree and by consequence a segregated approach can be adopted. Species and

temperature transport equations are solved decoupled in the following form (here below the equations for the fluid, see 2.1.2 for the equations for the solid):

$$\frac{d(\rho\omega_i)}{dt} + \nabla \cdot (\rho \boldsymbol{U} \omega_{\boldsymbol{i}}) - \nabla(\rho \mathcal{D}_{\mathrm{i}} \nabla \omega_{\mathrm{i}}) = 0 \tag{3.3}$$

$$c_p \frac{\partial(\rho T)}{\partial t} + c_p \nabla(\rho \boldsymbol{U} T) - \nabla(k \nabla \mathrm{T}) = 0 \tag{3.4}$$

After the predictor step, it is necessary to take into account the reactions, and this happens in the corrector step.

In the fluid cells, it consists of the resolution of the following system of equations (see Appendix A):

$$\begin{cases} \rho \dfrac{d\omega_i}{dt} = \displaystyle\sum_{j=1}^{NR} \tilde{R}_j^{hom} \nu_{ij} MW_i \\ \rho c_p \dfrac{dT}{dt} = Q^{hom} \end{cases} \tag{3.5}$$

where R_j^{hom} is the homogeneous reaction rate and Q^{hom} is the net heat of production of the gas phase species. The mass balance of the *i*th species is written for each component of the gas mixture.

As shown previously in 2.1.2.6, in the solid cells the expression of the corrector system has to take into account for additional terms. Indeed in these cells the reactants can adsorb on the catalytic surface, react through a number of elementary steps and desorb back in the gas phase inside the pores. Therefore, to describe the evolution of the catalytic cells it is necessary to:

✓ add the heterogeneous reaction term to gas phase balances. This takes into account the adsorption and desorption reactions at the catalytic surface;

✓ introduce a term to satisfy the total mass balance on the gas-phase. Since our solver has to be able to describe transient behavior, the mass balances of the gas phase has to include the sum of the production rates over each component due to chemisorption reactions.

✓ consider site conservation balances of the adsorbed species, according to e.g. (Maestri, Beretta et al. 2008). These include both surface and chemisorption reactions.

Mathematically the ODEs system becomes:

$$\begin{cases} \dfrac{d\omega_i}{dt} = \dfrac{R_{hom.i} MW_i}{\rho} + \dfrac{1}{\rho V_{CELL} \varepsilon}\left[a_{CAT} V_{CELL} \left(R_{het.i} MW_i - \omega_i \sum_{i=1}^{NC} R_{het.i} MW_i \right) \right] \\ \sum_{i=1}^{NC} m_i C_{p,i} \dfrac{dT}{dt} = -\left(\Delta \hat{H}_R^{hom} \tilde{R}^{hom} MW_{mix} V_{react} \varepsilon + \Delta \hat{H}_R^{het} \tilde{R}^{het} MW_{mix} V_{react} a_{cat} \right) \\ \Gamma_{sites} \dfrac{\partial \vartheta_i}{\partial t} = R_{i,sur} \end{cases} \tag{3.6}$$

where $R_{i,sur}$ is the production rate of the ith surface species and Γ_{site} denotes the catalyst site density, V_{cell} is the volume of the catalytic cell. The mass balance of the *i*th gas species is written for each component of the gaseous mixture, while the site conservation equation is written for each adsorbed species including the free catalytic sites for each catalytic face.

In order to account for the inner structure of the catalyst, the parameter a_{cat} has been introduced: it represents the catalytic surface available area per solid volume unit. As described in paragraph 2.1.1, this allows to model possible diffusive limitations and the consequent concentration profiles inside the solid volume. This was not possible with the previous version of the solver (Goisis and Osio 2011), which considered homogeneous concentrations within the solid volume and neglected the catalyst morphology.

In Figure 3.4 a physical interpretation of the numerical procedure is given. The predictor step represents the mass and energy exchange between single cells. The corrector step describes cells as an ensemble of perfectly mixed batch reactors.

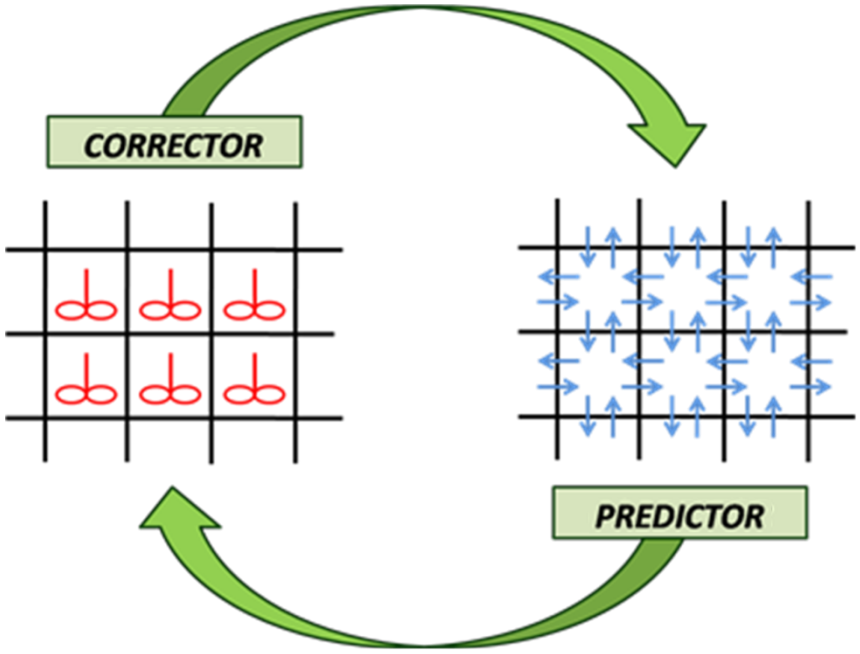

Fig. 3.4 - Physical interpretation of the predictor-corrector algorithm.

According to (Pope and Zhuyin 2008), even if this method requires the solution of the ODEs system for each cell of the computational mesh, the final solution obtained is second order accurate in time. Moreover it is much less computationally demanding than solving the entire PDEs system in a fully coupled approach.

The calculation of the formation rate of gaseous species is achieved by the OpenSMOKE library. For the computation of chemisorption reaction rate of both phases and the calculation of surface reaction rates the `CatalyticSMOKE` library has been used. The structure of both was described in chapter 2.

Now that both a mathematical model and a numerical framework to handle the computational cost have been developed, it is possible to describe the structure of the developed solver in each phase considered. How inter-phase phenomena will be taken into account will be the focus of the second part of the chapter.

3.3.2 `catalyticFOAM-multiRegion` structure for the solution of a single phase

The `catalyticFOAM-multiRegion` structure is organized in more levels, as shown in Figure 3.5.

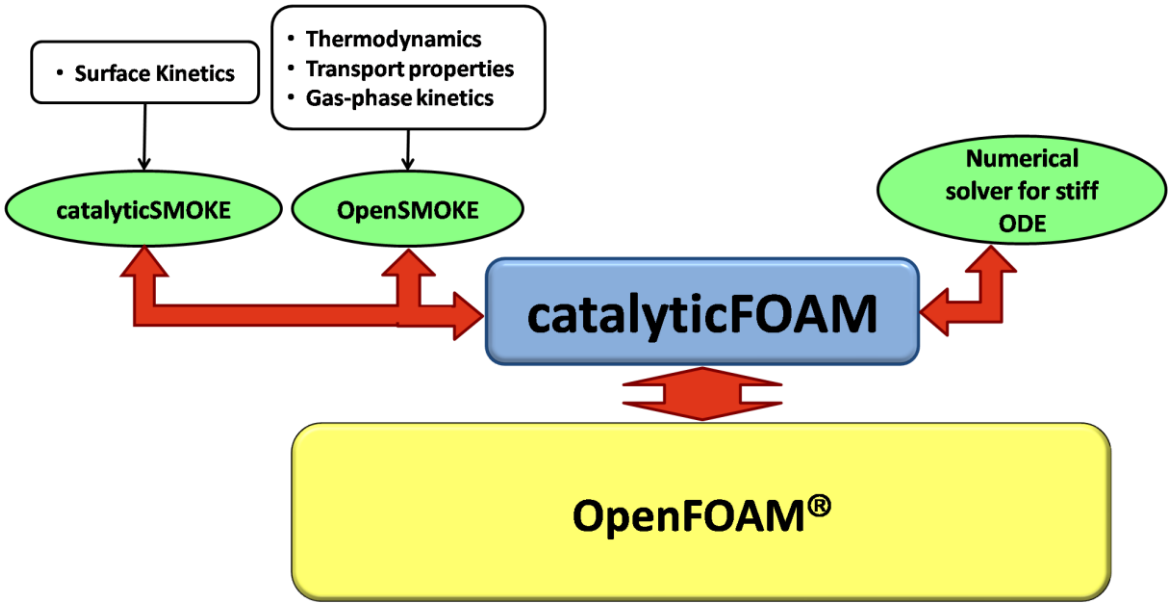

Fig. 3.5 - Schematization of the `catalyticFOAM` structure.

The whole program is based on the OpenFOAM® framework, which handles the discretization and solution procedures via Finite Volumes Methods and is described briefly in the previous chapter. The `catalyticFOAM-multiRegion` solver contains the entire set of equations and manages the solution procedure. At every iteration, the PDEs are transmitted to OpenFOAM®and solved. On the other hand, the ODEs system is solved for each cells by the BzzMath library (Buzzi Ferraris 2011, www.chem.polimi.it/homes/gbuzzi). The thermodynamic and transport properties of the gas phase are calculated by the OpenSMOKE library, using the CHEMKIN standard correlations (ReactionsDesign 2008). Furthermore, the computation of gas phase kinetic is achieved by the OpenSMOKE library. Instead, the surface kinetic is evaluated by the `catalyticSMOKE` library.

A detailed description of the solution loop achieved by `catalyticFOAM-multiRegion` is given in Figure 3.6. It involves the mathematical model shown in Chapter 2 and the numerical approach discussed in 3.1, and it distinguishes between the characteristic equations solved in the fluid and in the solid cells:

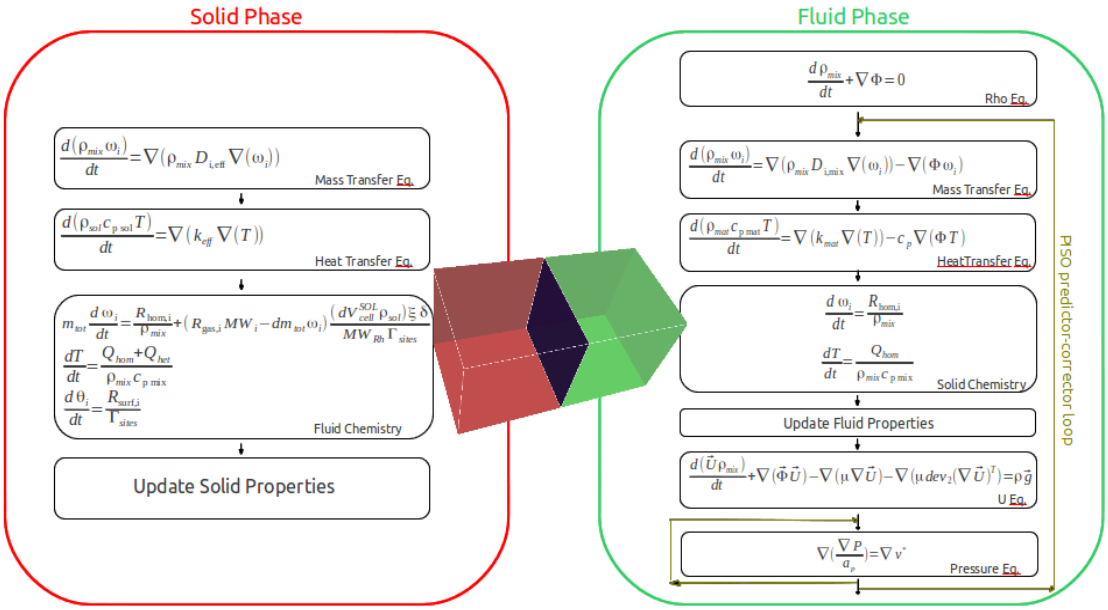

Fig. 3.6 -. Schematization of CatalyticFOAM-multiRegion solution procedure in the fluid and solid phase

Initially the geometric domain is discretized by the creation of the computational mesh and the procedure solution can start in each cell in which the computational domain has been discretized. Then temperature, pressure, velocity and species concentrations are initialized.

The iterative procedure starts with the implementation of the transport equations for each species, as regards both heat and mass transfer. Updated values of concentrations and temperature fields are thus computed. Then the ODEs systems are solved and the properties are updated. These steps characterize both the fluid and the solid phase, with the differences in the mathematical model shown in the previous chapter (2.1.2). Finally, in the case the computation is being performed for a fluid cell, the PISO loop starts: the Navier-Stokes and the continuity equations are solved and the velocity field is corrected explicitly. The whole procedure is iterated till the reaching of the end time.

3.3.3 Features to be implemented for inter-phase phenomena description

In the first part of this chapter the development process of the solver has been shown, from the mathematical model to the coding of a computational and numerical structure for the problem simulation. The main numerical issues related to the solution of the previously described mathematical model in complex catalytic systems have been addressed, leading to the choice for a segregated approach for the solving process. Then the numerical structures adopted to overcome the intrinsic issues of a segregated approach have been presented, as well as the final architecture of the solver as regards the solution process in each phase.

Aim of this work is to provide a tool capable of describing phenomena occurring in both phases, as well as intra-phase phenomena between them. To do this, it has been necessary to endow the solver with:

- the capability to handle multiple meshes and multiple regions, both for easier characterization of the different phases and numerical solution handling;
- coupling libraries describing the physics of the interface phenomena occurring between two phases and imposing proper conditions on both ends of interfaces between different phases during the computation.

The development of these features will be discussed in the second part of this chapter.

3.4 Introducing multiple regions structure

Before the development of this work, the only multiple-region partitioned solver available in the OpenFOAM® environment was the `chtMultiRegionFoam` solver, capable of handling only

heat transfer problems using OpenFOAM® internal libraries for coupling handling. On the other hand, neither libraries nor solvers for mass-transfer coupling existed in OpenFOAM®, as well as no convergence criteria was implemented for coupling at the interface. In this part of the chapter the main required features for the solver design listed above will be analyzed: firstly, multiple meshes structure will be described; secondly, the interface coupling will be discussed; finally, the numerical algorithm to reach coupling convergence will be presented.

3.4.1 The need for multiple regions

As anticipated in the previous section, the introduction of multiple regions and particularly modeling the solid phase as a separate phase with its own properties and variable fields leads to a sounder description of the physics of the problem discussed in Chapter 2, as it provides:

- ✓ capability to model heat and mass transfer limitations;
- ✓ capability to represent in the same system several regions with their own properties;
- ✓ accurate description of temperature and concentration distribution leading to more correct reaction rate computation.

The adopted strategy consists in the separation of the domain in distinct meshes (fig. 3.7), each of which representing a different region characterized as solid or fluid.

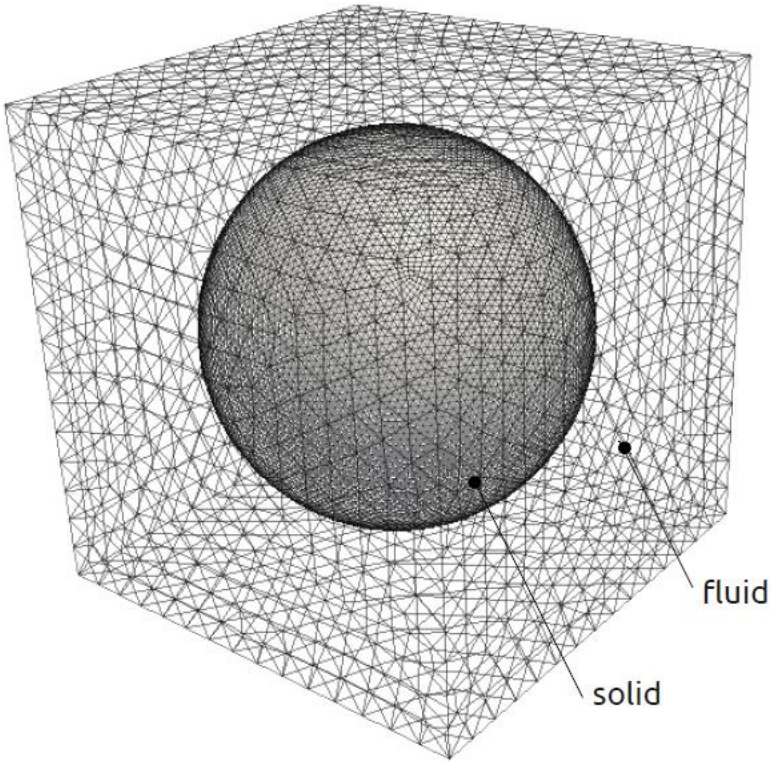

Fig. 3.7 – Mesh separation for multiphase representation

In this way, the new structureis capable of handling an arbitrary number of fluid and solid regions of arbitrary geometry in the same overall mesh (as shown in fig. 3.8). For solving purposes, the different regions are then structured in single separate meshes and it is thus possible to solve the mathematical model equations on each of them separately.

In addition to that, for solid phase characterization purposes, it will be necessary to associate each of the meshes corresponding to different regions with its own properties (such as density, diffusivity, thermal conductivity and catalyst activity) and fundamental equations, different from the ones used in the fluid phase, describing the phenomena taking place in it.

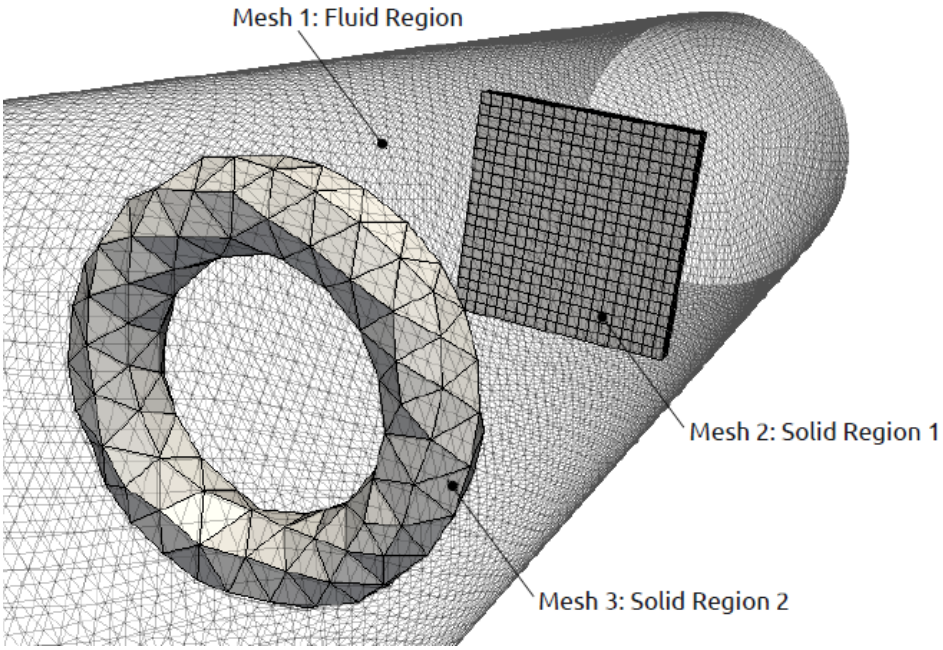

Fig. 3.8 – Example of mesh composed by three arbitrarily shaped regions

Among the main features and advantages of this multiple-regions/multiple-meshes approach, the most relevant are:

- ✓ multiple meshes are considered (one for each region), in which the solver can act separately;
- ✓ field variables stored separately on each mesh (each fluid and solid region);
- ✓ separate governing equations implemented on each region and solved on each cell of that region;
- ✓ full support for multi-region post-processing and data visualization, in the sense that it is possible to represent different fields in different regions contained in the same overall

domain.

In the following paragraphs, a practical overview of how this structure was implemented into the OpenFOAM® standard case structure is shown. Its ease of use and fast execution make it feasible and profitable for all those cases, where an accurate description of all the phases and regions involved is required.

3.4.2 A user-friendly mesh tool: Fluent® Gambit

In order to reproduce simple geometries, it is possible to use the meshing tool embedded in the OpenFOAM® framework, but the structure of input files makes it hard and time-consuming to use it for meshing non-elementary geometries.

In order to model complex geometries in an easy way, a complete, user-friendly mesh tool such as Gambit (Fluent, I. 2004) becomes necessary. Its usage within the OpenFOAM® framework is possible thanks to the `fluent3DMeshToFoam tool`, through which Gambit meshes information can be collected in a "`polyMesh`" dictionary readable from OpenFOAM® based solvers.

It is then easily possible to create mesh volumes of different geometries based on size, shape, and position. Furthermore, it is possible to deal with multiple volumes through useful tools for moving, splitting and merging volumes, providing the user a powerful and easy-to-use tool for the creation of complex geometries.

For volume meshing, beside the possibility of setting a precise number of intervals or intervals dimension for each edge/face/volume, it is also possible to provide a grading, single or double, at chosen degree, in order to make the mesh finer in portions of the domain where the simulation requires a higher degree of precision.

Finally, Gambit allows the naming and characterization of each patch and volume and transmits the information to the OpenFOAM® `polyMesh` dictionary after the mesh conversion has occurred. In this way patches and volumes are easily recognizable inside the fields characterization input files.

3.4.3 Splitting the regions in multiple meshes

The conversion of Gambit multi-region mesh to an OpenFOAM® dictionary involves the creation of several text files containing new information about the newly introduced multi-region pattern inside the `polyMesh` directory. Particularly, they contain the geometric characteristics of the so

called `zones`, which can now be identified as different entities, such as `cells`, `faces` and `points`.

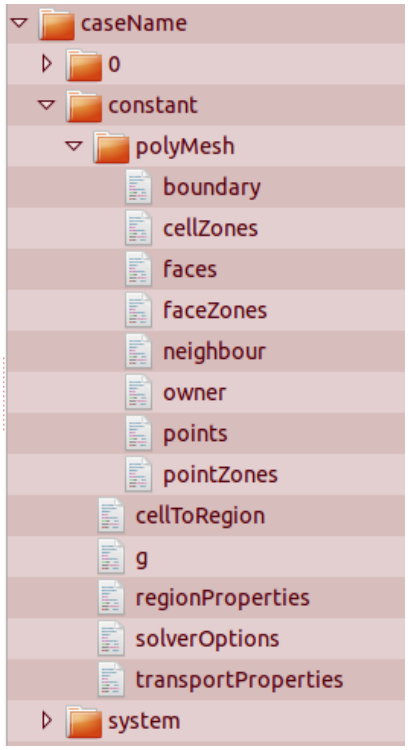

Fig. 3.9– `polyMesh` folder content after converting Gambit mesh to OpenFOAM format

As it can be seen from the Figures 3.9, 3.10, 3.11, 3.12 every time a multiplicity of regions is introduced (in the example reported above fluid and solid are the names chosen for the two regions) the dictionary `cellZones` reports a distinction between different cells (some labeled as fluid and others as solid);

```
2
(
fluid
{
type            cellZone;
cellLabels      List<label> 6(0 1 2 3 4 5);
}
Solid
{
type            cellZone;
cellLabels      List<label> 4 (6 7 8 9);
}
)
```

Fig. 3.10 – Example of cellZones file content

The file faceZones imposes a distinction between internal faces, which define the faces separating different zones at coupled boundaries, and default-interior faces, which indicate all the internal faces of each domain; if any punctual zones are defined during the meshing process, the file pointZones is written accordingly as well.

```
2
(
internal
{
type            faceZone;
faceLabels      List<label> 1(1);
flipMap         List<bool> 1(0);
}
Default-interior
{
type            faceZone;
faceLabels      List<label> 8 (0 2 3 4 5 6 7
8);
flipMap         List<bool> 8(0);

}
)
```

Fig. 3.11– Example of faceZones file content

```
0
()
```

Fig. 3.12– Example of pointZones file content

As OpenFOAM® needs to recognize the different regions as different meshes, it is necessary to physically separate them as they are just addressed as different interconnected zones after GAMBIT mesh creation. In order to perform this operation, a command already implemented in the OpenFOAM® environment can be used, namely splitMeshRegions -cellZones. This function automatically creates inside each of the OpenFOAM® case folders (0, constant and system) a number of sub-folders equal to the number of regions considered, each of which is named as the corresponding zone was originally named during mesh creation, as shown in figure 3.13.

These folders contain both geometrical properties of that region, physical information related to

the case setup and numerical information related to the solution methods as described in 2.2.1.1.

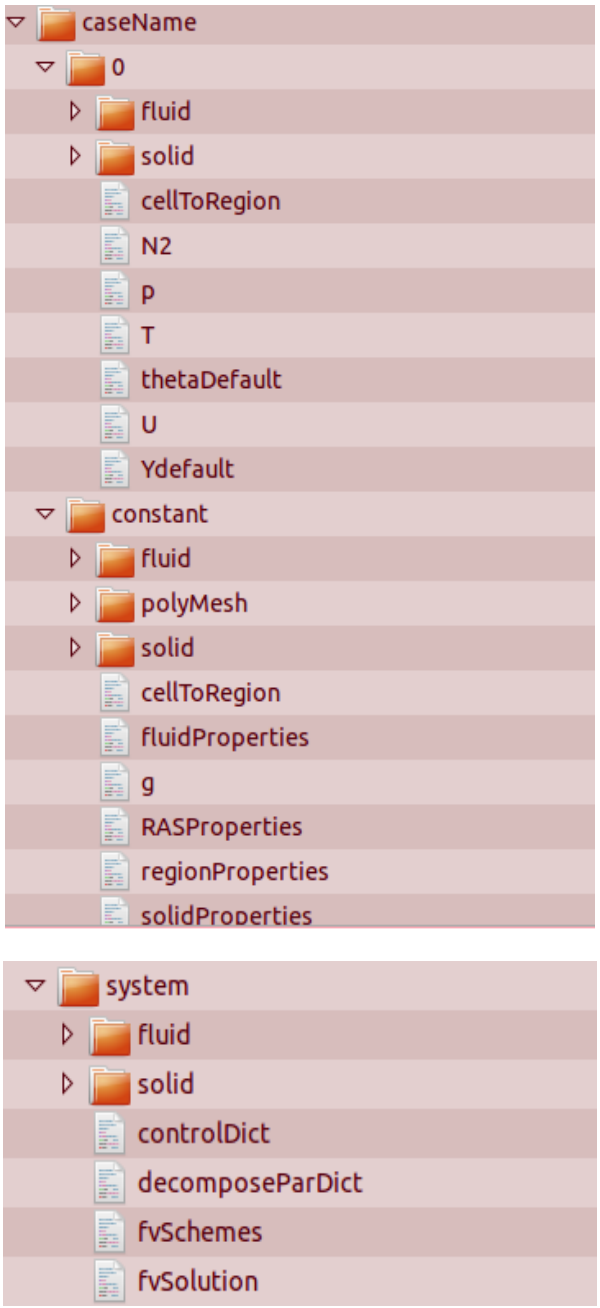

Fig. 3.13– Input folders `0`, `system`, and `constant` in a multi-region case

3.5 Coupling regions at the interface

Once a structure is provided to make possible the implementation of different fundamental equations on different regions, it is important to provide physical soundness to the problem by assuring appropriate conditions describing inter-phase heat and mass transfer phenomena occurring at the interfaces between those regions are imposed. These conditions, characteristic of conjugate heat/mass transfer problems, are the ones shown in the eqs. 3.7 and 3.8, imposing the

same value of the field variable on both sides of the interface and continuity of the flux through it:

$$\begin{cases} k_{eff,I} \left(\frac{\partial T_{SOL}}{\partial x} \right)_{(I)} = k_{fluid,I} \left(\frac{\partial T_{FLUID}}{\partial x} \right)_{(I)} \\ T_{SOL,I} = T_{FLUID,I} \end{cases} \tag{3.7}$$

$$\begin{cases} D_{eff,I} \left(\frac{\partial TC_{i,SOL}}{\partial x} \right)_{(I)} = D_{fluid,I} \left(\frac{\partial C_{i,FLUID}}{\partial x} \right)_{(I)} \\ C_{SOL,I} = C_{FLUID,I} \end{cases} \tag{3.8}$$

According to the literature (Craven and Campbell, 6th OpenFOAM Workshop 2011), two are the possible approaches to impose those conditions:

- ✓ **monolithic:** this approach involves a single coupled system of equations on a single matrix taking into account both the phases involved. When dealing with multiple regions with different properties, this approach can work just for loose inter-equation coupling. Furthermore, the management of the constitutive equations, the storage of field variables and all post-processing operations would become harder with a single matrix approach, as well as parallel processing handling (Clifford, 6th OpenFOAM Workshop 2011);
- ✓ **partitioned:** this approach involves governing equations solved separately on each of the coupled regions, imposing appropriate boundary conditions on both ends. To make the coupling effective, the procedure must be iterated until convergence is reached. If this can be seen as a negative aspect in terms of computational time, the advantage of this approach is that it works on multiple meshes even for stiff inter-equation coupling.

Since the equation system describing heterogeneous catalytic reactors shows stiff inter-equation coupling, the partitioned approach has been chosen to assure numerical stability to the routine.

The physical conditions previously shown (eq. 3.7 and 3.8) have thus been converted into a single mathematical condition for coding and implementation as shown below (eqs. 3.9 and 3.10). The partitioned approach implemented can be summarized as:

- ✓ constitutive governing equations are solved in each zone with the appropriate boundary conditions (eqs. 3.9 and 3.10). These conditions are called “Mixed” (Jaluria and Torrance, 2003), as opposed to Dirichlet/Neumann BCs, which impose different conditions on different

parts of the domain's boundary (Craven and Campbell,6th OpenFOAM Workshop 2011);

- ✓ while solving for the neighboring region, the conditions are updated with the variables values in the freshly solved coupled cell, and this procedure is iterated until convergence is reached.

$$\begin{cases} k_{OWN,I}\left(\frac{\partial T_{OWN}}{\partial x}\right)_{(I)} = k_{NBR,I}\left(\frac{\partial T_{NBR}}{\partial x}\right)_{(I)} \\ T_{OWN,I} = T_{NBR,I} \end{cases} \Rightarrow T_{I,OWN} = \frac{\frac{k_{OWN}T_{OWN}}{\Delta_{OWN}} + \frac{k_{NBR}T_{NBR}}{\Delta_{NBR}}}{\frac{k_{OWN}}{\Delta_{OWN}} + \frac{k_{NBR}}{\Delta_{NBR}}} \tag{3.9}$$

$$\begin{cases} D_{OWN,I}\left(\frac{\partial C_{OWN}}{\partial x}\right)_{(I)} = D_{NBR,I}\left(\frac{\partial C_{NBR}}{\partial x}\right)_{(I)} \\ C_{OWN,I} = C_{NBR,I} \end{cases} \Rightarrow C_{I,OWN} = \frac{\frac{D_{OWN}T_{OWN}}{\Delta_{OWN}} + \frac{D_{NBR}T_{NBR}}{\Delta_{NBR}}}{\frac{D_{OWN}}{\Delta_{OWN}} + \frac{D_{NBR}}{\Delta_{NBR}}} \tag{3.10}$$

In order to handle these boundary conditions automatically during the PDE system solution within a solver built in the OpenFOAM® framework, it has been necessary to code two new libraries which define two new boundary types, not previously available in OpenFOAM®.

Through this new boundary types, called respectively `concentrationCoupled` for species mass fractions and `temperatureCoupled` for temperature, it is possible to recall the boundary conditions discussed in this chapter continuously during the solving process in a simple and user-friendly way.

Here below in fig. 3.14, an example of how this looks in a multi-region case, in both the fluid and the solid coupled regions:

```
(
boundaryField
{
        <Region1Name>_to_<Region2Name>
        {
        type                concentrationCoupled;
        value         uniform 0;
        neighbourFieldName  <coupleSpeciesName>;
        }
}
)
*********************************************
*********************************************
(
boundaryField
{
        <Region1Name>_to_<Region2Name>
        {
        type                temperatureCoupled;
        value         uniform 0;
        neighbourFieldName  T;
        }
}
)
```

Fig.3.14 – Example input file for `concentrationCoupled` *and* `temperatureCoupled` *boundary type definition*

3.5.1 Design of a numerical structure for interface convergence

As previously stated, the chosen partitioned approach requires to iterate between the fluid and solid region in a conjugate mass/heat transfer problem in order to reach convergence at the interface values. In numerical simulations where the purpose is to reach and represent the steady state solution of the system, there is no need for inner loops as convergence on interface coupling is automatically reached at stationary and there's no interest in imposing it for every time step of integration. If, on the other hand, the interest is focused on the transient problem, it is important to guarantee that the interface boundary conditions previously shown are accurately met at every time step of integration. To provide this accuracy, an iterative procedure called PIMPLE loop (merged PISO-SIMPLE algorithm, Penntinen, Yasari at al. 2011, Ferziger and Peric 1997) has been implemented. Its structure (represented in fig. 3.15) can be summarized as follows:

1. Solution on fluid interface cells of the characteristic equations for heat/mass transfer with mixed boundary conditions at the interface:

$$\begin{cases} \dfrac{d(\rho_{mix}\omega_i)}{dt} = \nabla\left(\rho_{mix} D_{i,fluid} \nabla\omega_i\right) - \nabla(\phi\omega_i) \\ \dfrac{d\left(\rho_{mix} c_{p,mix}\, T\right)}{dt} = \nabla(k\nabla T) - Cp\nabla(\phi T) \end{cases} \tag{3.11}$$

with boundary conditions

$$\begin{cases} T_I^{fluid} = \dfrac{\dfrac{k_{fluid}T_{fluid}}{\Delta_{fluid}} + \dfrac{k_{eff}T_{solid}}{\Delta_{solid}}}{\dfrac{k_{fluid}}{\Delta_{fluid}} + \dfrac{k_{eff}}{\Delta_{solid}}} \\ C_{i,I}^{fluid} = \dfrac{\dfrac{D_{i,fluid}C_{i,fluid}}{\Delta_{fluid}} + \dfrac{D_{i,eff}C_{i,solid}}{\Delta_{solid}}}{\dfrac{D_{i,fluid}}{\Delta_{fluid}} + \dfrac{D_{i,eff}}{\Delta_{solid}}} \end{cases} \tag{3.12}$$

2. Solution of the characteristic equations for heat/mass transfer on solid phase cells, analogous to the previous ones but without the convective term, with mixed boundary conditions at the interface updated according to the fluid phase solution obtained from 3.11 and 3.12:

$$\begin{cases} \dfrac{d(\rho_{mix}\omega_i)}{dt} = \nabla\left(\rho_{mix} D_{i,eff} \nabla\omega_i\right) \\ \dfrac{d\left(\rho_{sol} c_{p,sol}\, T\right)}{dt} = \nabla\left(k_{eff}\nabla T\right) \end{cases} \tag{3.13}$$

with boundary conditions:

$$\begin{cases} T_I^{solid} = \dfrac{\dfrac{k_{fluid}T_{fluid}}{\Delta_{fluid}} + \dfrac{k_{eff}T_{solid}}{\Delta_{solid}}}{\dfrac{k_{fluid}}{\Delta_{fluid}} + \dfrac{k_{solid}}{\Delta_{solid}}} \\ C_{i,I}^{solid} = \dfrac{\dfrac{D_{i,eff}C_{i,solid}}{\Delta_{solid}} + \dfrac{D_{i,fluid}C_{i,fluid}}{\Delta_{fluid}}}{\dfrac{D_{i,eff}}{\Delta_{solid}} + \dfrac{D_{i,fluid}}{\Delta_{fluid}}} \end{cases} \tag{3.14}$$

3. Check for convergence: residuals of mass fractions/temperature values have to be lower than user defined absolute and relative tolerances, chosen in order to be appropriate for

the specific case/time step of integration chosen:

$$\left|\omega_i^{(k)} - \omega_i^{(k-1)}\right| \leq absTol_{\omega_i} \quad \left|\frac{\omega_i^{(k)} - \omega_i^{(k-1)}}{\omega_i^{(k-1)}}\right| \leq relTol_{\omega_i}$$

$$\left|T^{(k)} - T^{(k-1)}\right| \leq absTol_T \quad \left|\frac{T^{(k)} - T^{(k-1)}}{T^{(k-1)}}\right| \leq relTol_T$$

4. If both absolute and relative convergence criteria are reached, the solver can proceed to the following time step. Otherwise, for each integration time step, if convergence is not reached in a user defined maximum number of iterations, convergence failure is registered. This can occur if the convergence criteria imposed are too severe, if the system modeled is too numerically unstable or the discretization time is too coarse for the system itself.

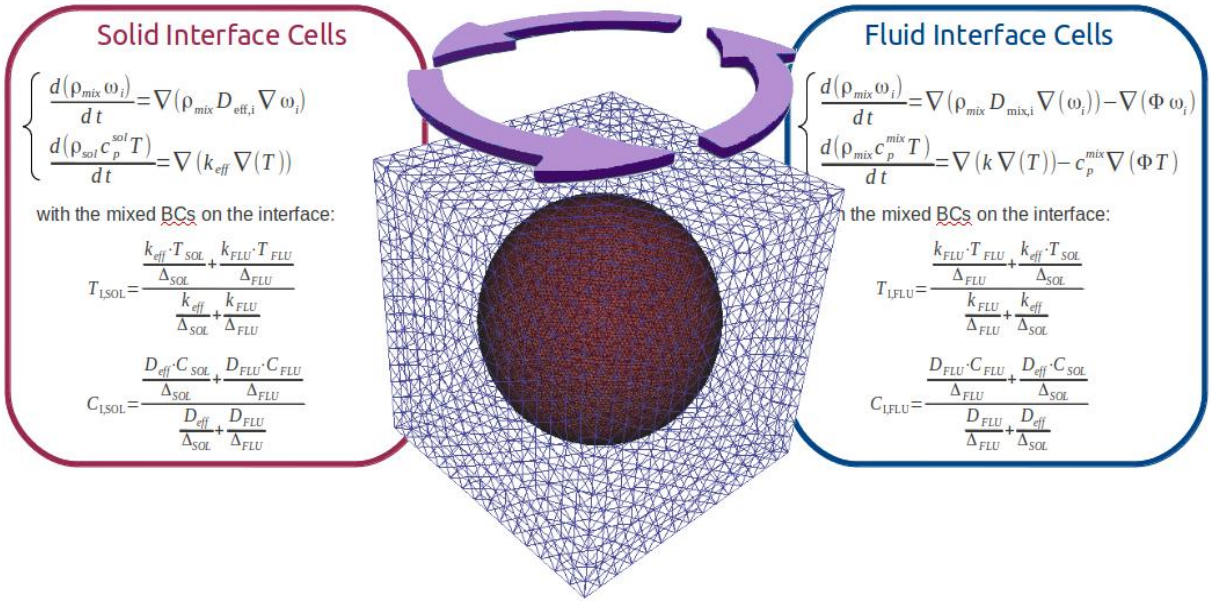

Fig. 3.15 – Pimple loop representation

3.6 Conclusions

In this chapter, several aspects of the development of the catalyticFOAM-multiRegion solver have been discussed.

In a first part of the chapter, after addressing the numerical issues due to the choice for a segregated approach in 3.2, the numerical strategies implemented to overcome these issues have been presented, namely the PISO algorithm and the staggered time splitting scheme.

After describing the embedding of those methods within the mathematical model described in Chapter 2, in the second part of this chapter the main focus has been the description and development of a coupling strategy to correctly represent inter-phase heat and mass transfer phenomena occurring between different regions. In 3.4 the developed multiple meshes/multiple regions structure has been then presented, while in 3.5 the coupling boundary conditions have been discussed and implemented through the coding of two new libraries, working in the PIMPLE loop framework described in the previous paragraph.

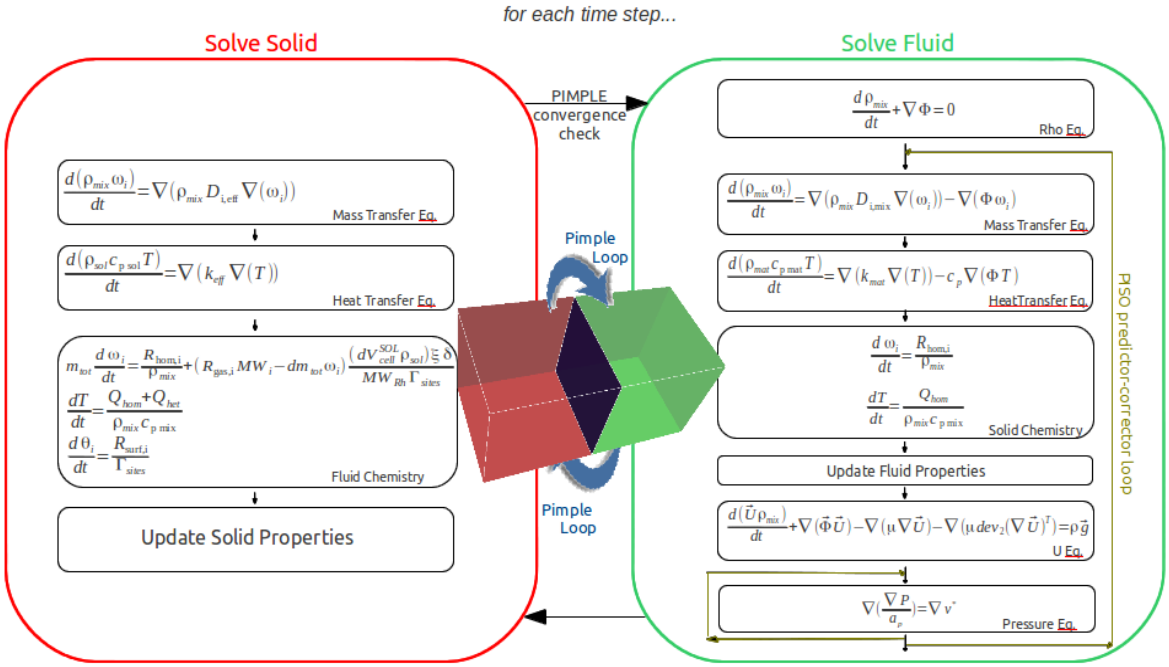

Fig. 3.16 – catalyticFOAM-multiRegion solver architecture

It is possible to merge the solver numerical structure developed for the solution of a single region system discussed in the first part of the chapter with the coupling strategy discussed in the second part of the chapter, thus obtaining the final architecture of the catalyticFOAM-multiRegion solver developed in this work.

Several numerical tests on this architecture, which is represented above in figure 3.16, have been performed in Chapter 4.

Chapter 4

Numerical tests

The main aim of this chapter is to illustrate some cases specifically thought to verifiy the architecture developed and proposed in Chapter 3. In section 4.1 the coupling strategy adopted for heat and mass transfer has been numerically verified through 1D simulations and comparison with analytical and fully-coupled numerical solutions. Afterwards, the operator splitting procedure proposed in 3.2.2 has been tested by simulating cases of increasing complexity, adding one equation at a time to the global solver architecture. Finally, in section 4.3, the importance of the equations order within the operator-splitting technique is discussed.

4.1 Coupling verification

As seen in Chapter 3, the coupling at the boundary interfaces (necessary with the partitioned approach proposed) is performed through the usage of two newly coded libraries (section 3.5). Here, the implemented mixed boundary conditions are reported for reference:

$$\begin{cases} k_{OWN,I}\left(\frac{\partial T_{OWN}}{\partial x}\right)_{(I)} = k_{NBR,I}\left(\frac{\partial T_{NBR}}{\partial x}\right)_{(I)} \\ T_{OWN,I} = T_{NBR,I} \end{cases} \Rightarrow T_{I,OWN} = \frac{\frac{k_{OWN}T_{OWN}}{\Delta_{OWN}} + \frac{k_{NBR}T_{NBR}}{\Delta_{NBR}}}{\frac{k_{OWN}}{\Delta_{OWN}} + \frac{k_{NBR}}{\Delta_{NBR}}} \tag{4.1}$$

$$\begin{cases} D_{OWN,I}\left(\frac{\partial C_{OWN}}{\partial x}\right)_{(I)} = D_{NBR,I}\left(\frac{\partial C_{NBR}}{\partial x}\right)_{(I)} \\ C_{OWN,I} = C_{NBR,I} \end{cases} \Rightarrow C_{I,OWN} = \frac{\frac{D_{OWN}T_{OWN}}{\Delta_{OWN}} + \frac{D_{NBR}T_{NBR}}{\Delta_{NBR}}}{\frac{D_{OWN}}{\Delta_{OWN}} + \frac{D_{NBR}}{\Delta_{NBR}}} \tag{4.2}$$

where OWN and NBR stand respectively, along the solution procedure, for the cell in which the computation is being performed at the current step and for the neighboring coupled cell. While temperature coupling involves just one equation, it is necessary to consider mass-transfer coupling boundary conditions for each of the species considered.

The solution of fundamental equations reported in chapter 2 with the boundary conditions illustrated above for each region until convergence on the boundary conditions previously shown leads to the structure called PIMPLE loop (section 3.5.1)

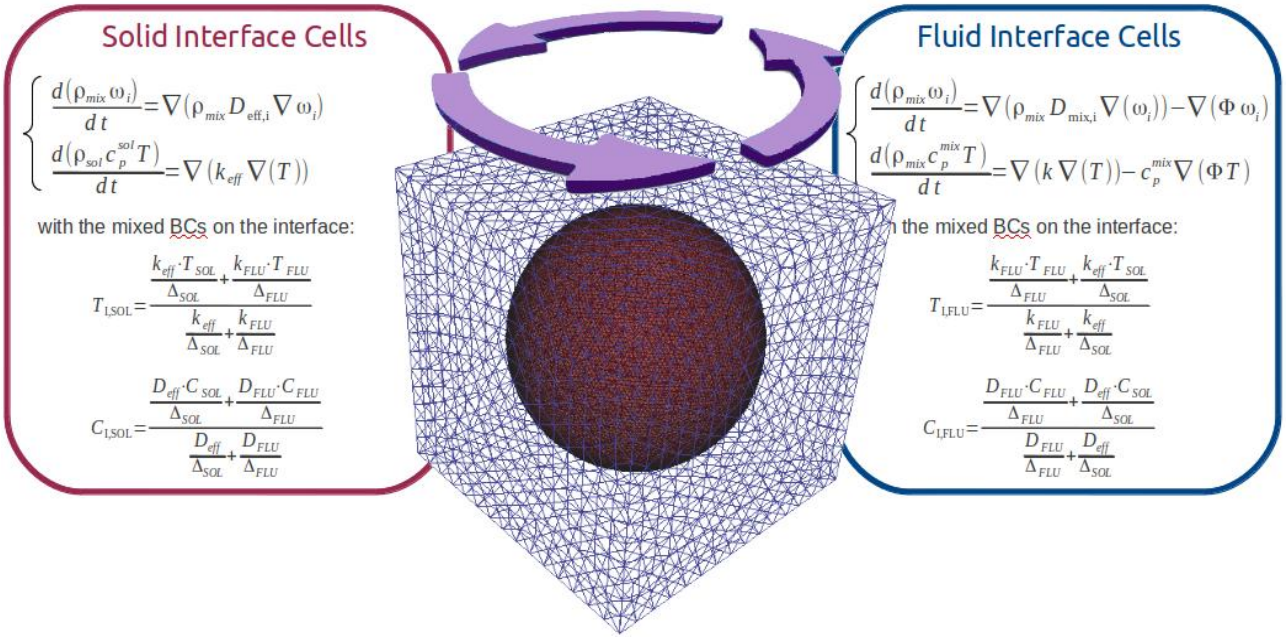

Fig. 4.1 – Pimple loop numerical structure for interface convergence

This endows the solver developed to take into account for both intra-phase phenomena and inter-phase heat and mass transfer. It is now necessary to test the effectiveness of the coupling strategy used, and this will be done by the simulation of cases in which it is easily possible to compute either the analytical solution at steady state or a fully coupled numerical solution during transient.

First, the solver has been tested for the solution of a 1-D conjugate heat transfer problem: analytical solution for steady state and numerical solutions for transient (obtained through a fully coupled solver using finite differences approximation (FDA) for derivatives discretization) have been compared with the solution deriving from the architecture proposed in Chapter 3. The same comparison has been then performed for a conjugate mass transfer case.

4.1.1 Conjugate Heat Transfer

In this case, two metallic bars of length 5 cm each with a common interface will be considered, the left one being made of aluminum (ρ=2800 kg/m^3, Cp=880 J/kg/K, k=200 W/m/K and the right one being made of steel (ρ=7800 kg/m^3, Cp=502 J/kg/K], k=60 W/m/K). As shown in fig. 4.2, the metallic bars are initially at a uniform 400 K temperature in the internal field, while the left and right extremities are at 500 K and 300 K respectively.

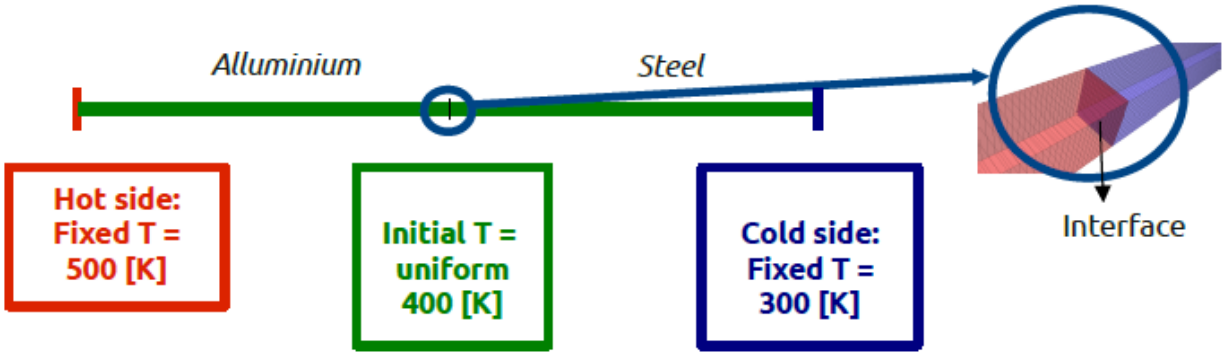

Fig. 4.2 – 1-D conjugate heat transfer: case presentation

In this way, besides providing a test for the coupling technique, the capability of the multiple-regions/multiple-meshes structure built to handle regions of the same phase, but different properties, will be exploited.

Here below (Fig. 4.3), the 1-D model for the description of the system is shown:

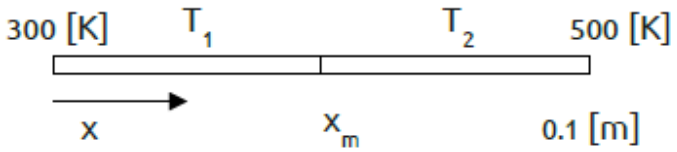

Fig. 4.3– 1D schematization for temperature field

The model equations (4.3), boundary conditions (4.4) and initial conditions (4.5) reported below completely define the problem from a physical and mathematical point of view:

$$\begin{cases} \frac{\partial T_1}{\partial t} = \alpha_1 \frac{\partial^2 T_1}{\partial x^2} \\ \frac{\partial T_2}{\partial t} = \alpha_2 \frac{\partial^2 T_2}{\partial x^2} \end{cases} \tag{4.3}$$

$$\begin{cases} T_1(0,t) = 300K \\ T_1(0.1,t) = 500K \\ T_1(m,t) = T_2(m,t) \\ k_1 \left.\frac{\partial T_1}{\partial x}\right|_m = k_2 \left.\frac{\partial T_2}{\partial x}\right|_m \end{cases} \tag{4.4}$$

$$\begin{cases} T_1(0,0) = 300K \\ T_1(0.1,0) = 500K \\ T_1(x,0) = 400K \end{cases} \tag{4.5}$$

Integrating Fourier's law of heat transfer (4.3) with the above boundary conditions at the ends of the two solids and at the coupled interface (4.4), and the initial conditions reported (4.5) it is possible to get the analytical solution for the problem, reported in equation 4.6.

$$\begin{cases} T_1 = \frac{200}{x_m} \frac{k_2}{k_2 + k_1} x + 300 \\ T_2 = \frac{200}{x_m} \frac{k_1}{k_2 + k_1} (x - 0.1) + 500 \end{cases} \tag{4.6}$$

It is now possible to compare this solution with the steady state one obtained by employing the solver here developed. As it is possible to see in fig.4.4, there is a good agreement between the two results.

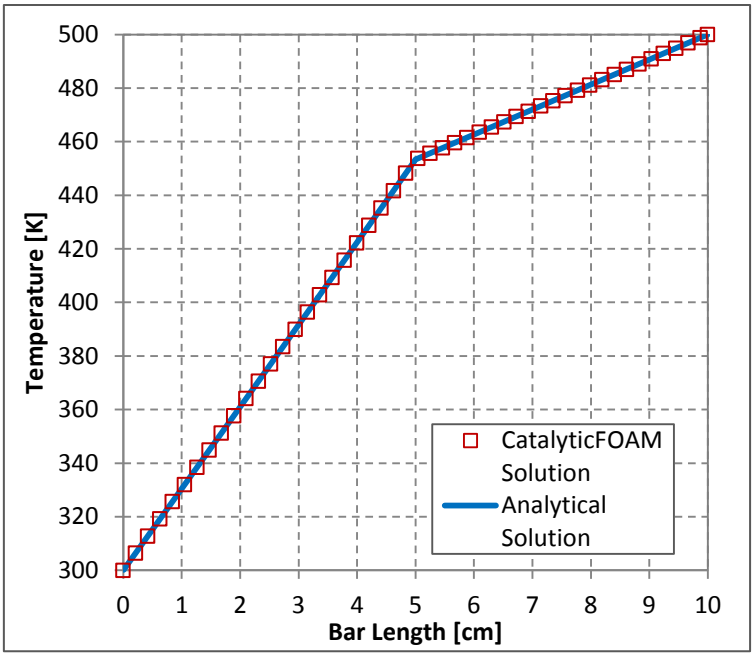

Fig. 4.4 – Comparison between solver and steady state analytical solution for heat transfer in 1D case

Furthermore, in order to fully test the effectiveness of the iterative PIMPLE loop for convergence coupling, a fully-coupled, finite difference approximation discretized solver has been built in MATLAB® for comparison with our solver transient solution.

The main difference between the two solvers stands in the coupling approach itself, as the MATLAB® code solves for both regions in a single block-matrix (fully coupled approach). This confirms the reliability of the segregated approach proposed, as regards both library for temperature coupling in different regions and iterative procedure (PIMPLE loop, Penttinen (2011)).

As shown below (fig. 4.5), the solver developed perfectly overlaps the MATLAB® solution, making a good prediction for temperature profiles along the 2 bars even in transient simulations.

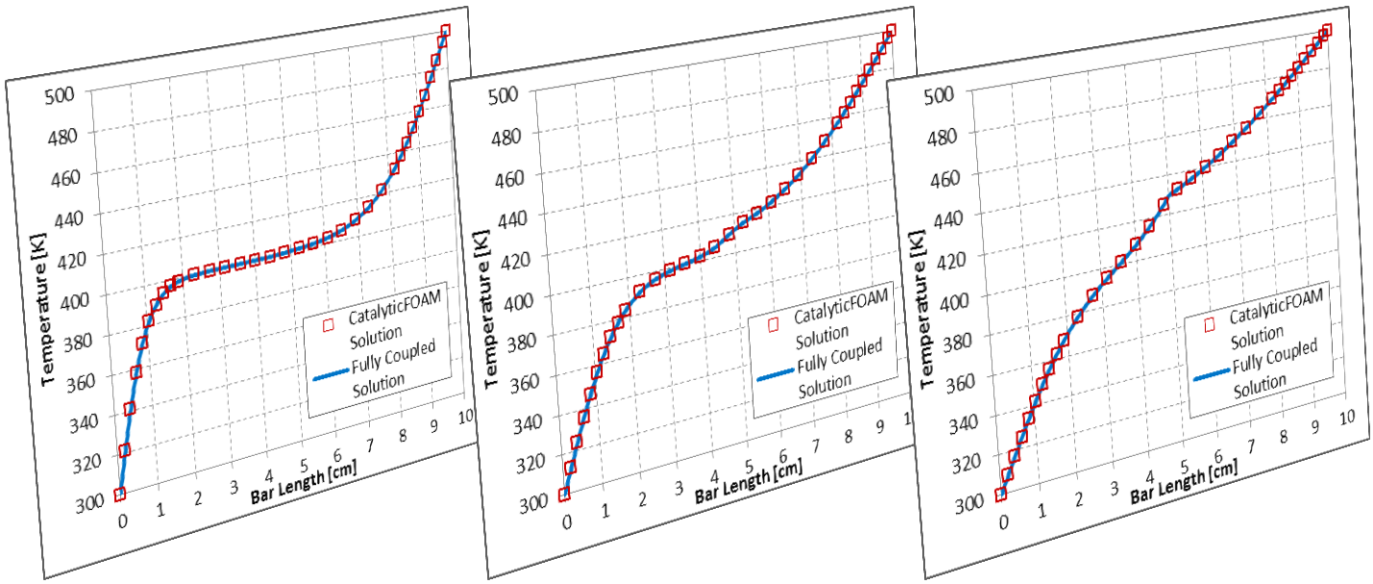

Fig. 4.5 – Comparison between fully coupled and catalyticFOAM solution in transient

In all the figures above, the Euclidean norm computed for the error between the fully coupled solution and the `CatalyticFOAM-multiRegion` solution has a value lower than $2 \cdot 10^{-6}$. The validity of the method proposed has thus been proven for a conjugated heat transfer problem.

4.1.2 Conjugate Mass Transfer

The library used for handling concentration coupling at the interface still needed to be tested, and this has been done through a simple conjugated mass-transfer problem. In this case, two fluid regions separated by a membrane are considered, as shown in figure 4.6. In order to fully reproduce the 1D case for which the analytical solution is known, the velocity field was not considered and the channels were considered to be stagnant. On one end of the system a fixed concentration of methane is imposed, and on the other a fixed concentration of oxygen.

Purpose of the simulation is to represent the concentration profiles for both species into the two regions. The diffusion coefficients assigned to left and right regions are respectively $2 \cdot 10^{-5}$ and 10^{-5} $\frac{m^2}{s}$. As stated in section 2.1, the solver can also calculate the diffusivities for each species in the mixture from its composition through the Fick's approach, implemented in the `OpenSMOKE` libraries.

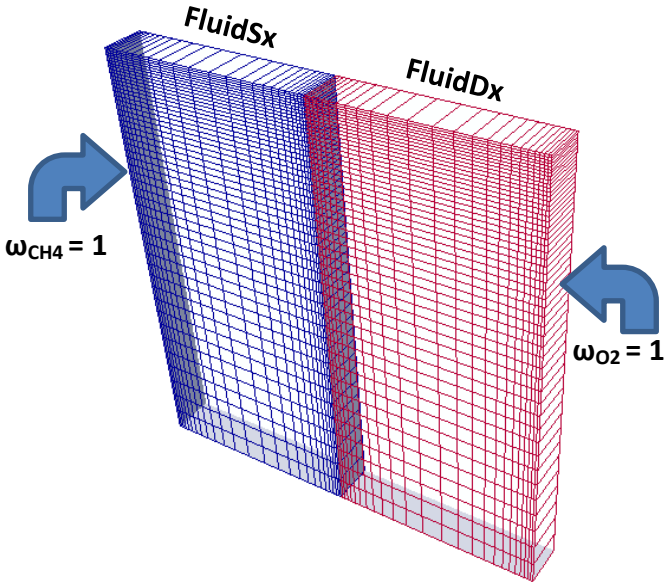

Fig. 4.6 – 1D conjugate mass transfer: case presentation

The mathematical description of the system consists of Fick's law (4.7) with specified initial conditions (4.8) and boundary conditions (4.9). Here below, the equations for methane are reported, and similar ones can be written for oxygen as well.

$$\begin{cases} \dfrac{\partial C_{CH4,1}}{\partial t} = D_1 \dfrac{\partial^2 C_{CH4,1}}{\partial x^2} \\ \dfrac{\partial C_{CH4,2}}{\partial t} = D_2 \dfrac{\partial^2 C_{CH4,2}}{\partial x^2} \end{cases} \tag{4.7}$$

$$\begin{cases} C_{CH4,1}(0,t) = 0.033[mol/m^3] \\ C_{CH4,2}(0.01,t) = 0[mol/m^3] \\ C_{CH4,1}(m,t) = C_{CH4,2}(m,t) \\ D_1 \dfrac{\partial C_{CH4,1}}{\partial x}\Big|_m = D_2 \dfrac{\partial C_{CH4,2}}{\partial x}\Big|_m \end{cases} \tag{4.8}$$

$$\begin{cases} C_{CH4}(0,0) = 0.033[mol/m^3] \\ C_{CH4}(0.01,0) = 0[mol/m^3] \\ C_{CH4}(x,t) = 0.015[mol/m^3] \end{cases} \tag{4.9}$$

The analytical solution can be obtained through integration of the above equations. For methane concentration, for example:

$$\begin{cases} C_1 = 0.033 - \dfrac{0.033}{x_m}\dfrac{D_2}{D_2 + D_1}x \\ C_2 = \dfrac{0.033}{x_m}\dfrac{D_1}{D_2 + D_1}(0.1 - x) \end{cases} \tag{4.10}$$

As done in the previous case, the `catalyticFOAM-multiRegion` solution obtained through a partitioned approach for coupling solving and PIMPLE Loop for convergence has been compared to the steady-state analytical solution. Here below (fig. 4.7), it is possible to notice once again the perfect match between the solver solution and the analytical one, for both oxygen and methane concentration fields. In the figure, the two lines represent the steady state analytical solution, while the squares represent the developed solver solution. The Euclidean norms (2-norm) of the error between the fully coupled and the developed solver solution for CH4 and O2 concentrations are respectively $3.12 \cdot 10^{-6}$ and $2.78 \cdot 10^{-6}$.

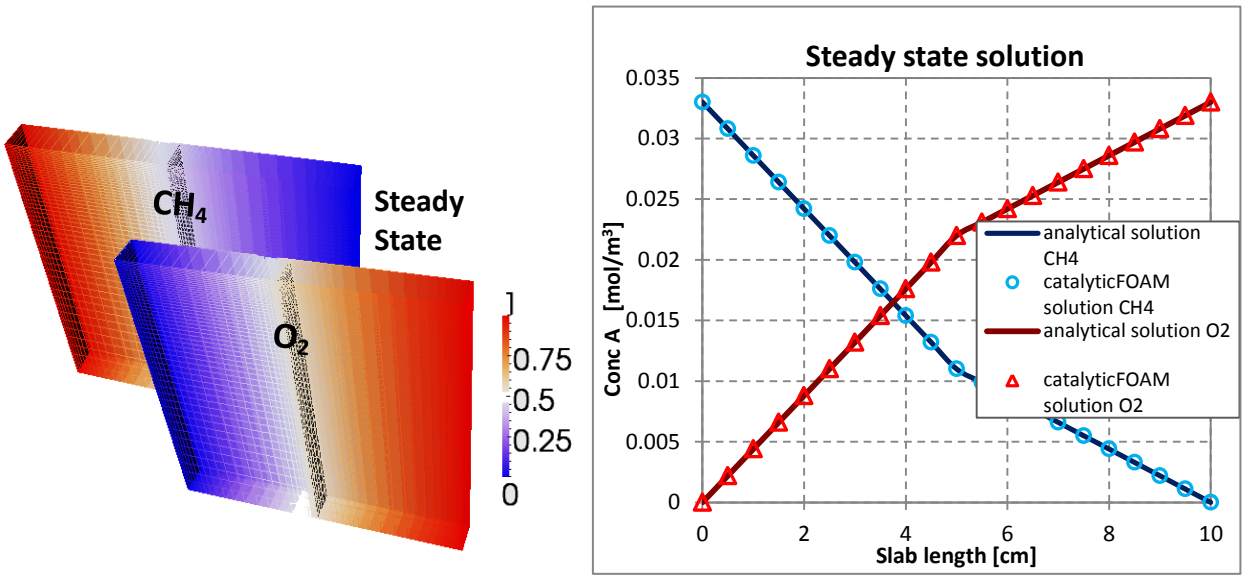

Fig. 4.7– Conjugate mass transfer – comparison with steady state solution

4.1.3 Conjugate Mass Transfer in a reacting environment

Till now, the coupling method has been tested in systems where the heat and mass transfer equations had no source term. The main aim of this section is to provide verification for mass transport equation even in presence of a source term lead by reaction.

An analytical solution for diffusion and reaction phenomena well-known in the literature is the one obtainable for a slab with fixed reactant concentration at the domain boundaries and pseudo-homogeneous first order reaction A→B inside the domain.

In the figure below (4.8), the geometry and boundary conditions for the case setup are shown:

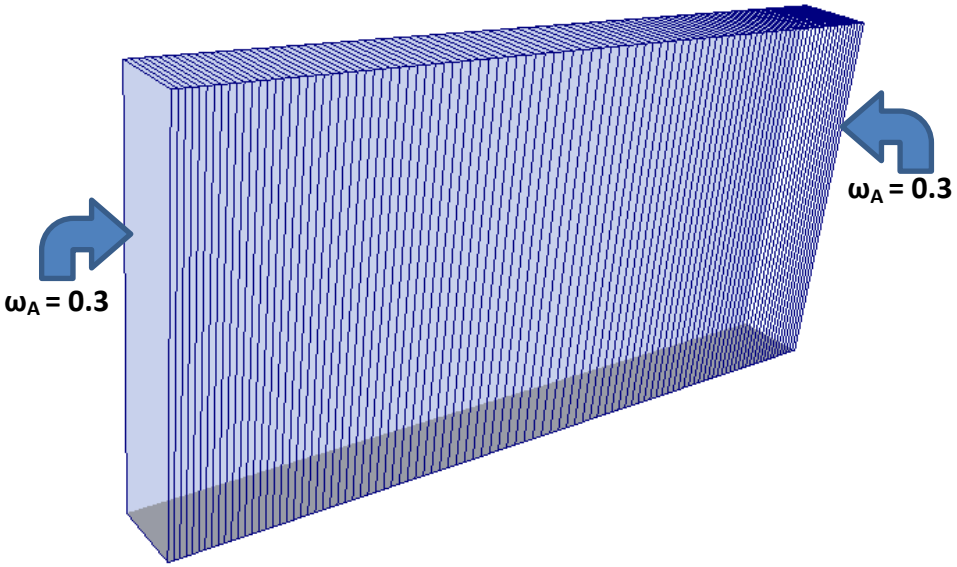

Figure 4.8 – Diffusion and reaction: case presentation

The system can be described by a mathematical model incorporating diffusive transport phenomena and reactive phenomena occurring in the solid slab:

$$\begin{cases} \dfrac{\partial C_{A,1}}{\partial t} = D_1 \dfrac{\partial^2 C_{A,1}}{\partial x^2} + R_{het} a_{cat} \\ \dfrac{\partial C_{A,2}}{\partial t} = D_2 \dfrac{\partial^2 C_{A,2}}{\partial x^2} + R_{het} a_{cat} \end{cases} \tag{4.11}$$

with boundary conditions:

$$\begin{cases} C_{A,1}(0,t) = 0.033[mol/m^3] \\ C_{A,2}(0.01,t) = 0.033[mol/m^3] \\ C_{A,1}(m,t) = C_{A,2}(m,t) \\ D_1 \dfrac{\partial C_{A,1}}{\partial x}\Big|_m = D_2 \dfrac{\partial C_{A,2}}{\partial x}\Big|_m \end{cases} \tag{4.12}$$

The analytical solution is the following:

$$C_A = C_A^S \frac{\cosh(\sqrt{(\frac{k}{D})}x)}{\cosh(\sqrt{(\frac{k}{D})}L)} \tag{4.13}$$

where C_A is the concentration value of reactant within the internal field, C_A^S is the fixed value of concentration in the boundaries, k is the reaction rate constant, D is the diffusion coefficient, L is the slab thickness, x is the longitudinal coordinate across the slab depth.

Even though the analytical solution is available only for a single region, a proof of the reliability of the coupling approach implemented can still be provided by splitting the slab in two different regions with the same properties. In this way the single region case solution will be effectively reproduced by the multi-region solver just if the coupling procedure operates correctly, thus giving a further proof of its reliability.

Once again, as shown in fig. 4.9, a perfect agreement between the two solutions is observed, confirming the reliability of the coupling method implemented.

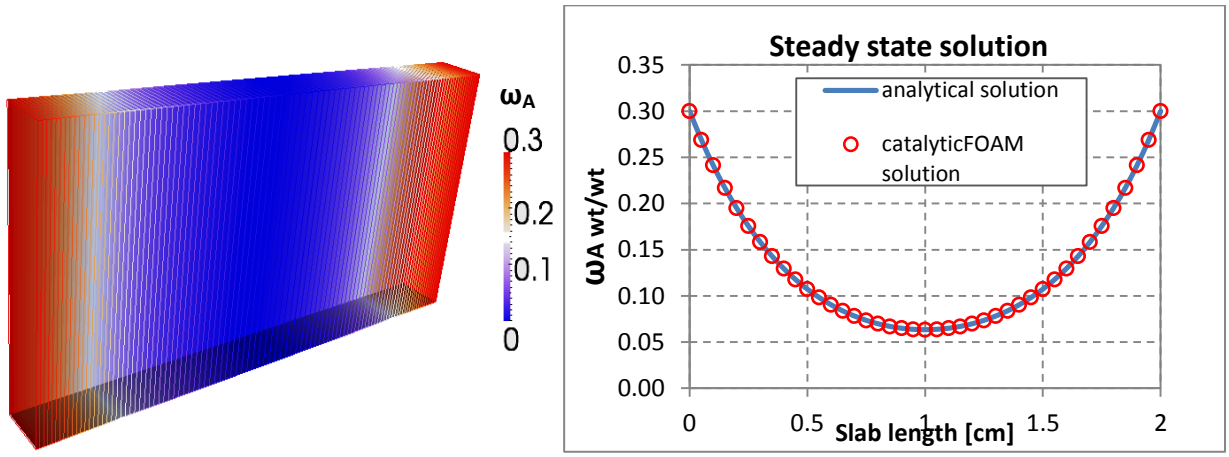

Fig. 4.9 – Diffusion and reaction: comparison with the analytical solution

4.2 Testing the operator splitting structure

After testing the coupling procedure proposed in section 3.5, some tests have been performed to show the reliability of the operator splitting procedure described in section 3.3. As reported in section 3.3.2, this numerical scheme consists of splitting the equations into sub-equations, and integrating each one separately and sequentially. Typically, each sub-equation describes only one part of the physics of the problem (in the case presented the two phenomena are the reaction term and the transport term). The results of the integration at each sub-step are combined to approximate the final solution with high accuracy (Strang 1968).

The main aim of the cases proposed is the testing of this numerical strategy through case studies of increasing complexity, i.e. involving an increasing number of equations in the architecture shown in section 3.6, starting from a simple diffusion/reaction case and adding one equation at a time. Particular attention will be given to the splitting structure numerical stability: in order to check its validity, the results obtained from the solver here presented (using operator-splitting

technique) will be compared to the MATLAB® resolution of the system through a solver in which no splitting between transport and reactive term is provided. This comparison has been made just in a limited set of simplified cases, since in more complex cases and with higher number of equations the case reproduction in a MATLAB® solver was too expensive in terms of time.

4.2.1 Testing diffusion and reaction

The case presented is a hexahedral 1D mesh composed of two different regions with a common interface. The left and right walls have a fixed molar fraction of, respectively, 0.6 and 0.4 $[\frac{mol_A}{mol_{TOT}}]$. In the left region the only phenomenon modeled is the compounds diffusion, while on the right region, besides diffusive phenomena, a first order pseudo-homogeneous reaction A→B occurs too.

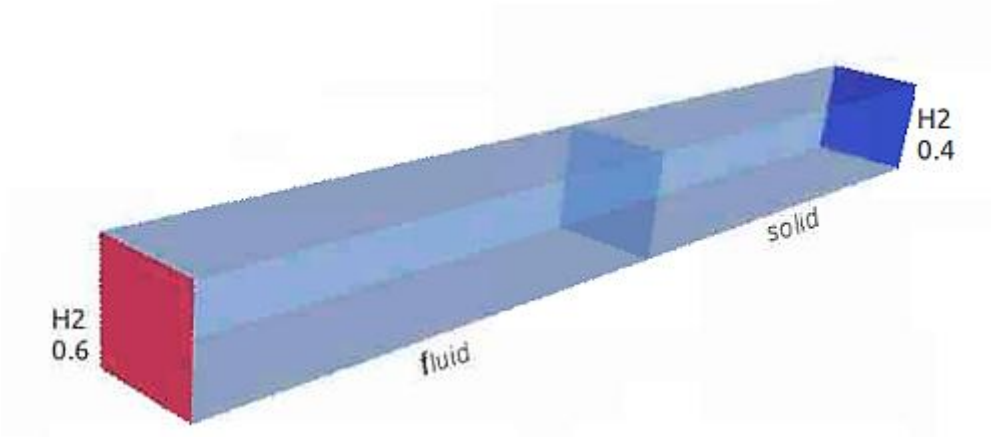

Fig. 4.10 – Diffusion and reaction: comparison with the analytical solution

The approach used in the following paragraphs aims at testing different numerical properties of the developed architecture, namely:

- the effect of a time step reduction on the solution;
- the effect of mesh refinement on the solution;
- the stability of the solution while varying operative conditions.

The values used for reaction rate and diffusion coefficients will be specified from case to case, and the solution obtained compared with a MATLAB® numerical solution not involving any operator splitting.

4.2.1.1 Effect of time-step

If the operator-splitting technique is stable, a reduction of discretization time should lead to a more accurate solution. For the case shown in fig. 4.10 a diffusion coefficient of $2 \cdot 10^{-5}$ m^2/s for the left zone, $1 \cdot 10^{-5}$ m^2/s for the right zone and a kinetic constant of 10 1/s for the reaction A→B occurring in the right zone are used. The results of this case at different time-steps are reported: as expected, as the time step decreases the `catalyticFOAM-multiRegion` solutions approach the coupled MATLAB® solution. The agreement has been shown in terms of norm-2 in table 4.1.

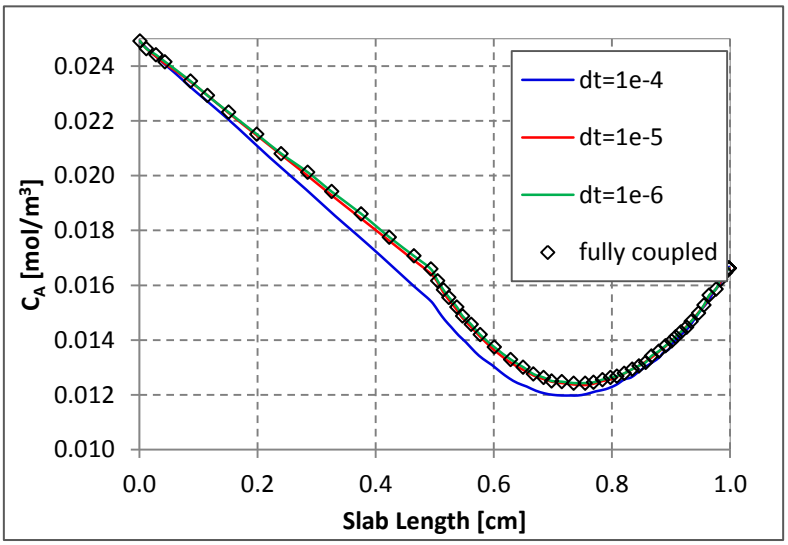

Fig 4.11 – Effect of time step in 1D case of diffusion and reaction

dt = $1 \cdot 10^{-4}$	dt = $1 \cdot 10^{-5}$	dt = $1 \cdot 10^{-6}$
$8.38 \cdot 10^{-5}$	$2.65 \cdot 10^{-5}$	$5.24 \cdot 10^{-6}$

Table 4.1 – Norm-2 of the errors between fully coupled and split solution

4.2.1.2 Effect of mesh refinement

Another test of the operator-splitting technique is the reduction of cell dimensions: smaller cell dimensions should lead to a more accurate solution. For the case shown in fig. 4.12 a diffusion coefficient of $2 \cdot 10^{-5}$ m^2/s for the left zone, $1 \cdot 10^{-5}$ m^2/s for the right zone and a kinetic constant of 10 1/s for the reaction A→B occurring in the right zone are used. The results of this case at different cell dimensions are reported: as expected, as the mesh refinement improves the `catalyticFOAM-multiRegion` solution approaches the coupled MATLAB® solution, as it is possible to notice from the values of the Euclidean norm computed for the error between the two

solutions (table 4.2).

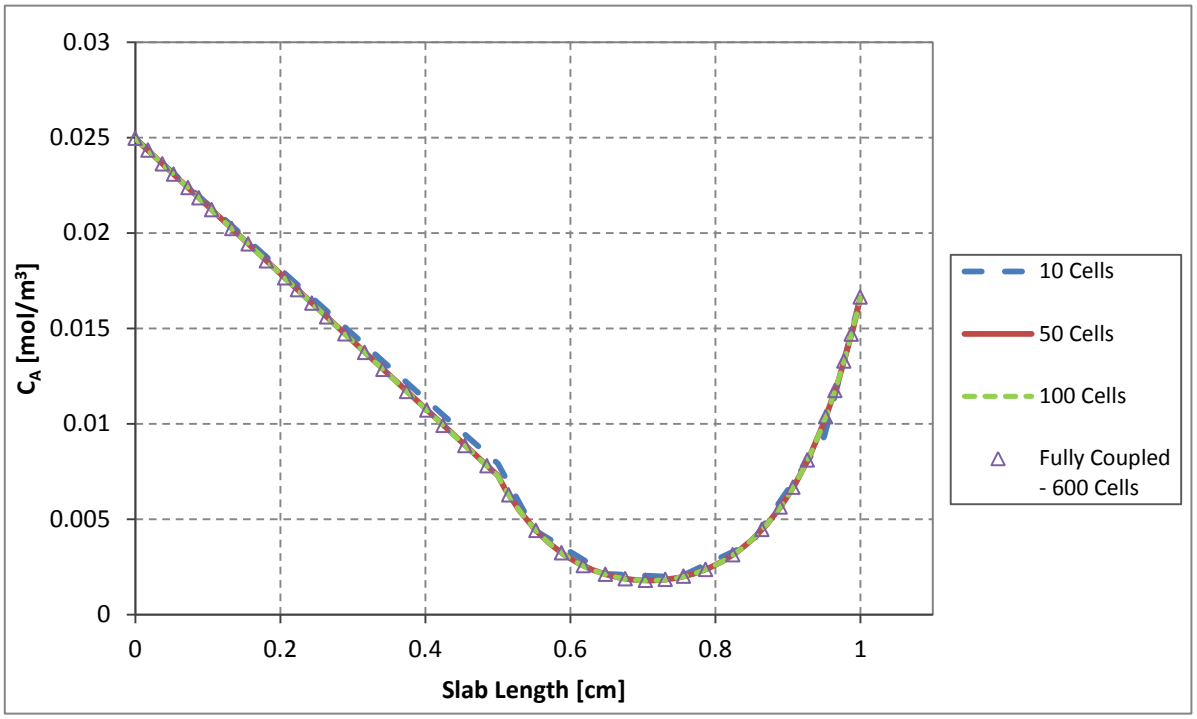

Fig 4.12– Effect of mesh refinement in 1D case of diffusion and reaction

10 cells	50 cells	100 cells
$6.41 \cdot 10^{-4}$	$5.71 \cdot 10^{-5}$	$1.86 \cdot 10^{-5}$

Table 4.2 – Norm-2 of the errors between fully coupled and split solution

4.2.1.3 Numerical stability in a wide set of conditions

The next series of simulations shows the 1-D case described at the beginning of this section in a wide variety of operating conditions. Particularly, 12 different combinations of kinetic constants and diffusion coefficients are used both in the `catalyticFOAM-multiRegion` split solver and in the MATLAB® coupled solver.

This test has been made in order to test the numerical stability of the splitting operator technique in "extreme" conditions: in case of high diffusion coefficient and/or low reaction rate, the system is in kinetic control, which means that the rate determining step is reaction. On the other hand, if reaction is fast and/or diffusion is slow diffusion is rate determining step. Finally, if reaction is very fast and/or diffusion is very slow, the system is in mass transfer regime, which means that all the reactant in contact with the catalyst immediately reacts, as shown below in Figure 4.13.

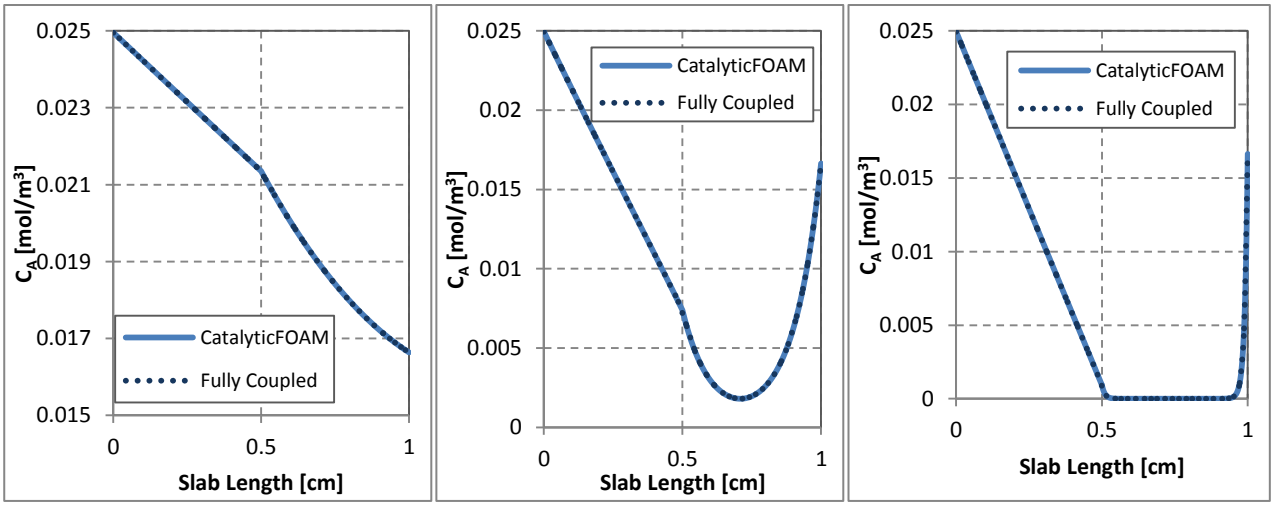

Fig. 4.13– Chemical, diffusive and mass transfer regime at different operating conditions

In figure 4.13, beside observing the different operative regimes occurring with varying conditions, it is possible to notice the good agreement between the developed solver numerical solution, involving operator splitting as described in 3.2, and the Matlab® coupled solution, including the reactive source term in the transport equations themselves.

Extending the approach to the whole range of operating conditions to be tested, the `catalyticFOAM-multiRegion` solution curve and the MATLAB® coupled solver solution curve still overlap. The 12 different profiles show the characteristics described above: the graphs with k=0.1 and $D=2\cdot10^{-4}$and $2\cdot10^{-5}$, together with the case k=1 and $D=2\cdot10^{-4}$ are in kinetic control; graphs at k=1000, $D=2\cdot10^{-5}$and $2\cdot10^{-6}$ are in mass transfer control. All the other cases are in diffusive control.

(x axis: Slab Length [cm] , y axis: C_A [mol/m^3])

$2\cdot10^{-6}$	$2\cdot10^{-5}$	$2\cdot10^{-4}$	Diff/k
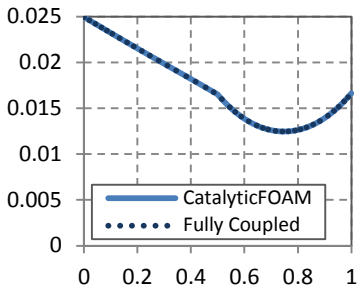	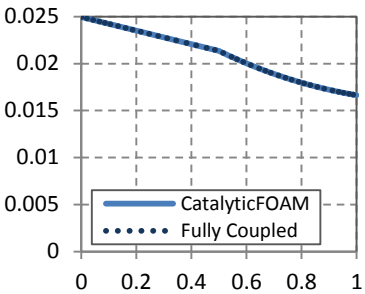	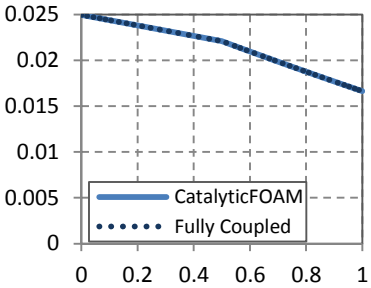	0.1
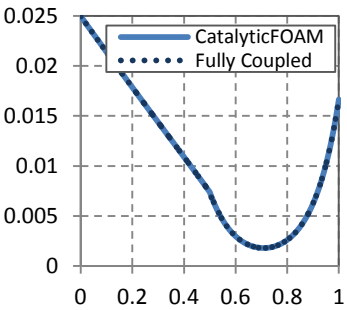	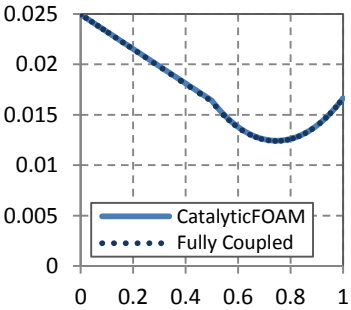	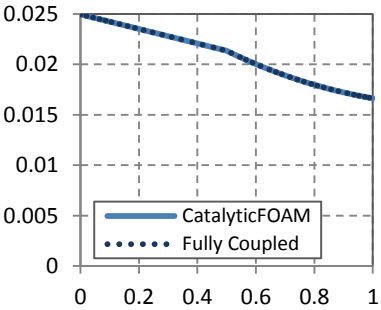	1
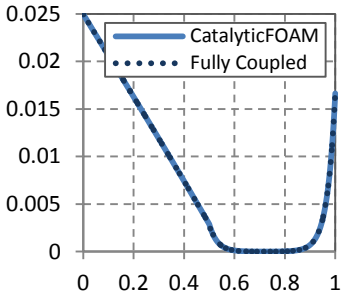	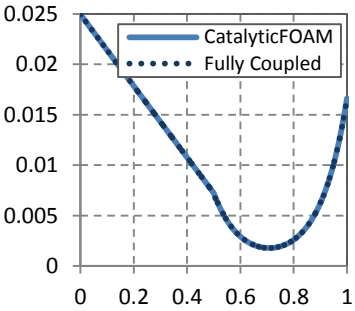	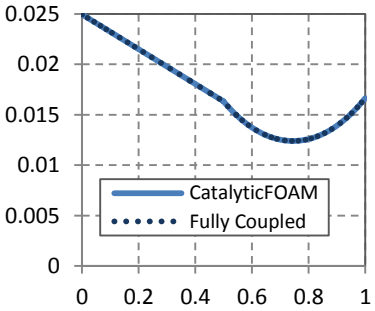	10
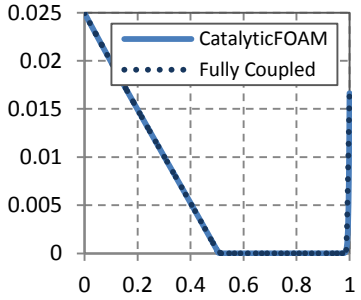	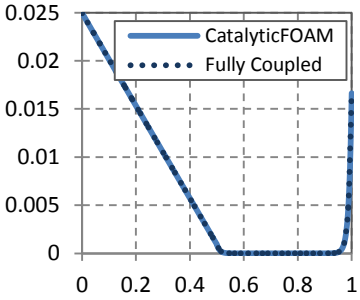	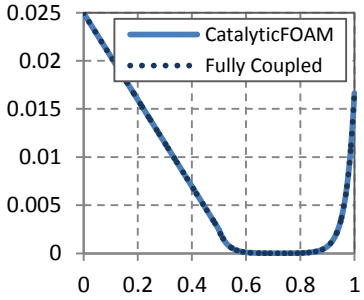	1000

Fig. 4.14– Comparison between split `catalyticFOAM-multiRegion` *solver and coupled MATLAB® solver for diffusion and reaction in 1-D system for a wide variety of conditions.*

4.2.2 Complex kinetic schemes

In the following case, the diffusion with reaction set of equations has been tested with a complex kinetic scheme: it consists of 21 homogeneous and 18 heterogeneous reactions involving 9 gaseous species ad 5 site species. The reaction rates are evaluated with the UBI-QEP method (Shustorovich and Sellers 1998; Goisis and Osio 2011).

The possibility to model complex kinetic schemes, considering a high number of gas and site species, is essential for a more correct representation of the chemical phenomena. Beside the change in the kinetic scheme, the case is identical to the one presented at the beginning of this section, as numerical complexity has been introduced by the kinetic scheme itself.

What can be observed in fig. 4.15 is a qualitative correct trend of H_2 (reactant) concentration throughout the double region domain: in the left part of the domain it is possible to notice a straight line, which shows the effect of diffusion according to the imposed boundary condition. In the right part of the domain a curve with a minimum can be observed, consequence of the reactive phenomenon which consumes hydrogen.

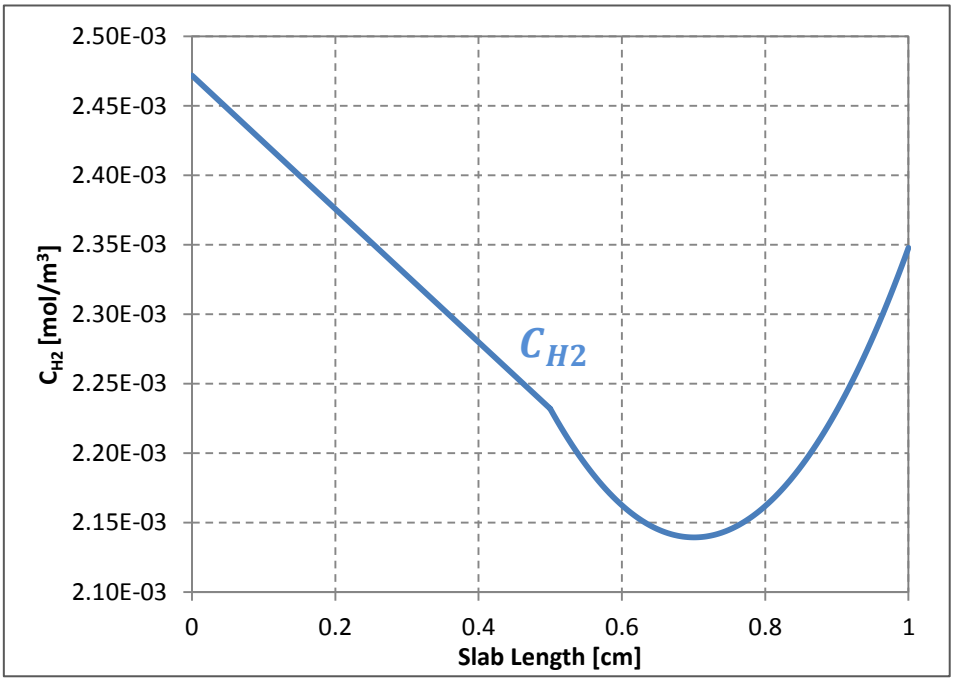

Fig. 4.15- 1-D case with diffusion and reaction using complex kinetic schemes

4.2.3 Coupling with the Navier Stokes equations

In the following cases, in addition to diffusion, reaction and use of complex kinetic schemes, we introduce non-elementary geometries and the solution of Navier-Stokes equations for pressure and velocity fields calculation in the operator-splitting framework described in 3.3.2.

4.2.3.1 Two channels separated by a catalytic layer

A first example of bi-dimensional mesh case is now presented. As shown in Fig. 4.16, it is composed of two hexahedral channels in which a gas mixture with the following molar compositin: 4% H_2, 1% O_2 and 95 N_2. Between the two channels there is a solid catalytic region constituted by a supported catalyst (Rh on α-Al) in which the fluid can diffuse and react, following the complex kinetic scheme introduced in 4.2.2 and reported in Appendix B.

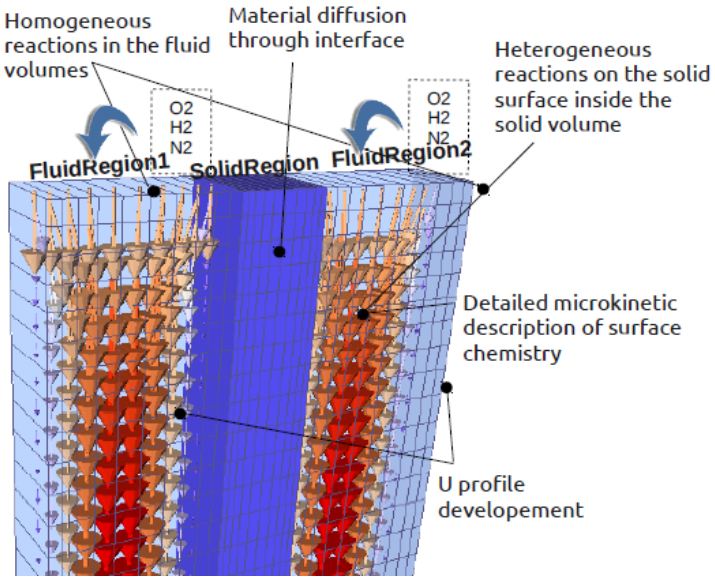

Fig. 4.16 – two 2D channels: case setup and description

The novelty and additional complexity of this case with respect to the previous one stands in the implementation of more than two regions in the same simulation, with more than one coupled interface to be considered within the developed framework.

First, velocity profiles have been investigated in both the fluid channels: the curves plotted are identical for both the channels due to the symmetry of the problem with respect to the only symmetry axis, and show a sound profile with a maximum corresponding to the middle of the channel once the profile is fully developed (fig. 4.17).

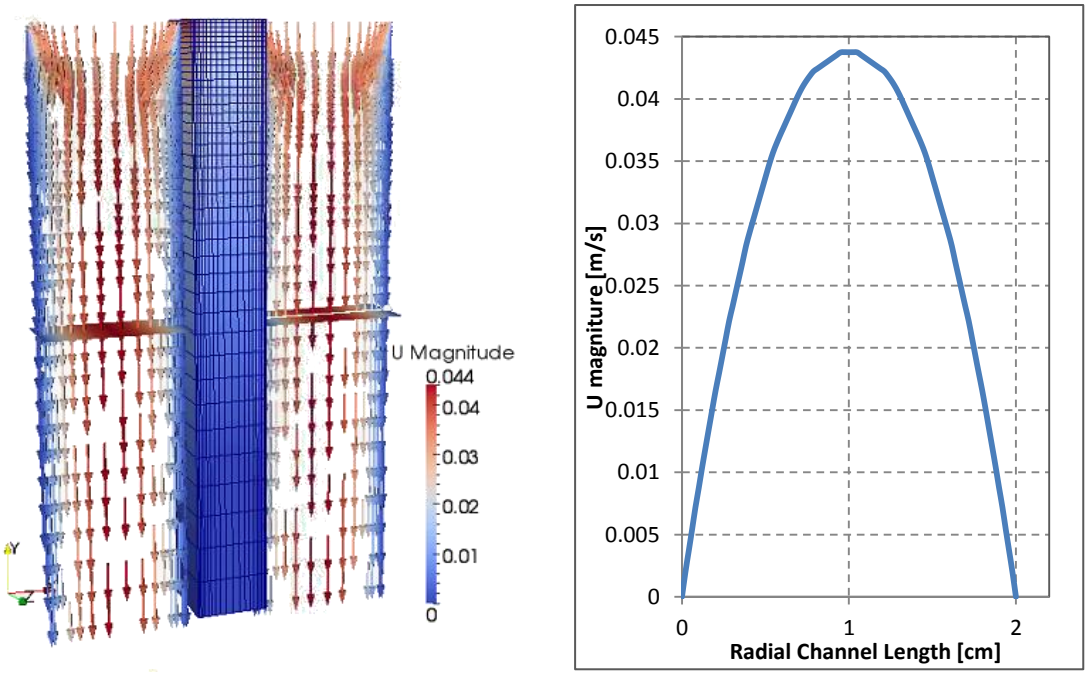

Fig. 4.17– Two 2D channels: velocity field development in the channels

The concentration profiles of both a reactant and a product have been then considered, with the aim of confirming both the coupling at the interface when more than two phases are involved and the diffusive limitations in the solid catalyst are taken into account and correctly represented.

As shown in figures 4.18a-b below, sound reactant and product mass fractions profiles are obtained in both the fluid and in the solid phase. In the fluid phase, the reaction occurring on the catalytic surface inside the solid volume produces a sudden reduction of reactants in the zone close to the solid phase, and a consequent increase of products mass fractions due to the reaction itself and the following desorption and diffusion from the catalytic surface to the channel where the gaseous mixture flows.

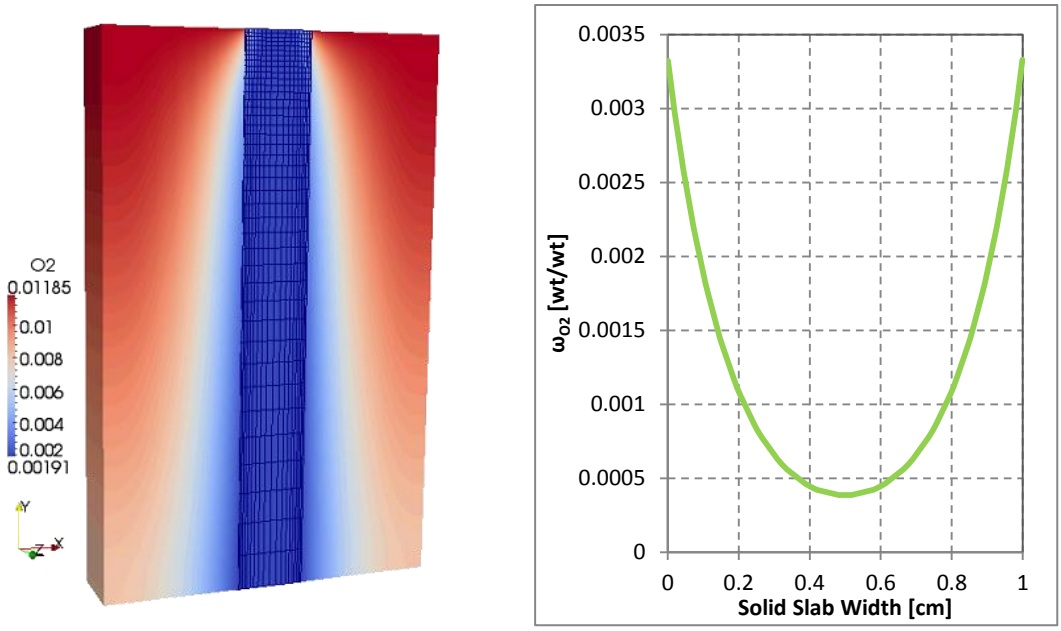

Fig. 4.18a – Two 2D channels: massive fractions reactant profiles inside the solid catalytic phase

As regards the mass fraction profiles inside the solid phase, it is possible to confirm the capability of the developed solver architecture to correctly predict and describe diffusive limitations inside the catalytic layer itself. Because of those limitations, it is possible to identify a symmetric profile with a minimum in the center of the layer when considering the reactant mass fractions and a maximum when considering the products mass fractions.

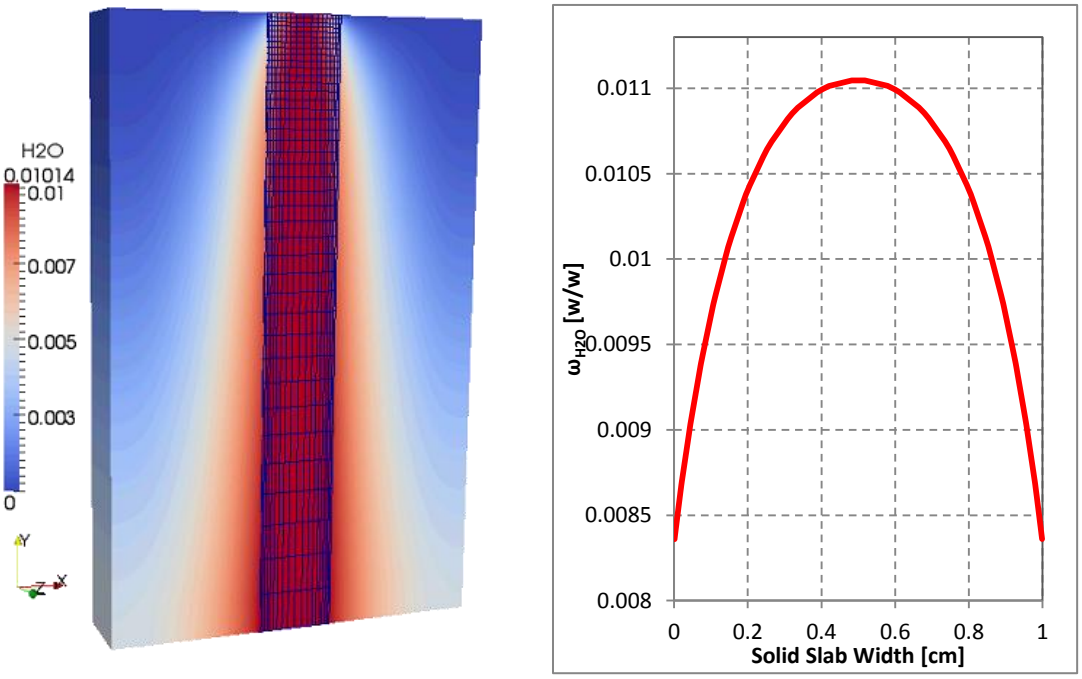

Fig. 4.18b – two 2D channels: massive fractions product profiles inside the solid catalytic phase

4.2.3.2 Channel with catalytic solid particle

The mesh of a second representative case is shown in fig. 4.19: it is a hexahedral channel containing fluid reactants moving at inlet velocity of 0.1 $\frac{m}{s}$; inside the channel, a cylindrical solid supported catalyst (Rh on α-Al) allows reactants to adsorb and react. The reaction scheme used is H_2 on Rh UBI-QEP scheme, according to the complex reaction scheme described in Goisis and Osio 2011 (appendix C). Products then desorb from the catalytic surface and flow to the outlet of the channel. The diffusive coefficient in the fluid phase is calculated according to the composition of the mixture, while the effective diffusivity in the solid phase is computed from the gaseous one through a reduction factor, as described in 2.1.2.5.

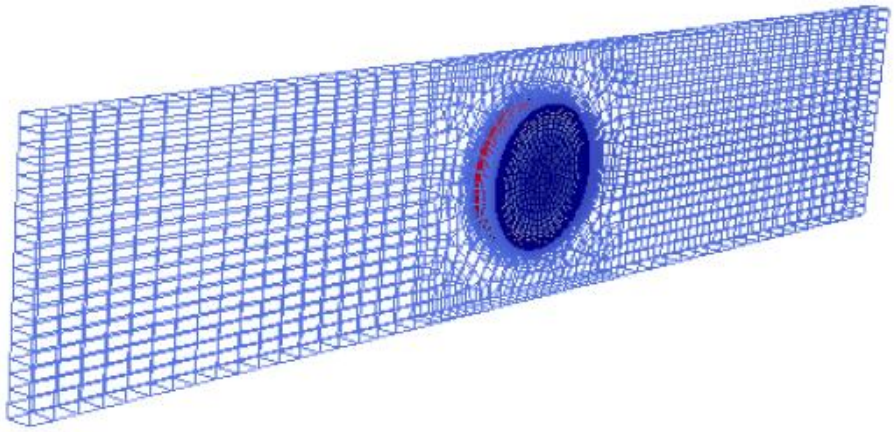

Fig. 4.19 – Channel with catalytic solid particle: mesh used for the simulation

A very important factor to be considered is the mesh grading next to the solid-fluid interface: in fact, both in the fluid and in the solid phase, the cells need to be much thinner than elsewhere in the domain in order for a physically sound solution to be obtained. This is due to the presence of the highest gradients in the whole domain concentrated in the zone close to the interface, where the multi-region coupling also occurs.

A correct physical description of the system should include:

- non-slip condition at the walls (both of the channel and of the cylindrical object) for the velocity field;
- Poiseuille velocity profile in laminar flow, with maximum value along the symmetry axis once the profile is fully developed;
- velocity increase across the object due to the section restriction and decrease in the zone behind it;

- velocity reduction in the zone immediately behind the cylindrical obstacle.

As it is possible to notice in fig.4.20a-b, the velocity profiles correctly describe the system as mentioned above.

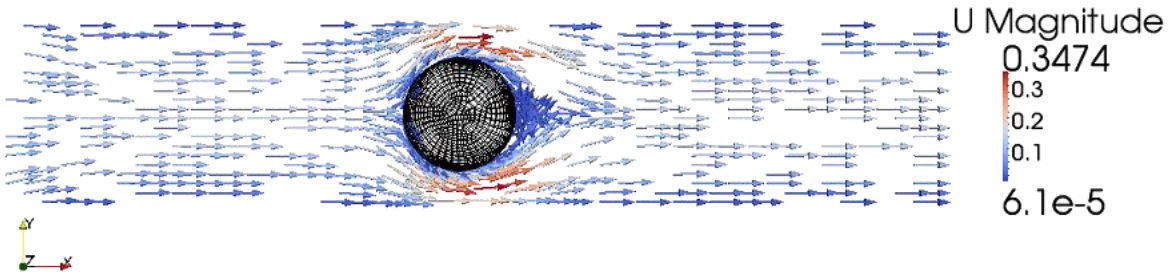

Fig. 4.20a – 2-D case: velocity profiles around the cylindrical catalyst

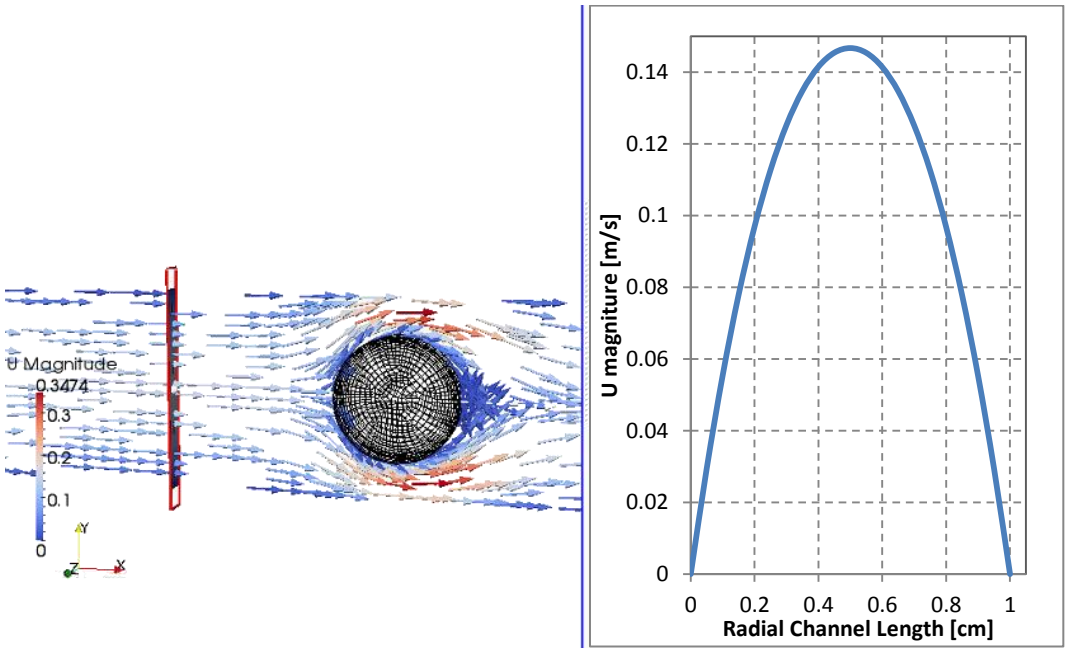

Fig. 4.20b – 2-D case: fully developed velocity profile before the obstacle

As regards concentration profiles, a physically sound description would consider reactant adsorption and reaction inside the catalyst pellet, as well as desorption of the products from the catalytic surface back into the gaseous mixture flowing into the channel. As shown in picture 4.21a and 4.21b, those profiles are correctly predicted by the developed solver inside the fluid phase.

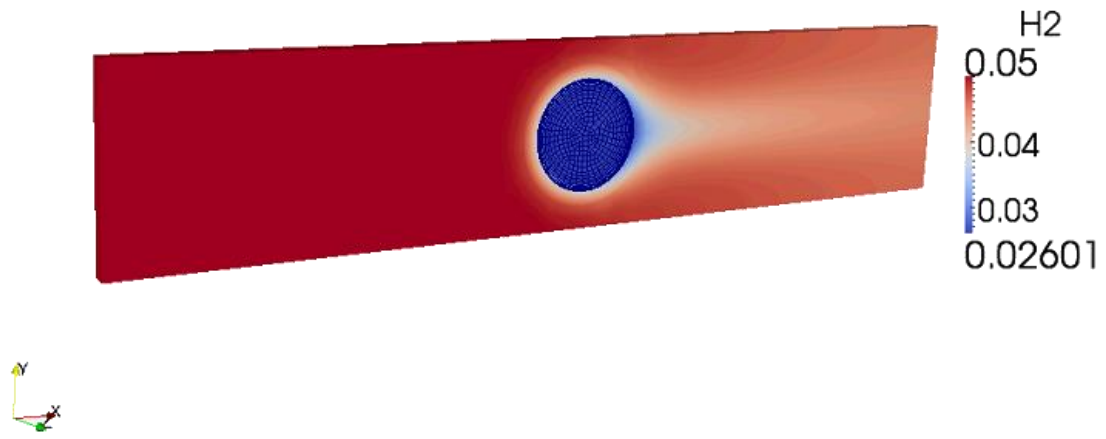

Fig. 4.21a – 2-D case: H2 mass fraction map in the channel

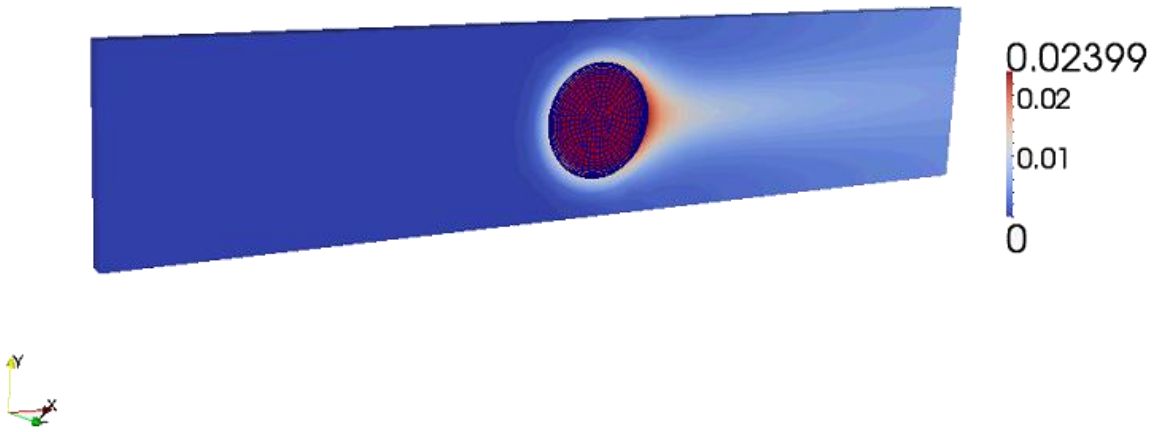

Fig. 4.21b – 2-D case: H2O mass fraction map in the channel

However, one of the main features of the solver developed in this work is the correct description of intra-phase phenomena occurring inside the catalytic solid phase, making it possible to take into account for diffusive limitations and incomplete catalyst volume utilization. For this reason, the mass fractions profiles of reactant in the fluid phase are shown in figures 4.22 and 4.23, describing (as expected) a minimum inside the solid particle due to the diffusive limitations.

Beside this, important considerations on the validity of the solver solution can be made based on the symmetry of the solutions obtained. In particular, the profile is not symmetric along the x-axis because the reactant convective flux inside the pipe makes the domain asymmetrical. It is nevertheless physically sound, having a maximum next to the solid-fluid boundaries where the reactant flux impacts the solid surface and a minimum inside the solid center in the bottom area of the solid, due to diffusive, convective and reactive phenomena. This is shown in figure 4.22 below:

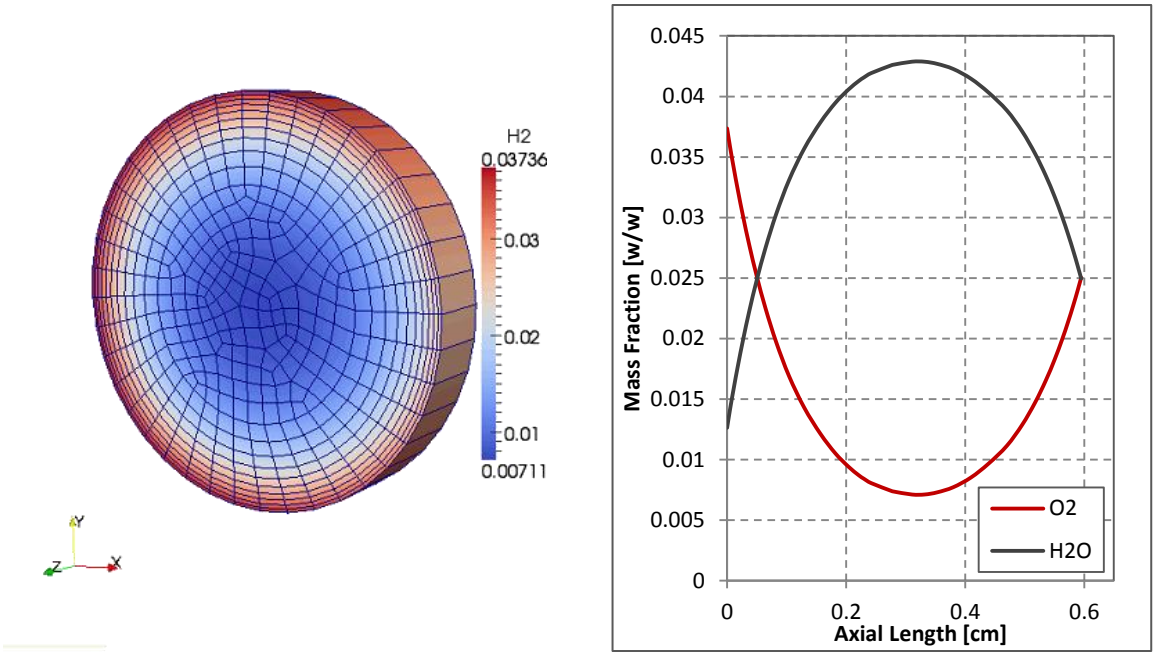

Fig. 4.22 – 2-D case: mass fractions profiles of reactant and products along the flow coordinate x

On the other hand, being the system axial symmetric with respect to the channel symmetry axis, a sound solution must be symmetric as well along the radial coordinate, both in the fluid and in the solid phase. As illustrated below in figure 4.23, the massive fractions profiles inside the catalyst particle show indeed a perfect symmetry.

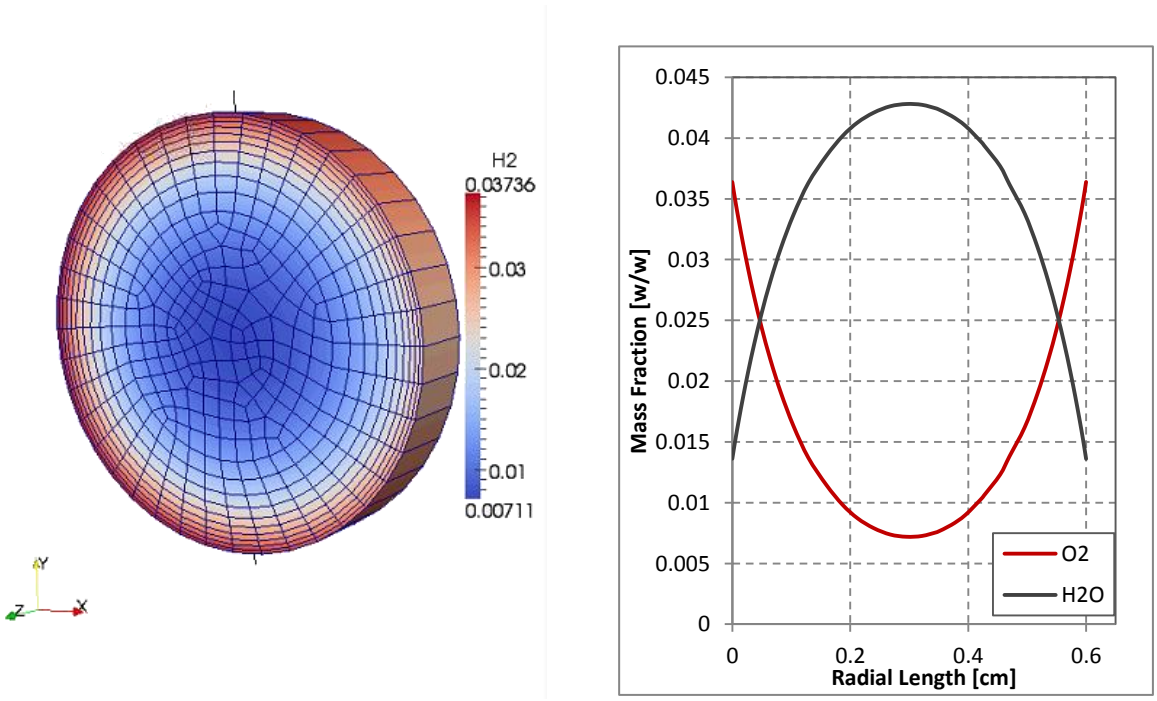

Fig. 4.23 – 2-D case: mass fractions profiles of reactant and products along the radial coordinate y

4.3 The importance of equations order when using operator splitting

In Section 3.3, the global architecture of the solver developed in this work has been shown, focusing in particular on the operator splitting technique chosen for implementation. In that context, however, the reason for the order of the equations to be embedded in the framework has not been investigated. Purpose of this paragraph is to discuss its importance, as it can affect the stability and accuracy of the solver architecture itself.

In a previous work (Goisis and Osio 2011) the splitting operator technique proposed was different from the one developed in this work and presented in 3.2.2:.

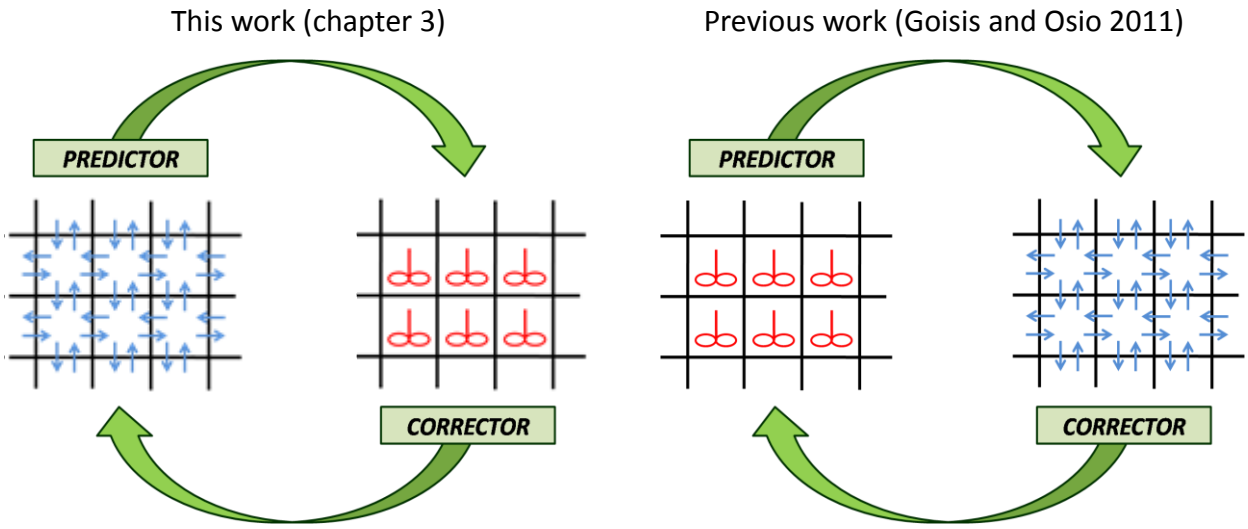

Fig. 4.24 - Physical interpretation of the two predictor-corrector routines (Goisis and Osio 2011)

As shown in the figure above, while the splitting technique presented in this work chooses the transport step as predictor and the reactor step as corrector, the previous work suggested a reversed order. At first instance, no particular order can be addressed as the optimal one, as a few studies have been made on the topic by now.

However, from the examples shown in the figures below, it can be inferred that the splitting technique presented in this work gives good results in several cases, where the one with reversed equations order proved to be numerically unstable or gave inconsistent results.

Reactive term solved last (3.2.2) Reactive Term solved first (Goisis and Osio 2011)

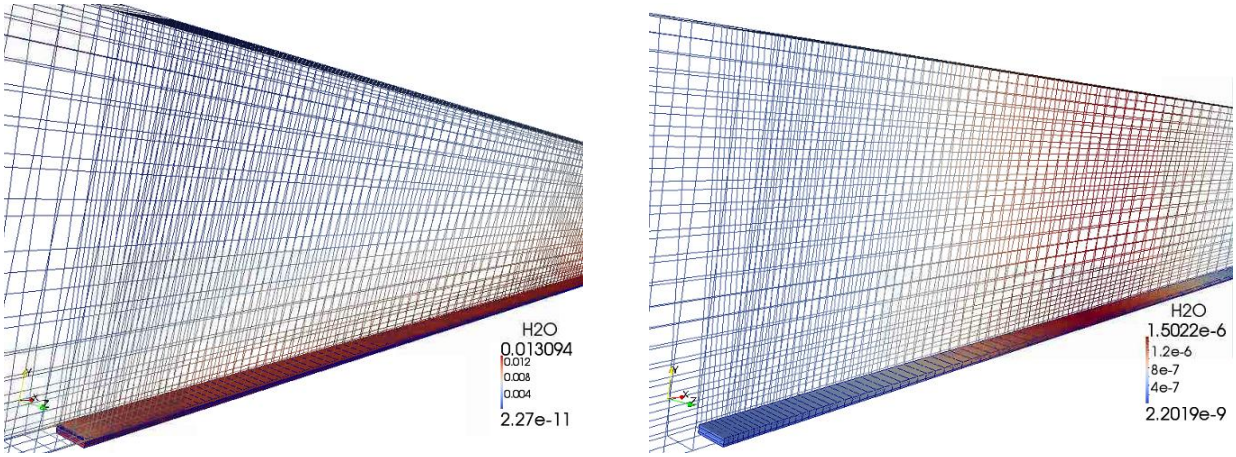

Fig. 4.25a – Annular reactor

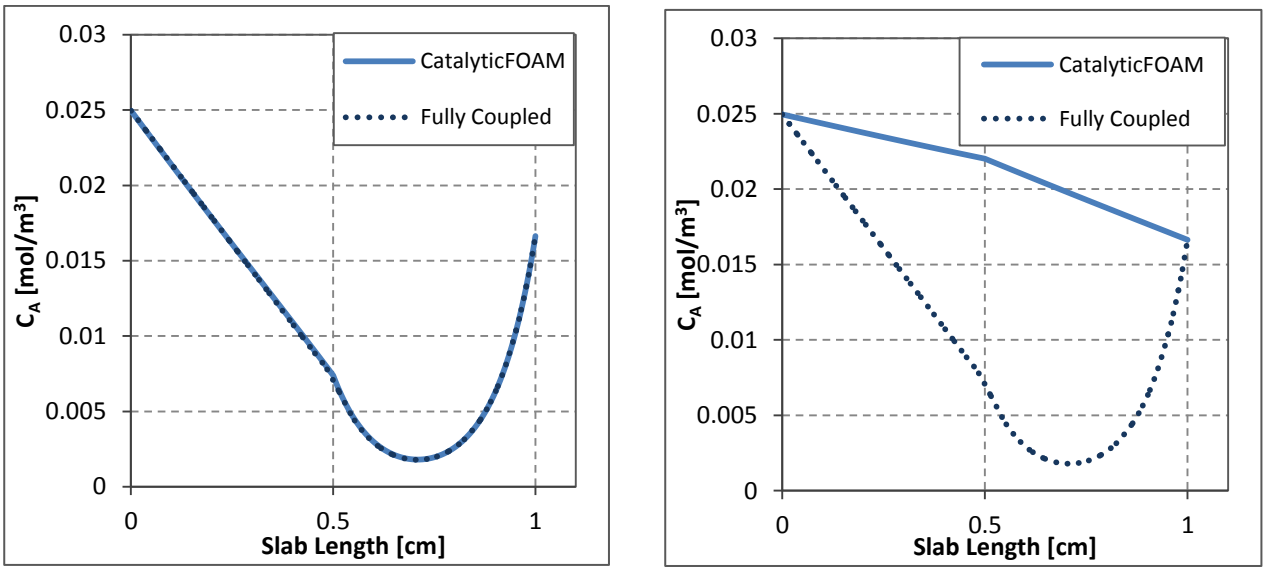

Fig. 4.25b – 1D diffusion with reaction case

The two couples of simulations, shown in figures 4.25a-b, are the results of identical cases (same mesh, same boundary and initial conditions) simulated with this work's splitting technique and the previous work's one (Goisis and Osio 2011).

Since the only difference between the results reported in the left column and the corresponding reported in the right column is the order equation within the splitting operator technique, it is clear the great importance it has when implementing an operator splitting algorithm: this does not imply that a different equation order from the one proposed leads necessarily to a wrong solution, but it shows evidence that the order proposed shows indeed a better numerical stability and accuracy in the same simulation conditions.

Confirmation of what has been stated above can be found in the literature (Sportisse, 2000), where the advantages of choosing the stiff operator as the last in the splitting order are pointed out. "[…] the operator sequence is crucial and the stiff operator has always to be last in splitting process. […]". This is mainly because "stiffness has a stabilizing effect and the local errors for fast species do not propagate".

For this reason the stiff operator needs to be located after the non-stiff one within the operator splitting, as shown in the splitting operator architecture proposed in 3.2.2. Further analysis is however required for a deeper insight in the problem.

4.4 Conclusions

The effectiveness of the operator splitting methodology for the staggered time step solution of the transport and reactive terms and the coupling strategy proposed has been tested through several cases, in which the solver solution in simple transport problems has been compared with the analytical stationary solution or with fully-coupled transient solutions. Moreover the feasibility of the complete numerical algorithm has been tested in cases of increasing complexity, which showed physically sound results for composition and velocity fields. Finally, the relevance of the correct operator splitting technique to assure numerical stability has been underlined through a series of specifically chosen test cases. In Chapter 5, the solver will be validated by comparison with experimental data.

Chapter 5

Experimental validations

In order to assess the reliability of the solver, it is now necessary to test its predictive ability.

First, a description of the system and the case setup is provided. Afterwards, a validation of the solver developed is presented, through a comparison between numerical results and experimental data. Further insight on the different regimes occurring in the system at different temperatures is given as well through an analysis of mass fraction profiles inside the catalytic layer. Finally, an analysis of the transient and steady state solutions of the system is provided.

5.1 Case setup and description

The test case selected is taken from (Maestri, Beretta et al. 2008). Maestri and co-workers developed a dynamic two-dimensional model of a catalytic annular reactor and validated it comparing model and experimental results. The analysis is performed by simulating a catalytic system whose behavior has been well described in the literature: short contact time hydrogen

combustion is performed under rich conditions (H2/O2/N2 = 4/1/95% v/v) in order to reproduce conditions similar to those of the partial oxidation of CH_4.

The surface reactivity has been accounted for using the detailed microkinetic model for H_2 combustion on Rh of Vlachos and co-workers has been used. This kinetic scheme consists of 18 reactions and 5 adsorbed species, and it is reported in Appendix B. Details on the kinetic schemes along with its experimental validations are provided in (Maestri, Vlachos et al. 2009).

The simulations were performed under isothermal conditions. A schematic representation of the catalytic reactor is given in Figure 5.1.

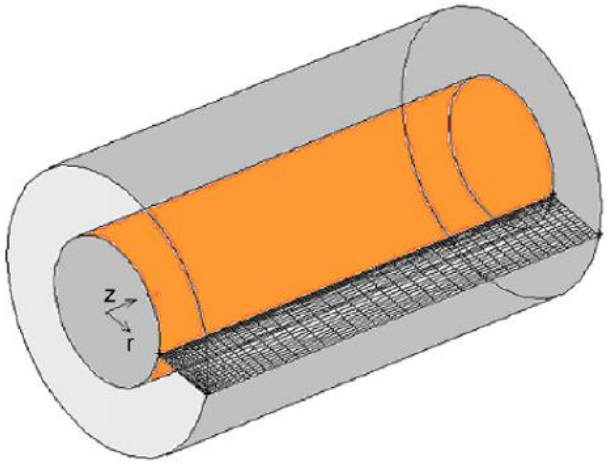

Fig. 5.1 - Sketch of the annular catalytic reactor, adapted from (Maestri, Beretta et al. 2008).

The Rh/α-Al_2O_3 catalyst is deposited over the surface of the inner wall of the reactor (colored in orange), forming a uniform and well adherent catalytic layer (1.5 cm long, 50 µm thick).

Operating conditions	
Inner radius	0.235 cm
Outer radius	0.450 cm
Reactor length	1.5 cm
Catalytic Layer Thickness	50 µm
O_2 mole fraction	0.01 (-)
H_2 mole fraction	0.04 (-)
N_2 mole fraction	0.95 (-)
Pressure	1 atm

Table 5.1 - Simulation parameters.

The operating conditions and the geometric parameters of the reactor are presented in Table 5.1 above. The ratio between catalytic area and effective reactor volume (V_{react}), described in session 2.1.1.2 is known and is called a_{cat}. In this case, its value was determined as 500 $\frac{m_{CAT}^2}{m_{REACTOR}^3}$, on the basis of H_2 and CO chemisorption experiments.

The spatial discretization of the geometrical domain was simplified in order to reach the steady state conditions with a smaller computational effort. Specifically, thanks to the symmetry of the annular reactor, it is possible to consider only one slice of this reactor. This is very convenient because this allows one to consider a 2D mesh instead of a 3D one. The 2D mesh is obtained considering the slice of a cylinder with a width of 5°. The number of required cells is thus 72 times lower than the one required for a 3D grid. A schematic view of the overall mesh is presented in the Figure5.2.

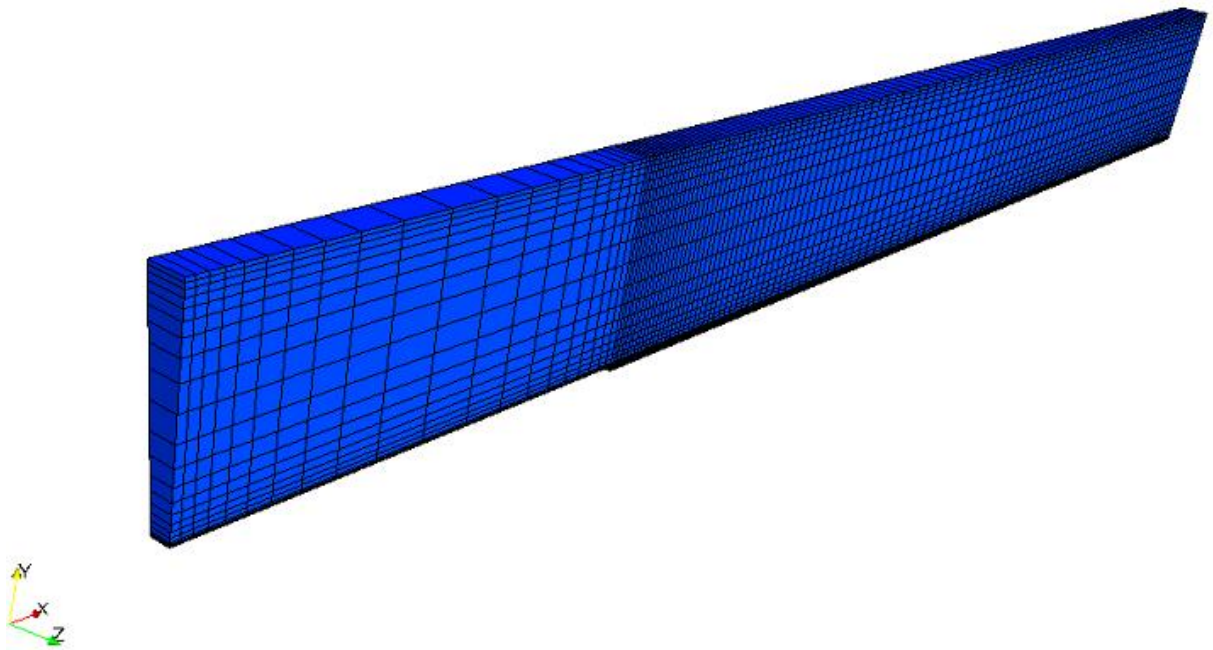

Fig. 5.2 - 2D mesh used for the numerical simulation.

As shown in Figure 5.2, the geometrical domain is divided in a series of cells by partitioning the axial and radial coordinates. In order to account for the presence of solid and gas phases, multiple meshes have been provided as described in Section 3.4: the simulations are performed over an optimized mesh for the fluid phase composed by 120 units in axial direction and 22 units in the radial one for an overall amount of 2640 cells, while for the solid phase the mesh is constituted by 120 units in the axial direction and 7 in the radial direction, for an overall amount of 840 cells.

In addition the grid is refined with a specific grading, i.e. the length of each cell of the mesh is not constant. The expansion ratio of the cells is calculated as the ratio among the length of the first and the last cell along one edge of a block. This enables the mesh to be graded, or refined, in specified directions for a specific factor. The introduction of a non-constant step grid allows one to describe certain areas of the system in a more detailed way.

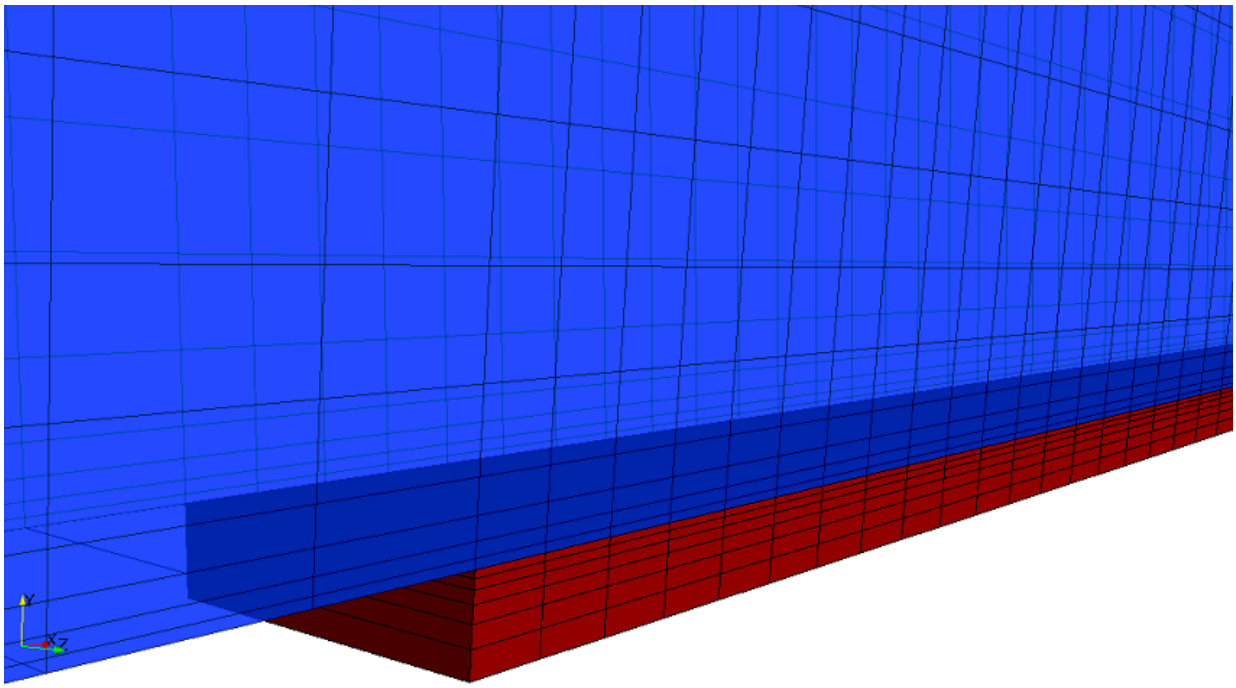

Fig. 5.3 - Importance of radial grading, specifically at the interface

In the case in point, this is particularly important because the zone close to the catalyst is interested by strong normal gradients, both from the fluid and from the solid side. The mesh is thus highly refined near the catalytic wall in the radial direction. A further grading was introduced in the axial direction to provide a proper description of the rapid consumption of reactants at the reactor inlet. Furthermore, particular attention has to be given to the cells dimensions at the coupled interface, in the sense that their size in the radial direction must not differ much from one side to the other in order for the coupling partitioned scheme to be numerically stable without the need of many PIMPLE loop iterations. This is shown in figure 5.3, where a particular of the mesh at the interface between the solid and fluid phase is provided. Further insight on mesh grading in the solid is given later in this chapter, when mass transfer regime conditions are investigated.

5.2 Comparison with experimental data

In this section the model results are compared with experimental data at different reactor temperatures **(**Maestri, Beretta et al. 2008**).** First, a brief description of the previous modeling results from the literature will be given. Then, the results simulated with the solver developed in this work will be shown, together with an analysis of concentration profiles in the fluid and solid phase, in order to assess the possible role of mass transfer limitations at the different temperatures investigated.

5.2.1 Modeling results from the literature

In figures 5.4a-b the red triangles are the experimental data points. The blue line represents the obtained conversions of O_2 at different temperatures. The green lines depict the numerical simulation reported in the reference article (Maestri, Beretta et al. 2008), while the blue line represents the modeling result of the previous thesis work (Goisis and Osio, 2011).

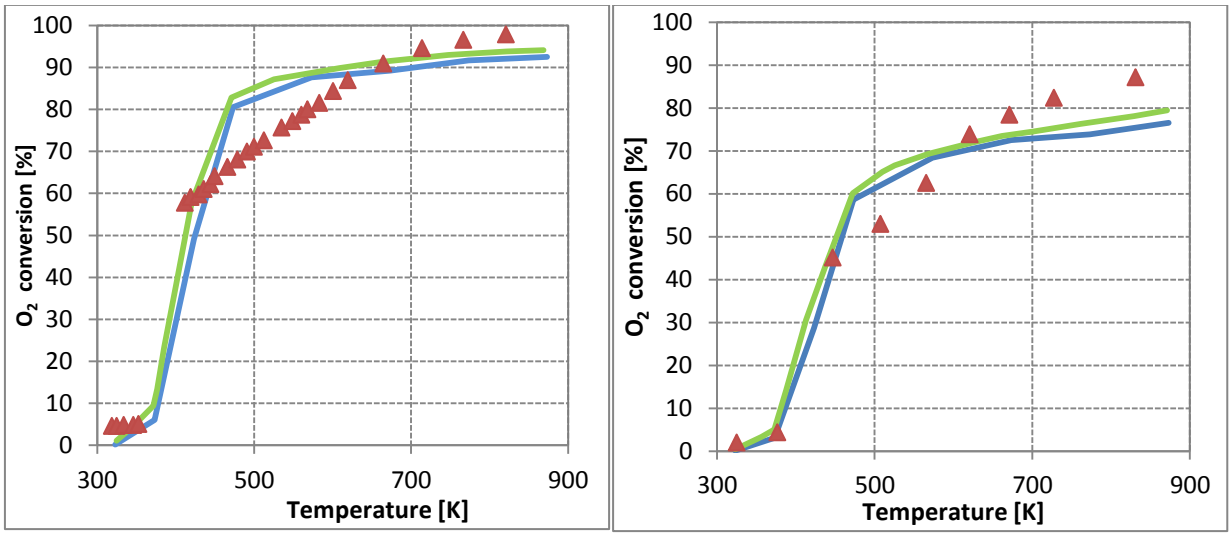

Figure 5.4 a-b. Conversion of O_2 vs. temperature at flow rate of 0.274 Nl/min and 0.578 Nl/min

The experimental data show that the combustion starts at about 373.15 K with a very low conversion of O_2. Then there is a rapid increase of the conversion of O_2 in a narrow range of temperatures. In the temperature range between 373.15 K and 573.15 K the system is then hypothesized to be in chemical regime. By increasing the temperature, the slope of the conversion profile decreases till the reaching of a plateau because of the establishment of the external diffusive regime. At this flow rate, the highest conversion is reached at about 773.15 K and is close to 100%. The model is able to reproduce the fast rise of conversion observed for temperatures just above 370 K, as well as the plateau observed at higher temperatures. Indeed the increase of the inlet velocity causes convective fluxes to grow at expenses of the diffusive flows and makes the oxygen conversion decrease consequently, being it limited by the fully external diffusive regime.

The models proposed overestimate the oxygen conversion at low temperatures and underestimates it at high temperatures. The reasons of these discrepancies are investigated in the following:

- ✓ The predicted conversion in the low temperature range is overestimated. As previously discussed, the system is supposed to be in chemical controlled regime in that range of

temperatures. Since both models (Maestri et. al 2008, Goisis and Osio 2011) are not able to describe intra-porous diffusion processes, the computed conversion is higher than the real one.

- ✓ The numerical solution qualitatively follows the trend to a plateau but does not reach the measured value. Indeed, from the previous plots it is noticeable that the experimental data show an enhanced conversion with respect to the model predictions. The reasons of this discrepancy in the high temperature range are discussed by Maestri and co-workers (Maestri et. al 2008): the main hypothesis is that Rh evaporation and redeposition downstream the catalytic bed occurred. This brought to the creation of zones of low catalytic activity outside the catalytic bed. Even if at low temperatures these contributions are negligible, at higher temperatures a rise of the oxygen conversion is observable.

Both the addressed discrepancies from the experimental data are discussed in the next paragraph, employing this time the solver developed in this work, namely `CatalyticFOAM-multiRegion`.

5.2.2 CatalyticFOAM-multiRegion Results

The new architecture developed in Chapter 3 allows the solver proposed in this work to model intra-phase phenomena in both gas and solid phase, as well all inter-phase phenomena between them. This allows taking into account diffusive limitations inside the catalyst, which was not possible to consider in previous works, where the catalyst morphology was neglected (Goisis and Osio 2011, Maestri et al. 2008).

First, the catalyst has been modeled with an infinite diffusion coefficient, in order to reproduce the case without any diffusive limitations as proposed in the literature. Afterwards, a sound value for diffusivity inside the solid volume has been chosen according to the correlations shown in table 3.1, selected to be 1/20 of the computed value for the compound in the gas mixture present inside the solid pores. According to this value it has been possible to reproduce the experimental data in the low temperature range, as shown in figure 5.5 below:

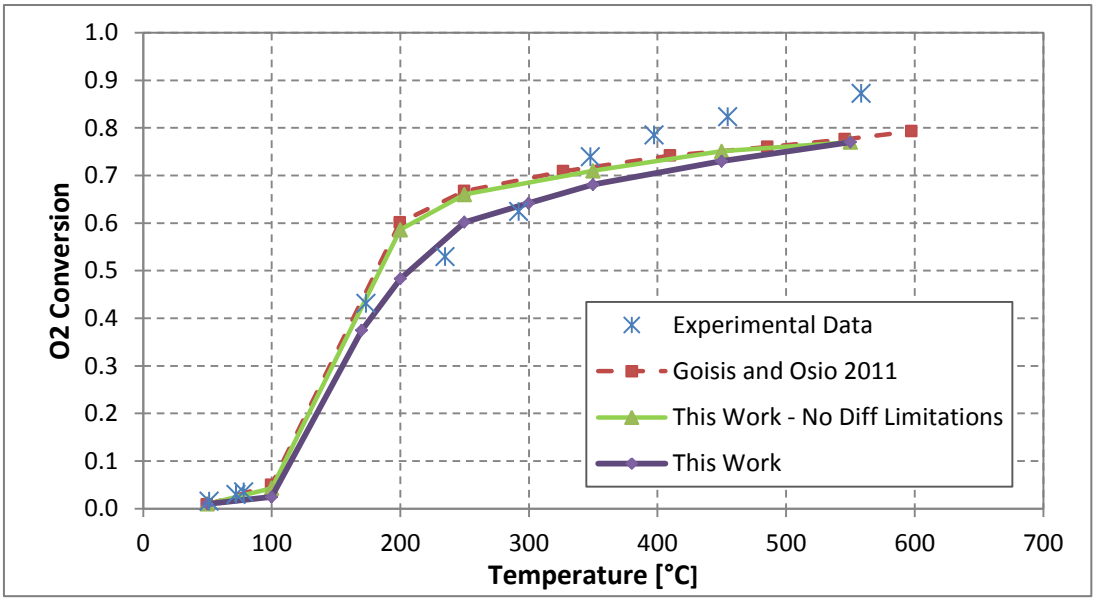

Fig. 5.5 -. Conversion of O2 vs. temperature for a flow rate of 0.578 Nl/min

The model shows a good agreement with the one of the previous work by Goisis and Osio (2011) when an infinite value for the diffusivity in the solid catalytic phase is considered, thus reproducing the external mass transfer limit at high temperatures and the measured conversion profile at low temperatures, but overestimating the experimental data in the medium temperature range.

On the other hand, it is possible to notice that the `catalyticFOAM-multiRegion` model is capable of satisfactorily predicting the conversion profile even in the medium temperature range when a reduced diffusion coefficient in the solid phase is taken into account, still getting the same values of conversion in the high and low temperature ranges. This gives evidence of the importance of diffusive limitations in the solid phase in the system considered: further investigation on the concentration profiles along the catalytic layer width is given in section 5.4.1, confirming the influence of different regimes on the conversion profiles observed.

When a lower flow rate is considered (0.247 Nl/min), the model still fits perfectly the experimental data in the low temperatures range, while the discordance with previous work simulations is higher because of the reduced flow itself. Without modeling intra-phase phenomena occurring inside the 50 µm thick catalytic layer, the solver predicted a fast transition from a chemically controlled regime to an inter-phase mass transfer controlled regime around 200°C. On the other hand, it is evident from figure 5.6 below the importance that modeling of these phenomena has in order to reproduce the actual physical behavior of the system. Further analysis on concentration

profiles in both the fluid and solid phase across different regimes has been made later in the chapter.

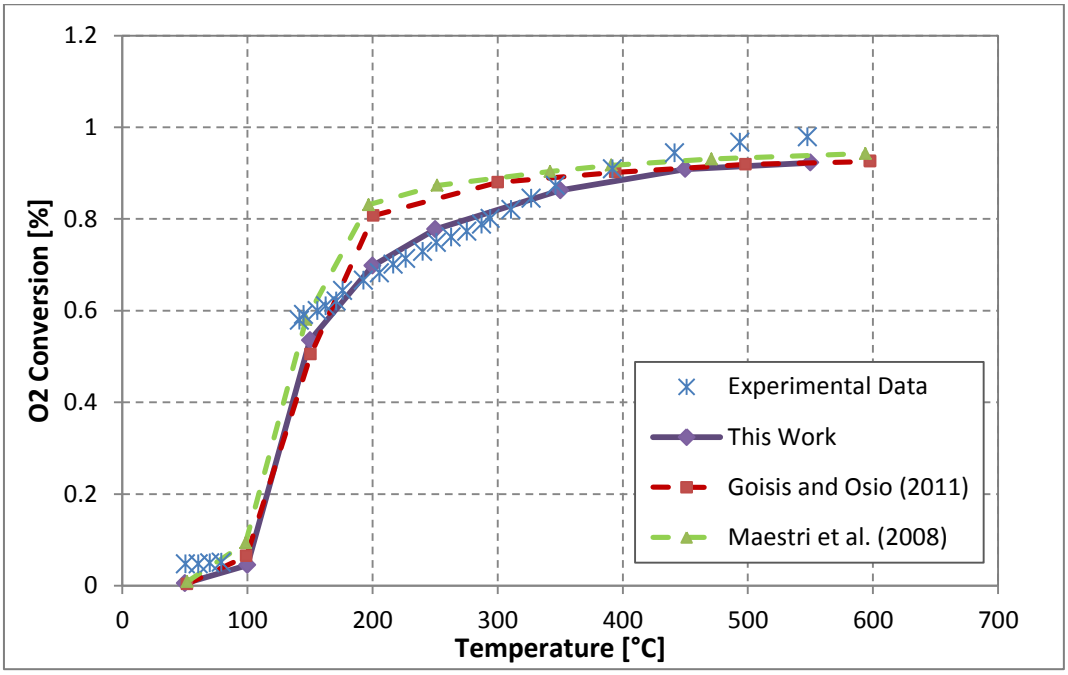

Fig. 5.6 - Conversion of O2 vs. temperature for a flow rate of 0.247 Nl/min

It is then possible to investigate also the underestimation of conversion values occurring at high temperatures: as discussed by Maestri et al. (2008), the "conversion enhancing mechanism" observed in the experimental data cannot be due to homogeneous gas phase chemistry playing a role at high temperatures, as the fraction of H* which is predicted to desorb in the gas phase at 500°C is many orders of magnitude lower than the one identified as necessary to trigger gas-phase chemistry. However, as mentioned previously in the chapter, an alternative hypothesis for this has been formulated (Maestri, Beretta et al.2008), involving the creation of zones of low catalytic activity outside the catalytic bed.

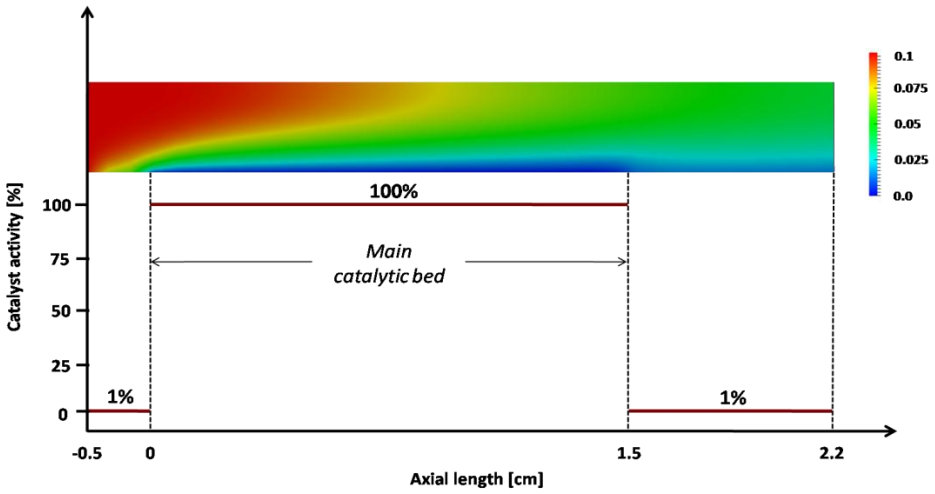

Fig. 5.7 - Activity of the catalytic bed vs. axial reactor length.

The previous hypothesis is investigated by considering the two sections with low catalytic activity upstream and downstream the catalytic bed, as shown in figure 5.7. A catalyst layer of 0.2 cm is then added upward the main bed. Another one is added downstream, with a length of 0.7 cm. The catalytic activity of these beds is lowered to 1% of that of the main bed. In figure 5.8 the effect of this hypothesis is shown.

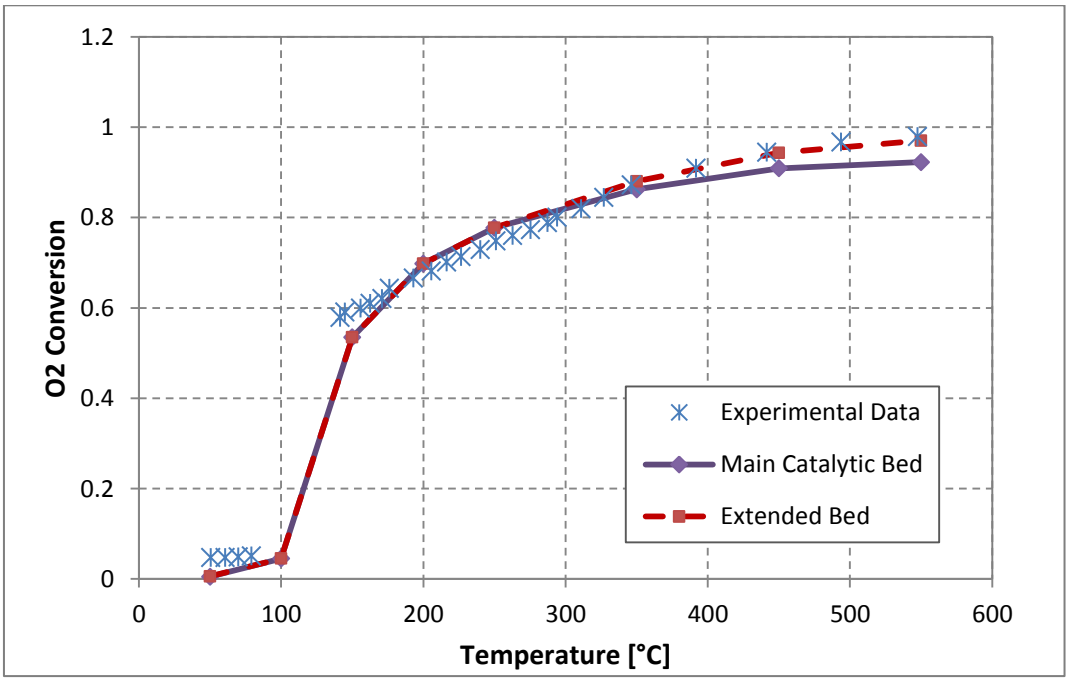

Fig. 5.8 - O_2 conversion vs. temperature for different catalytic bed at 0.274Nl/min.

The additional low activity sections beside the main bed, which work in chemical regime due to the low amount of catalyst (Maestri, Beretta et al. 2008), lead to an increase of conversion. At low temperatures, on the other hand, the contribution is almost negligible. Together with the effect of modeling of intra-phase phenomena embedded in the developed solver, this produces a perfect agreement with the experimental data in the whole range of temperatures considered. The simulations performed at 0.548 Nl/min show the same good agreement with the experimental data.

5.2.1 Chemical, diffusive and external mas transfer regimes

As can be inferred from the previous analysis, one of the most important features related to the modeling of the chosen system is the transition between different controlling regimes in different temperature conditions. In particular, the conversion plots below show a range in which a chemical-controlled regime holds, from 423 K to approximately 523 K, and a progressive transition to a purely mass-transfer controlled regime at higher temperatures. In order to provide further insight on these regimes, oxygen mass fraction profiles along the radial direction of the reactor taken at the outlet zone inside the solid layer are hereby shown (fig.5.9):

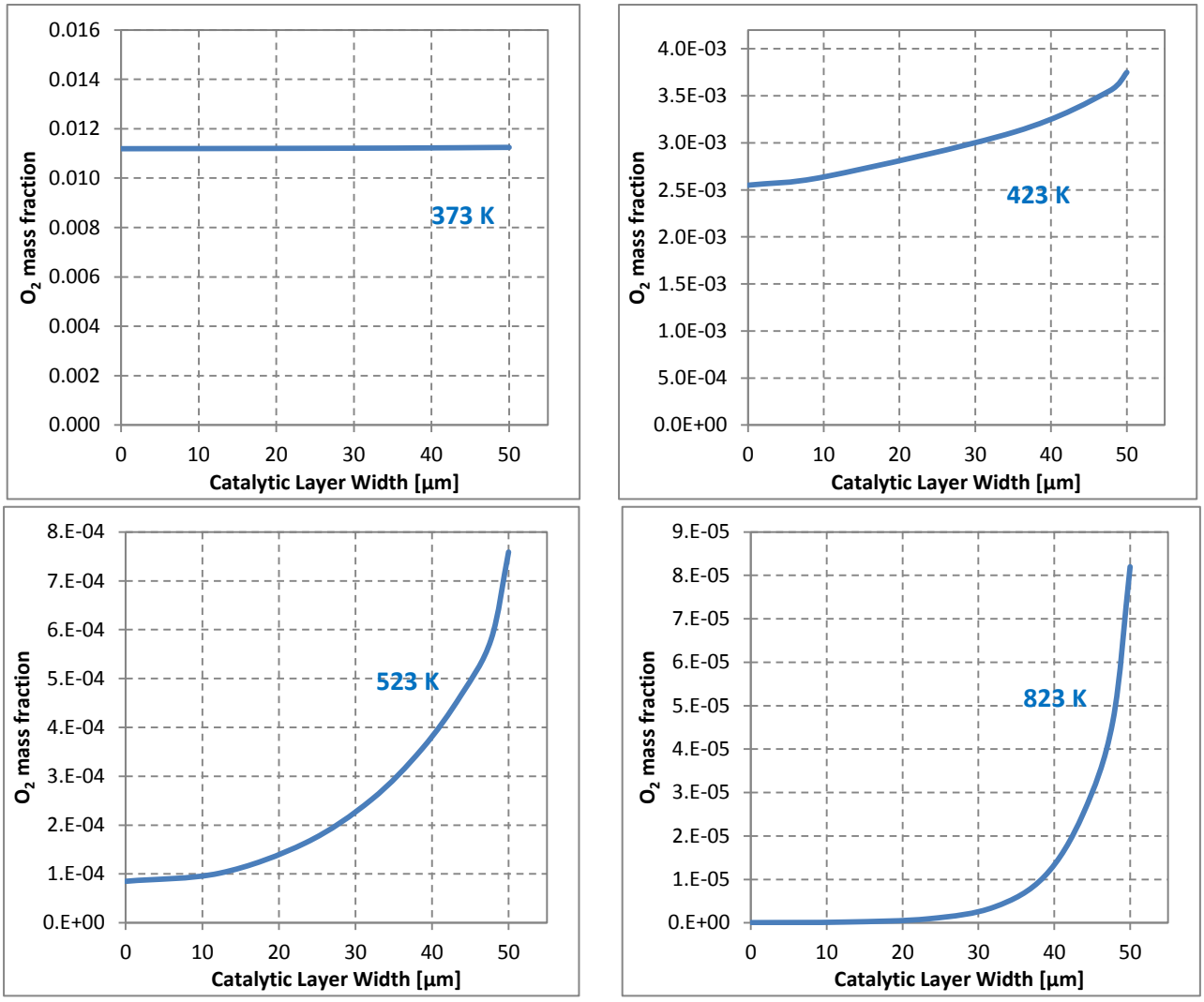

Fig. 5.9 - O_2 mass fraction along radial reactor direction in the solid phase at different temperatures

It is thus possible to confirm the strong influence of diffusive intra-phase limitations inside the 50 µm thick catalytic solid phase in the middle range of temperatures, making the actual profile of conversion lower than the one predicted by previous works (Maestri et al. 2008, Goisis and Osio 2011). In chemical-controlled regime, the heterogeneous reaction is the rate determining step and there is a slight drop in reactant concentration inside the solid phase due to intra-phase diffusive limitations, correctly predicted by the solver developed as seen in the previous paragraph. At higher temperatures, on the other hand, the oxygen mass fraction profile follows a steep decrease immediately after the surface of the catalytic layer, making its fraction practically zero after the first few micrometers of the layer. This happens because the diffusive phenomenon becomes the rate determining step.

An important issue related to the representation of the profiles shown in figure 5.10 is the mesh refinement inside the catalytic solid. The presence of strong gradients in a few micrometers of thickness close to the surface of the catalytic layer make it necessary for the mesh to be very detailed in that zone in order to reproduce the profiles shown before. On the contrary, if the chosen mesh is not enough refined in this zone, the mass transfer regime cannot be described properly.

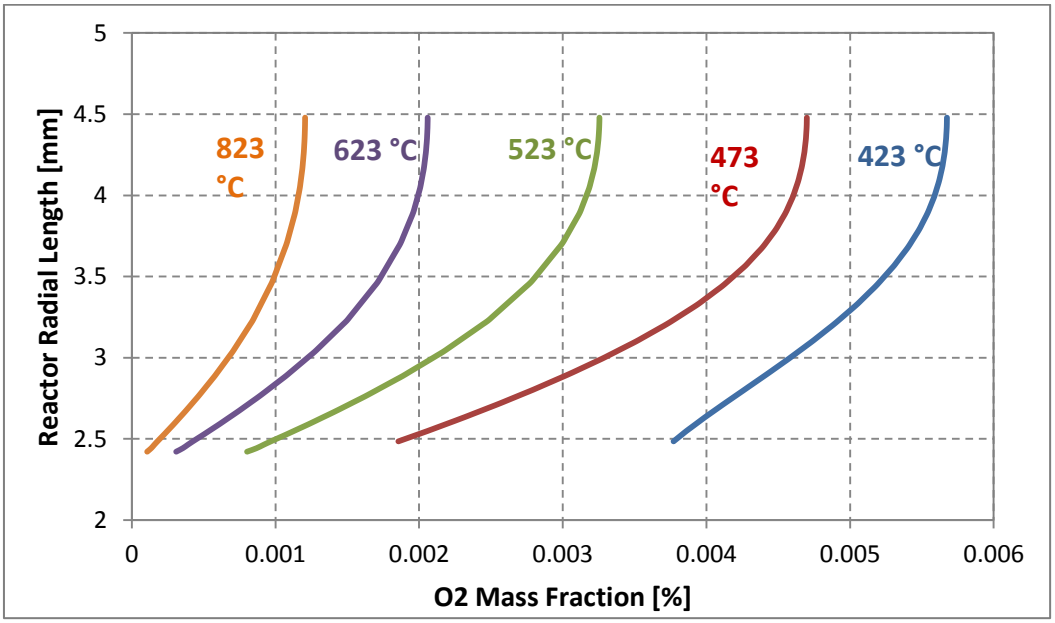

Figure 5.10 - O_2 mass fraction along radial reactor direction at different temperatures

On the other hand, the mass fraction profiles in the fluid phase are characterized by lower gradients and do not require at first instance a very refined mesh: nevertheless, as discussed previously in section 5.1, it is important for the cells on both sides of the interface to have similar dimensions: in the fluid cells close to the solid-fluid interface a geometrical subdivision as refined as their solid counterparts is required, in order to assure numerical stability of the coupling procedure adopted and described in section 3.6.

5.3 Transient and steady-state analysis

In this section an analysis of the dynamic behavior of the reactor start-up is described, providing both steady-state concentration profiles and an insight on the Rate Determining Step (RDS) of the considered kinetic mechanism. Initially, the reactor is filled with N_2 at the operating temperature of 523 K. The other operating parameters are reported in Table 5.1. The reacting mixture is

continuously fed into the reactor with a flow rate of 0.274Nl/min. The ignition of the mixture is instantaneous and the steady-state is achieved in about 200 ms.

The velocity profile is completely developed after 60 ms (fig. 5.11), as shown in Figure 5.4: this represents the steady state condition for velocity. Of course within the solid phase the velocity field is null everywhere.

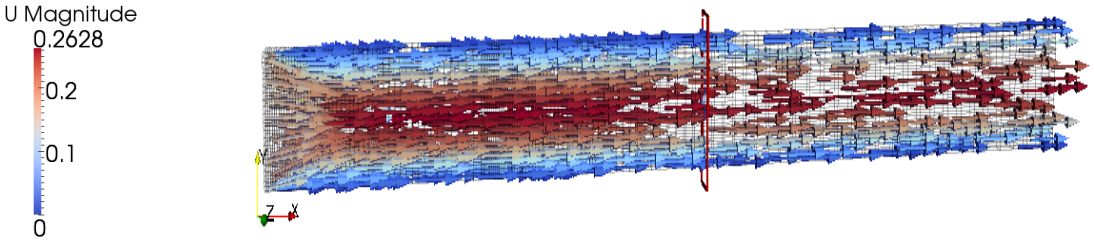

Fig. 5.11 - Velocity magnitude [m s^{-1}]profiles at 523.15 K at 60 ms.

In Figure 5.12 the O_2 profiles at different times are reported. The catalytic layer is located in the lower part of the figures as a 50 µm thick solid layer.

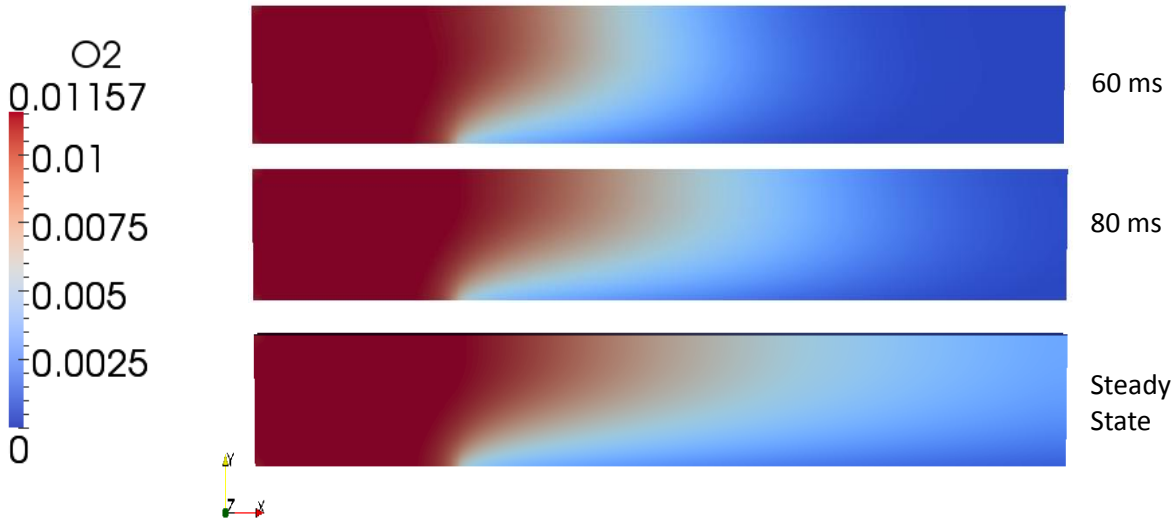

Fig. 5.12 - O_2 mass fraction profiles at 0, 2 and 15 ms at 523.15 K.

In the very first part of the reactor near the catalyst an abrupt decrease of O_2 concentration is observed. This reveals the presence of strong axial composition gradients.

Furthermore, it is possible to notice the formation of a boundary layer in which the O_2 is quickly consumed. The layer is established as soon as the reactants approach the catalyst and the reactions occurring inside the solid phase create axial and radial gradients.

In fig. 5.13 the detail of O_2 mass fraction inside the solid phase is shown: it is possible to notice the oxygen mass fraction gradient inside the solid thin layer.

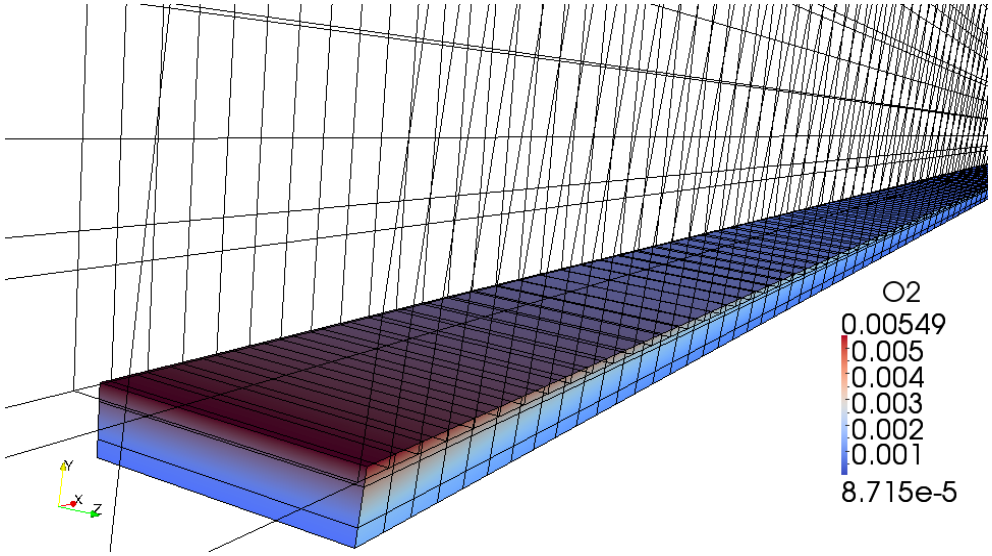

Fig. 5.13 - O_2 mass fraction profiles at 60 ms at 523.15 K in the catalytic layer.

The non-uniform profile inside the solid phase is created by the mass transfer and reaction equations solved inside the solid phase, able to represent intra-solid diffusive limitations.

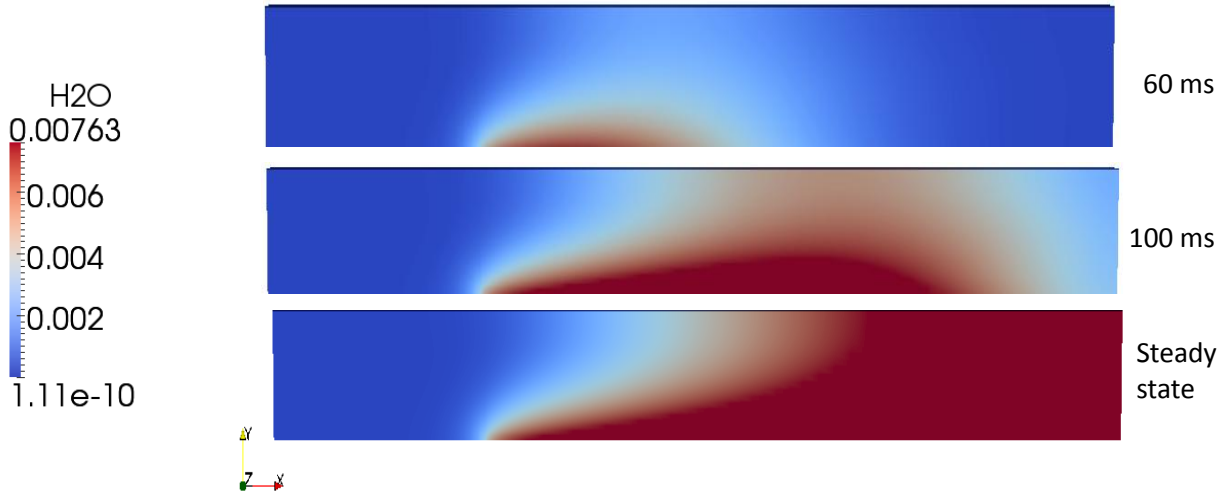

Fig. 5.14 – H2O mass fraction profiles at 60, 100 ms and Steady State at 523.15 K in solid phase

In Figure 5.14 the profiles of H_2O are reported. It can be observed that the H_2O mole fraction has an opposite behavior with respect to the reactants profiles, both for the fluid phase and for the solid phase. After 60 ms the formation of the boundary layer can be observed.

As soon as the reactants enter the reactor, H_2O formation is predicted. This can be also observed in Figure 5.15, where the H_2O profiles inside the solid phase are shown.

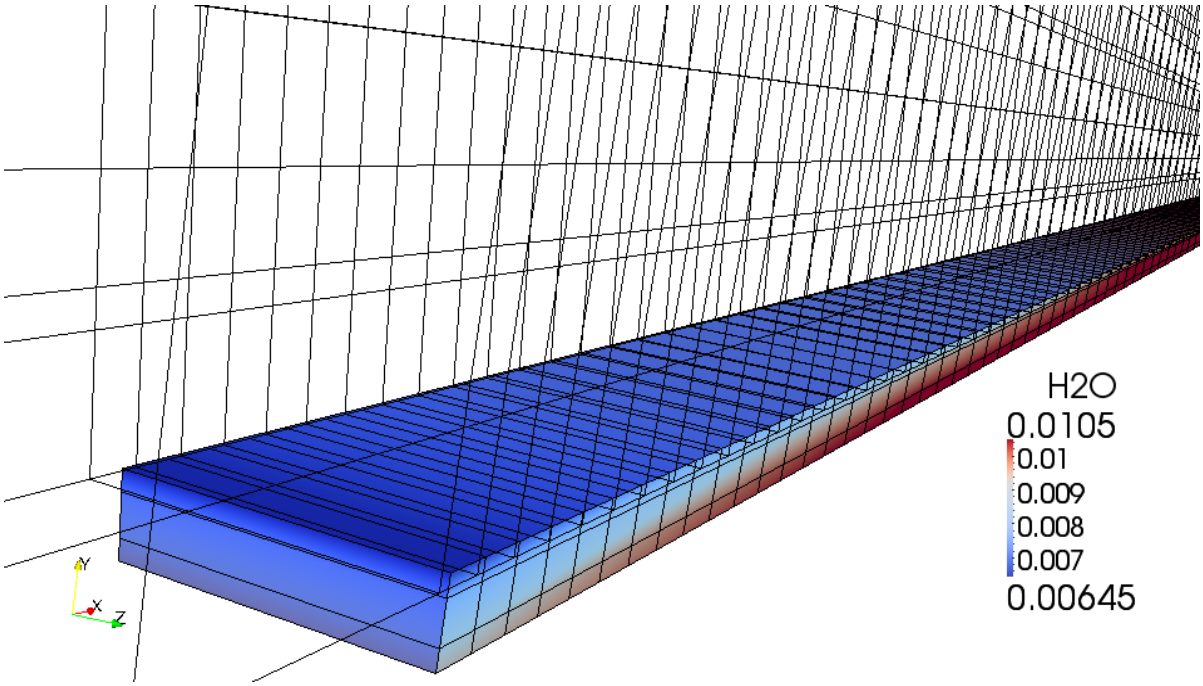

Fig. 5.15 – H2O mass fraction profiles at 523.15 K in the catalytic layer

It is clear that reactants (such as O2) should have higher mass fraction values along the solid/fluid interface than in the internal part of the volume, while products (as shown in fig. 5.8) have higher mass fraction values inside the volume. The lower product concentration along the fluid-solid interface is due to the continuous contact of this surface with fresh, reactant-rich fluid which creates a radial gradient in product concentration enhancing water retro-diffusion in the fluid phase. This last phenomenon does not occur in the internal solid cells.

The analysis proceeds by observing the coverage profiles on the catalyst surface inside the solid phase. In Figure 5.16 the profiles of adsorbed species and free site fraction along the axial reactor coordinate are reported taken at half width of the solid catalytic layer. A fast adsorption of species on the catalytic surface at the very beginning of the reactor can be noticed. In fact, the free site fraction is lower at the beginning of the reactor (higher concentration of adsorbed species) than at the end, and has a relatively low value.

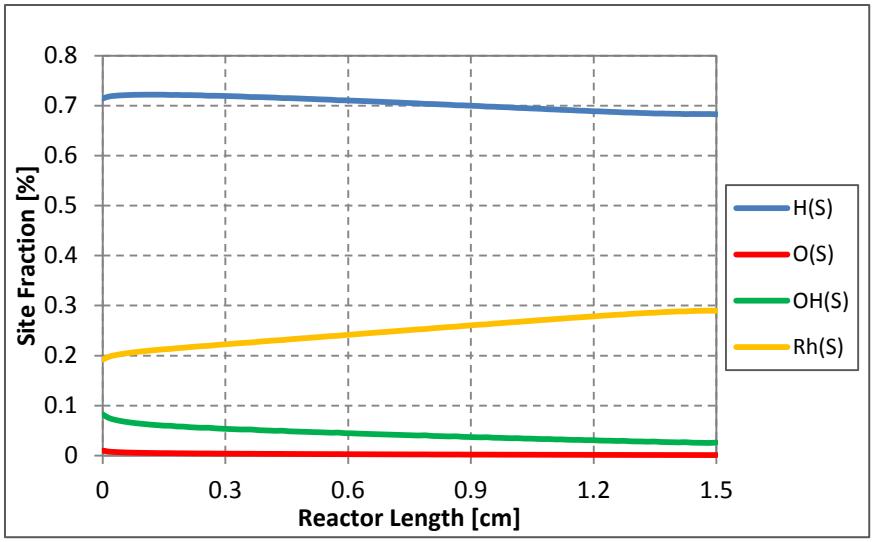

Fig. 5.16 – Site species axial distribution(y = 25 µm, T = 523 K)

The Most Abundant Reaction Intermediate (MARI) is the H(S) as shown in Figure 5.16. The accumulation of this species on the catalyst indicates the presence of a bottleneck in the reaction mechanism. On the other hand, within the same graph, it is possible to notice that the amount of O* on the catalyst is very low.

Since the model provides a detailed description of the solid phase, it is also possible to plot the adsorbed species mass fractions profiles along the solid thickness: similarly to H_2 mass fraction, H(S) is lower near the solid-fluid interface than inside the solid volume. This happens because the continuous flowing in the fluid phase enhances species desorption in that area. By consequence, free sites fraction is higher near the interface.

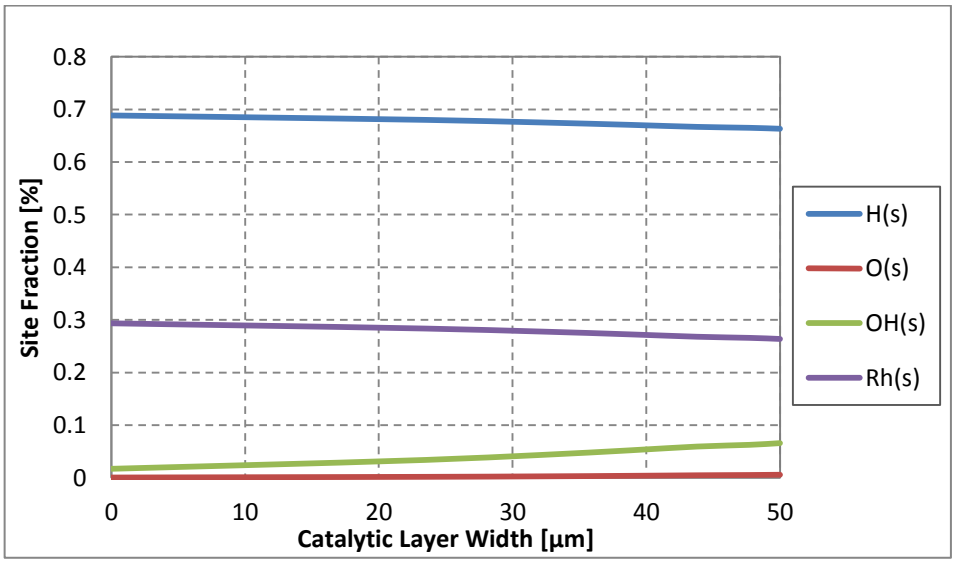

Fig. 5.18 - Intra-solid radial profiles. (y = 25 µm, T = 523 K)

5.4 Conclusions

In this chapter, a validation of the solver developed has been presented through a comparison between the numerical results and the experimental data. In particular, the importance of the description of intra-phase phenomena inside the catalytic solid phase has proven to be critical in order to accurately predict conversion profiles in the considered system. The capability of the solver to describe inter-phase phenomena and intra-phase phenomena in both the solid and the fluid phase allows the model to properly describe the experimental data.

Conclusions

In this work catalyticFOAM, a solver for the detailed simulation of gas-solid catalytic reactors based on a microkinetic description of surface chemistry has been extended to describe in detail phenomena occurring within the solid (catalytic) phase. This allows for the descriptions of systems where heat and mass transfer limitations inside the catalytic phase can play a role, and intra-catalyst phenomena cannot be neglected.

In order to make possible the solution of different equations in different domains with their own properties, a multiple-meshes/multiple-region structure has been developed, allowing the characterization of intra-phase phenomena in both the catalytic solid phase and the gas phase.

A segregated approach has been adopted for taking into account inter-phase phenomena occurring between different phases, involving an iterative algorithm for coupling neighboring regions. At this scope, new libraries have been coded which allow for coupling at the interface to be automatically implemented during the computation. A new numerical framework has thus been proposed, capable of describing both intra-phase phenomena in the fluid and solid regions and inter-phase phenomena occurring between them. The possibility to investigate systems with geometries of arbitrary complexity, considering an arbitrary number of different regions with their own equations and properties, confers generality and flexibility to the solver.

The effectiveness of both the segregated coupling strategy proposed and the operator splitting methodology for the solution of the transport and reactive terms have been tested through several cases, in which the solver solution in simple transport problems has been compared with the analytical solution or with a fully-coupled solution. Moreover the feasibility of the complete numerical algorithm has been tested in cases of increasing complexity, which showed physically sound results for composition and velocity fields.

Finally, the reliability and predictive capability of the developed solver have been tested by comparing the numerical results with the experimental data. In particular, the importance of the description of intra-phase phenomena inside the catalytic solid phase has proven to be critical in order to accurately predict conversion profiles in the catalytic system considered. The capability of the solver to describe inter-phase phenomena and intra-phase phenomena in both the solid and

the fluid phase allows the model to satisfactorily fit the experimental data, representing a breakthrough with respect to the literature. The results highlight the great generality and flexibility of the catalyticFOAM solver.

Future developments deal with improving the reliability and applicability of catalyticFOAM, specifically:

- ✓ Improvement of computational efficiency of the code in order to reduce the simulation time, which can be high in the simulation of complex geometries or kinetic schemes
- ✓ Extension of the code parallelization, already present in the mono-region version of catalyticFOAM, to the multi-region version of the solver.

Appendix A

In this section the derivations of conservation equations of mass and energy for a batch reactor are provided.

A1. Total mass conservation

The expression of the total mass balance for a batch reactor can be written as:

$$\frac{dm_{tot}}{dt} = \sum_{i=1}^{NC} \frac{dm_i}{dt} \qquad (A.1)$$

Splitting the source term in the homogeneous and heterogeneous terms:

$$\sum_{i=1}^{NC} \frac{dm_i}{dt} = V_{react} \sum_{i=1}^{NC} \hat{R}_i^{hom} MW_i + A_{cat} \sum_{i=1}^{NC} \tilde{R}_i^{het} MW_i \qquad (A.2)$$

Where NC indicates the number of species , $\hat{R}_i^{hom}$is the consumption/production rate of the i-th specie due to homogeneous reactions in $\left[\frac{mol}{m_{react}^3 s}\right]$, $\tilde{R}_i^{het}$is the consumption/production rate of the i-th specie due to heterogeneous reactions in $\left[\frac{mol}{m_{cat}^2 s}\right]$, $V_{react}$is the reactor volume in $m_{react}^3$and $A_{cat}$the total catalytic surface in m_{cat}^2.

In order to express the area of the catalytic surface of each computational cell, the parameter $a_{cat}$is introduced, defined as the specific catalytic area per unit of reactor volume:

$$\alpha_{cat} = \frac{A_{cat}}{V_{react}} \; in \; [m^{-1}] \qquad (A.3)$$

Since the sum of production rates in the gas phase is zero, the equation can be written as:

$$\frac{dm_{tot}}{dt} = \sum_{i=1}^{NC} (a_{cat} V_{react} \tilde{R}_i^{het} MW_i) = a_{cat} V_{react} \sum_{i=1}^{NC} \tilde{R}_i^{het} MW_i \qquad (A.4)$$

A2. Species mass conservation

The generic expression for the mass balance of the *i*th species is defined as the accumulation (derivative of mass over time) equal to the net mass flow (inlet minus outlet mass flows) plus the mass generation due to the reactions (R_i). The mathematical formula is:

$$\frac{dm_i}{dt} = m_i^{IN} - m_i^{OUT} + R_i V_{react} \qquad (A.5)$$

The inlet and outlet mass flows are neglected because we adopt a batch reactor model, i.e. the system is thermodynamically closed. Splitting the reaction term into homogeneous and heterogeneous, and considering a generic catalytic cell in which both homogeneous reactions in the gaseous pores and heterogeneous reactions on the catalytic surface occur:

$$\frac{d(m_{tot}\omega_i)}{dt} = \omega_i \frac{dm_{tot}}{dt} + m_{tot} \frac{d\omega_i}{dt} = \tilde{R}_i^{hom} MW_i V_{react} + a_{cat} V_{react} \tilde{R}_{ik}^{het} MW_i \qquad (A.6)$$

Recalling the expression for the total mass balance derived in section A.1:

$$\frac{d\omega_i}{dt} = \frac{\tilde{R}_i^{hom} MW_i V_{react}}{m_{tot}} + \frac{a_{cat} V_{react} \tilde{R}_{ik}^{het} MW_i}{m_{tot}} - \frac{\omega_i}{m_{tot}} a_{cat} V_{react} \sum_{i=1}^{NC} \tilde{R}_{ik}^{het} MW_i \qquad (A.7)$$

Introducing the density:

$$\frac{d\omega_i}{dt} = \frac{\tilde{R}_i^{hom} MW_i}{\rho_{mix}\varepsilon} + \frac{a_{cat}\tilde{R}_{ik}^{het} MW_i}{\rho_{mix}\varepsilon} - \frac{\omega_i}{\rho_{mix}\varepsilon} a_{cat} \sum_{i=1}^{NC} \tilde{R}_{ik}^{het} MW_i \qquad (A.8)$$

Grouping the surface terms:

$$\frac{d\omega_i}{dt} = \frac{\tilde{R}_i^{hom} MW_i}{\rho_{mix}\varepsilon} + \frac{1}{\rho_{mix}\varepsilon}\left(a_{cat}\tilde{R}_{ik}^{het} MW_i - \omega_i a_{cat} \sum_{i=1}^{NC} \tilde{R}_{ik}^{het} MW_i \right) \qquad (A.9)$$

The final expression for the mass conservation of the ith species is:

$$\frac{d\omega_i}{dt} = \frac{\tilde{R}_i^{hom} MW_i}{\rho_{mix}\varepsilon} + \frac{a_{cat}}{\rho_{mix}\varepsilon}\left(\tilde{R}_{ik}^{het} MW_i - \omega_i \sum_{i=1}^{NC} \tilde{R}_{ik}^{het} MW_i \right) \qquad (A.10)$$

A3. Energy conservation equation

The equation for the energy conservation in a batch reactor is written as follows

$$\frac{dH_{tot}}{dt} = 0 \qquad (A.11)$$

The total enthalpy of the system is expanded as follows:

$$H_{tot} = \sum_{i=1}^{NC} m_i \, \widehat{H}_i \qquad (A.12)$$

By consequence, for the primary derivation rules:

$$\frac{dH_{tot}}{dt} = \frac{d(\sum_{i=1}^{NC} m_i \, \nu_i \widehat{H}_i \,)}{dt} = \sum_{i=1}^{NC} \frac{d(m_i \nu_i \widehat{H}_i \,)}{dt} = \sum_{i=1}^{NC} m_i \frac{d(\nu_i \widehat{H}_i \,)}{dt} + \sum_{i=1}^{NC} H_i \frac{dm_i}{dt} = \qquad (A.13)$$

Expressing the enthalpy variation with differentials with respect to pressure, temperature and composition, it becomes:

$$\sum_{i=1}^{NC} m_i \frac{\partial(\nu_i \widehat{H}_i\ )}{\partial T}\frac{dT}{dt} + \sum_{i=1}^{NC} m_i \frac{\partial(\widehat{H}_i\ \nu_i)}{\partial p}\frac{dp}{dt} + \sum_{i=1}^{NC} m_i \frac{\partial(\nu_i \widehat{H}_i\ )}{\partial \omega_i}\frac{d\omega_i}{dt} + \sum_{i=1}^{NC} \nu_i H_i \frac{dm_i}{dt} = \qquad (A.14)$$

Since the Joule-Thomson effect is considered neglectable ($\frac{\partial \widehat{H}_i}{\partial p}$=0) and the mixture is considered to be ideal, ($\frac{\partial \widehat{H}_i}{\partial \omega_i} = 0$), and being $\frac{\partial \widehat{H}_i}{\partial T} = C_{p,i}$, then the expression becomes:

$$\sum_{i=1}^{NC} m_i C_{p,i} \frac{dT}{dt} + \sum_{i=1}^{NC} \nu_i H_i \frac{dm_i}{dt} = 0 \qquad (A.15)$$

By consequence:

$$\sum_{i=1}^{NC} m_i C_{p,i} \frac{dT}{dt} = -\sum_{i=1}^{NC} \nu_i H_i \frac{dm_i}{dt} \qquad (A.16)$$

It is possible to express the term $\frac{dm_i}{dt}$ following the mass species conservation above, considering that in the generic solid cell both homogeneous reactions and heterogeneous can happen:

$$\sum_{i=1}^{NC} m_i C_{p,i} \frac{dT}{dt} = -(\sum_{i=1}^{NC} \nu_i \widehat{H}_i^{hom} \tilde{R}_i^{hom} MW_i V_{react} \varepsilon + \nu_i \widehat{H}_i^{het} \tilde{R}_i^{het} MW_i V_{react} a_{cat}) \qquad (A.17)$$

And remembering the definition of reaction enthalpy:

$$\sum_{i=1}^{NC} m_i C_{p,i} \frac{dT}{dt} = -\left(\Delta \widehat{H}_R^{hom} \tilde{R}^{hom} MW_{mix} V_{react} \varepsilon + \Delta \widehat{H}_R^{het} \tilde{R}^{het} MW_{mix} V_{react} a_{cat}\right) \qquad (A.18)$$

which expresses the temperature evolution in time.

Appendix B

In this Appendix the kinetic schemes used for the numerical simulations described in the previous chapters are provided.

H_2 over Rh in UBI-QEP format

The UBI-QEP heterogeneous kinetic scheme of H_2 over rhodium catalyst from (Maestri, Vlachos et al. 2009) is provided in this section. This detailed microkinetic model is able to predict integral data of multiple processes. The parameters of the reaction mechanism been derived according to a multi-scale methodology: activation energies are predicted using the UBI-QEP theory, coverage effects are accounted for using Density Functional Theory(DFT), and pre-exponentials are calculated using transition state theory (TST).

In the input file reported the reactions are written in sequence, followed by the turn over frequency A (unitless and s^{-1}), the exponential beta (-), the bond index (-), the temperature dependence (-), the type of kinetic method (UBI) and the type of reaction. All these parameters are required in order to compute the reaction rates.

```
MATERIAL MAT-1
!*****************************************************************
SITE/RH_SURFACE/    SDEN/2.49E-9/
    Rh(s)   H2O(s)  H(s)    OH(s)   O(s)   OH(s) H2O(s)
END
!*****************************************************************
HEATS_OF_CHEMISORPTION / 300 /
    O(s)   /      1.5   /     100.0  /    O(s)  -26                    //
    H(s)   /      1.5   /     62.3   /    H(s)  -2.5                   //
    OH(s)/  2.0   /     70.0   /    O(s)  -33   /     H2O(s)  25  //
    H2O(s) /      2.5   /     10.8   /    OH(s) 25    /     H2O(s) -4.5 //
END
```

```
!****************************************************************
REACTIONS
H2      +Rh(s)   +Rh(s)     =H(s)    +H(s)     7.73E-01   0.9387  0.5
                                        UBI   2   ADS
H(s)    +H(s)    =>H2        +Rh(s)    +Rh(s)   5.56E+11  -0.4347  0.5
                                        UBI   2   DES
O2      +Rh(s)   +Rh(s)     =>O(s)     +O(s)   4.81E-02   1.9965  0.5
                                        UBI   2   ADS
O(s)    +O(s)    =>O2        +Rh(s)    +Rh(s)   4.31E12    1.1995  0.5
                                        UBI   2   DES
OH(s)   +Rh(s)   =>H(s)      +O(s)             5.2E12    -0.2659  0.3
                                        UBI   5   SUP
H(s)    +O(s)    =>OH(s)     +Rh(s)            4.69E12   -0.8196  0.3
                                        UBI   5   SUP
H2O(s)  +Rh(s)   =>H(s)      +OH(s)            5.74E11    0.0281  0.55
                                        UBI   5   SUP
H(s)    +OH(s)   =>H2O(s)    +Rh(s)            1.8E9      1.2972  0.55
                                        UBI   5   SUP
H2O(s)  +O(s)    =>OH(s)     +OH(s)            2.08E13   -2.113   0.3
                                        UBI   8   SUP
OH(s)   +OH(s)   =>H2O(s)    +O(s)             7.22E10   -0.2902  0.3
                                        UBI   8   SUP
OH      +Rh(s)   =>OH(s)                       2.66E-1   -0.2891  0.5
                                        UBI   1   ADS
OH(s)            =>OH        +Rh(s)            1.14E13   -0.95    0.5
                                        UBI   1   DES
H2O     +Rh(s)   =>H2O(s)                      7.72E-2    1.4067  0.5
                                        UBI   1   ADS
H2O(s)           =>H2O       +Rh(s)            2.06E13   -1.8613  0.5
                                        UBI   1   DES
H       +Rh(s)   =>H(s)                        1.93E-1    1.5313  0.5
                                        UBI   1   ADS
H(s)             =>H         +Rh(s)            2.4E12     1.3208  0.5
                                       UBI   1   DES
O       +Rh(s)   =>O(s)                         4.46E-2   -1.9236  0.5
                                       UBI   1   ADS
O(s)             =>O         +Rh(s)             9.74E12   -1.9701  0.5
                                        UBI   1   DES
```

Nomenclature

A_{cat} – catalytic area [m^2]

a_{cat}– ratio between the real area of the catalyst and the reactor volume [m^{-1}]

C_i – concentration of I species [mol m^{-3}]

c_p–specific heat of the gas mixture[J mol^{-1} K^{-1}]

$\boldsymbol{d}$– vector distance through the centroid of adjacent cells [m]

D– diffusivity [m^2 s^{-1}]

D_{eff} - effective diffusivity in porous solid [m^2 s^{-1}]

D_{bulk} – bulk diffusivity [m^2 s^{-1}]

$\boldsymbol{g}$ – gravity acceleration [m s^{-1}]

H – enthalpy [J]

H_{tot} – total enthalpy [J]

k – thermal conductivity of the gas-phase [W $m^{-1}K^{-1}$], kinetic constant [s^{-1}]

k_{eff} - effective thermal conductivity of the porous solid [W $m^{-1}K^{-1}$]

$k_{diffusivity}$ = reduction factor for species diffusivity in solid phase [-]

M– transport term

m_{tot}– total mass [kg]

MW–molecular weight [kg mol^{-1}]

n – mole [mol]

N–point in the centre of the neighbouring control volume

N_C – number of computational cells [-]

NR – number of reactions [-]

N_S- number of chemical species [-]

NS – number of surface species [-]

NU - number of unknowns [-]

p – pressure [N m^{-2}], centroid of the cell [-]

Q^{het}– net heat of production of the adsorbed species [J]

Q^{hom}– net heat of production of the gaseous species [J]

r – coordinate normal to the catalytic surface [m]

r_o – outer radius [m]

r_i - inner radius [m]

R –constant of perfect gas [J mol^{-1} K^{-1}], molar production rate [mol s^{-1}]

R_{het} – heterogeneous reaction rate

R_{hom} – homogeneous reaction rate

R_{surf} – surface reaction rate

S– source term [-]

S_f– surface vector

T – temperature [K]

T_0 – reference temperature [K]

t– time [s]

$\boldsymbol{U}$– velocity vector [m s^{-1}]

$\boldsymbol{u}$– secondary variables vector

V – volume [m^3]

V_{react} – reactor volume [m^3]

V_{cell}– volume of the cell [m^3]

V_{react}–total volume of the reactor [m^3]

W_{cat} – catalyst weight [kg]

$\boldsymbol{x}$ – position vector [m]

$\boldsymbol{x_p}$– coordinate of the centroid [m]

Greek letters

α_{cat}–ratio between geometric and effective catalytic area [-]

Γ_{sites} – catalyst site fraction [mol m^{-2}]

Γ– generic transport property

Δ – distance between the cell center and the interface

ΔH – heat of reaction [J mol^{-1}]

Δx - distance between the centers of the circles [m]

ε – void fraction [-]

μ– dynamic viscosity [kg s^{-1} m^{-1}]

ν– stoichiometric coefficient [-]

ρ– density [kg m^{-3}]

$\boldsymbol{\varphi}$ – primary variables vector

ϕ – generic scalar field

Ψ– generic nonlinear function

ω– mass fraction [-]

ϑ_i– site fraction of the *i*th component [-]

ξ – fraction of catalyst active phase over total catalyst mass [kgActive/kgCat]

δ – fraction of active sites available over total active sites [molAvailable/molTotAct]

Superscripts

|| – vector magnitude

* – adsorbed species

~ – molar property

ˆ – massive property

^{0} – initial value

^{gas} – gas-phase

^{het} – referred to heterogeneous phase

^{hom}– referred to the homogeneous phase

^{n} – new computed value

^{IN} = inlet

^{OUT} = outlet

Subscripts

$_{I}$ – index of the generic species

$_{j}$ – index of the generic species or reaction

$_{k}$ – index of the reaction

$_{OWN}$ –index for the cell in which the computation is being performed

$_{NBR}$ – index for the neighboring cell at the interface of the cell in which the computation is being performed during partitioned coupling procedure

$_{solid}$ – solid phase

$_{bulk}$ – bulk phase

$_{eff}$ – effective

$_{sol}$ – solid phase

$_{D}$ – discretized form of the generic quantity

$_{MIX}$ – mixture

Bibliography

Aghalayam, P., Y. K. Park, et al. (2000). "Construction and optimization of complex surface-reaction mechanisms." Aiche Journal 46(10): 2017-2029.

Ahrens J., Geveci B. and Law C.(2005). “ParaView: An End-User Tool for Large Data Visualization.” In the Visualization Handbook. Edited by C.D. Hansen and C.R. Johnson. Elsevier.

Bird, R. B., W.E. Stewart and E.N. Lightfoot (2002). "Transport Phenomena. 2 ed." New York: J. Wiley.

Buzzi-Ferraris, G. (1998). "Metodi numerici e software in C++." Wiley Longmann Italia.

Buzzi-Ferraris, G. (2011). "BzzMath 6.0 from (www.chem.polimi.it/homes/gbuzzi)."

Clifford, I. (2011). “Block Coupled simulation using OpenFOAM”. 6th OpenFOAM workshop.

Clifford I. on block coupled approach, CFD forum online (http://www.cfd-online.com/Forum/)

Craven and Campbell (2011). “MRconjugateHeatFoam: A Dirichelet-Neumann partitioned multi-region conjugate heat transfer solver”. 6th OpenFOAM Workshop .

Deutschmann, O., C. Correa, et al. (2003). "Experimental and numerical study on the transient behaviour of partial oxydation of methane in a catalytic monolith." Chemical Engineering Science 58: 633-642.

Deutschmann, O., S. Tischer, et al. (2008). "DETCHEM™ Software Package, http://www.detchem.com." Karlsruhe 2.2 ed.

Deutschmann, O., S. Tischer, et al. (2011). "DETCHEMTM User Manual - Version 2.3.".

Dumesic, J. A., G. W. Huber, et al. (2008). "Microkinetics: Rates of Catalytic Reactions." Handbook of Heterogeneous Catalysis. Ertl, et al., Editors.

Faravelli, T., A. Cuoci, et al. "http://creckmodeling.chem.polimi.it/."

H. Ferziger H. and Peric M.(1999). "computational Methods for Fluid Dynamics." 2nd Edition. Springer.

Fluent, I. (2004). "GAMBIT 2.2 - Tutorial Guide " www.fluent.com.

Gear, C. W. (1971). "Numerical Initial-Value Problems in Ordinary Differential Equations." Prentice-Hall, Englewood Cliffs, NJ.

Goisis and Osio (2011). “Computational fluid dynamics of gas-solid catalytic reactors based on microkinetic description of surface chemistry“. Msc Thesis in Chemical Engineering, Politecnico di Milano.

Gokhale, A. A., S. Kandoi, et al. (2004). "Molecular-level descriptions of surface chemistry in kinetic models using density functional theory." Chemical Engineering Science 59(22-23): 4679-4691.

Hartmann, M., L. Maier, et al. (2010). "Catalytic partial oxidation of iso-octane over rhodium catalysts: An experimental, modeling, and simulation study." Combustion and Flame 157: 1771-1782.

Issa, R. I. (1986). "Solution of the implicitly discretized fluid flow equations by operator-splitting." J. Comp. Physics 62: 40-65.

Jaluria and Torrance (2003). “Computational Heat Transfer” Taylor & Francis 2003”.

Jasak, H. (1996). "Error Analysis and Estimation for the Finite Volume Method with Applications to Fluid Flows." PhD Thesys; Imperial College; London.

Kim J.H., Okhoa J.A., Whitaker S., (1987). Transport Porous Med. 2, 327.

Koop, J. and O. Deutschmann (2009). "Detailed surface reaction mechanism for Pt-catalyzed abatement of automotive exhaust gases." Applied Catalysis B: Environmental 91: 47–58.

Maestri, M. (2011). "Microkinetic Analysis of complex chemical processes at surfaces." [in press] Wiley VCH.

Maestri, M., A. Beretta, et al. (2008). "Two-dimensional detailed modeling of fuel-rich H2 combustion over Rh/Al2O3 catalyst." Chemical Engineering Science 63: 2657-2669.

Maestri, M. and K. Reuter (2011). "Semiempirical Rate Constants for Complex Chemical Kinetics: First-Principles Assessment and Rational Refinement." Angewandte Chemie-International Edition 50(5): 1194-1197.

Maestri, M., D. G. Vlachos, et al. (2009). "A C(1) Microkinetic Model for Methane Conversion to Syngas on Rh/Al(2)O(3)." Aiche Journal 55(4): 993-1008.

Manca, D., G. Buzzi-Ferraris, et al. (2009). "The solution of very large non-linear algebraic systems." Computers and Chemical Engineering 33: 1727-1734.

Mangani, L. (2008). "Development and Validation of an Object Oriented CFD Solver for Heat Transfer and Combustion Modeling in Turbomachinery Applications." PhD Thesis, University of Florence.

Mezedur M.M., Kaviany M., Moore W.(2002). AIChE J. 48, 15.

Mhadeshwar, A. B. and D. G. Vlachos (2005). "A thermodynamically consistent surface reaction mechanism for CO oxidation on Pt." Combustion and Flame 142(3): 289-298.

Mladenov, N., J. Koop, S. Tischer and O. Deutschmann (2010). "Modeling of transport and chemistry in channel flows of automotive catalytic converters." Chemical Engineering Science 65(2): 812-826.

Mu, D., Z.-S. Liu, C. Huang and N. Djilali (2008). “Determination of the effective diffusion coefficient in porous media including Knudsen effects” Microfluidics & Nanofluidics, 4 (3), 257-260.

Nowak U., Frauhammer J., Nieken U. (1996). Comp. Chem. Eng. Vol. 20 No. 5 547

OpenFOAM® (2011). "The Open Source CFD Toolboox - User Guide."

OpenFOAM® (2011). "www.openfoam.com - OpenFOAM®: open source CFD."

Patankar, S. V. and D. B. Spalding (1972). "A calculation procedure for heat, mass and momentum transfer in three-dimensional parabolic flows." Int. J. Heat Mass Transfer 15: 1787.

Penntinen, Yasari et al. (2001). “A PimpleFoam tutorial for channel flow, with respect to different LES models”. A course at chalmers University of technology taught by Hakan Nilsson.

Pope, S. B. and R. Zhuyin (2008). "Second-order splitting schemes for a class of reactive systems." Journal of Computational Physics 227(8165-8176).

Quarteroni, A. and A. Valli (1999). "Domain decomposition methods for partial differential equations (Numerical mathematics and scientific computation)." Oxford University Press.

ReactionsDesign (2008). "CHEMKIN-PRO® Software - Input Manual." http://www.cadfamily.com/download/CAE/Chemkin-Tutorial/Input.pdf.

Ren, Z. and S. B. Pope (2008). "Second-order splitting schemes for a class of reactive systems." Journal of Chemical Physics 227: 8165.

Reuter, K. (2009). "First-Principles Kinetic Monte Carlo Simulations for Heterogeneous Catalysis: Concepts, Status and Frontiers." Wiley-VCH, Weinberg.

Schlögl, R. (2001). "Theory in heterogeneous catalysis - An experimentalist's view." Cattech 5(3): 146-170.

Shustorovich, E. a. H. S. (1998). "The UBI-QEP method: a practical theoretical approach to understanding chemistry on transition metal surfaces." Surface Science Reports 31(1-3): 5-119.

B. Sportisse (2000). An analysis of operator splitting techniques in the stiff case, Journal Computational Physics 161 (1) 140–168.

Strang, G. (1968). "On the construction and comparison of difference schemes." SIAM Journal of Numerical Analysis 5: 506.

Tischer, S., Jiang, Y., Hughes, K., Patil, M. et al.(2007) "Three-Way-Catalyst Modeling - A Comparison of 1D and 2D Simulations," SAE Technical Paper 2007-01-1071, doi:10.4271/2007-01-1071.

Thiele, E.W. (1939). "Elation between catalytic activity and size of particle". Industrial and Engineering Chemistry, 31 , pp. 916–920

Van Doormaal, J. P. and G. D. Raithby (1985). "An evaluation of the segregated approach for predicting incompressible fluid flows." National Heat Transfer Conference, Denver, Colorado.

Versteeg, H. K. and W. Malalalsekera (1995). "An introduction to Computational Fluid Dynamics." Longman Scientific & Technical.

Vlachos, D. G., S. Kaisare, et al. (2008). "Stability and performance of catalytic microreactors: simulations of propane catalytic combustion on Pt." Chemical Engineering Science 63: 1098-1116.

Vlachos, D. G., M. Stamatakis, et al. (2011). "A review of multiscale modeling of metal-catalyzed reactions: Mechanism development for complexity and emergent behavior." Chemical Engineering Science 66(19): 4319-4355.